The Dissertation Committee for Robert Joe McKee certifies that this is the approved version of the following dissertation:

Composite Expansions for Active and Inactive Motions in the Streamwise Reynolds Stress of Turbulent Boundary Layers

Committee:

Ronald Panton, Supervisor

Janet Ellzey

Ofodike A. Ezekoye

Jack Howell

Christopher Freitas

Composite Expansions for Active and Inactive Motions in the Streamwise Reynolds Stress of Turbulent Boundary Layers

by

Robert Joe McKee, B.S.M.E.; M.S.M.E.

Dissertation

Presented to the Faculty of the Graduate School of

The University of Texas at Austin

in Partial Fulfillment

of the Requirements

for the Degree of

Doctor of Philosophy

The University of Texas at Austin

May 2008

Dedication

To Catherine L. McKee who persistently encouraged my somewhat displaced dream of obtaining a Doctorate and consistently gave of her time and love to make this journey possible and to support my efforts to reach this goal.

Acknowledgements

Many people have supported and encouraged me during my efforts towards this degree. First and foremost among these people is my supervisor, Dr. Ronald Panton who richly deserves my highest praise and my heart felt appreciation for his consistent belief in my ability, his in-depth and enlightening instruction, and his patience with my significant time constraints.

In addition, I thank other facility members at the University of Texas at Austin including my committee members, Dr. Janet Ellzey, Dr. Ofodike Ezekoye, and Dr. Jack Howell along with other professors, including Dr. David Bogard, all of whom encouraged, guided, and taught me a great deal.

I thank my employer, Southwest Research Institute, where management encourages and provides opportunities for the staff to seek higher education. I have also enjoyed the encouragement of my son Dr. David W. McKee, and coworkers Dr. Christopher Freitas, Dr. Jack Simonis, Dr. Klaus Brun, Mr. Danny Deffenbaugh, and others at SwRI. I also appreciate the consistent support of Ms. Lora Neill in accommodating business requirements to my academic schedule and in aiding with formatting this document.

I owe a sincere thank you to the other turbulence researchers who have supplied data from their work to Dr. Panton, and thus to myself, for use in this analysis including David DeGraaff, Jens Osterlund, Michael Stanislas, Ivan Marusic, Luciano Castillo, Hassan Nagib, and their colleges.

Composite Expansions for Active and Inactive Motions in the Streamwise Reynolds Stress of Turbulent Boundary Layers

Publication No._____

Robert Joe McKee, Ph.D.

The University of Texas at Austin, 2008

Supervisor: Ronald Panton

Abstract: The proper scaling and prediction of the streamwise Reynolds stress in turbulent boundary layers has been a controversial issue for more than a decade as its Reynolds Number dependence can not be removed by normal scaling. One issue that may explain the unusual behavior of the streamwise Reynolds stress is that it is affected by both active and inactive motions per the Townsend hypothesis. The goal of this research is to develop a composite expansion for the streamwise Reynolds stress in turbulent boundary layers that considers active and inactive motions, explains various Reynolds Number dependencies, and agrees with available data.

Data for the Reynolds shear stress and the streamwise Reynolds stress from six sources are evaluated and as appropriate plotted on inner and outer scales. A new asymptotic representation for the Reynolds shear stress, <uv>+, that meets the requirements for a proper composite expansion is developed and applied. This new Reynolds shear stress composite expansion agrees with data and allows predictions of <uv>+ for any Reynolds Number.

The streamwise Reynolds stress, <uu>+, can be separated into active and inactive parts and the Reynolds shear stress can be used to represent the active part. The inactive streamwise Reynolds stress, <uIuI>#, is separated from the complete <uu>+ in part of this work.

An outer correlation equation with the correct asymptotic limits for the inactive streamwise Reynolds stress is developed and shown to fit the outer part of the <uIuI># data. A separate inner correlation equation for inner inactive streamwise Reynolds stress is developed and fit to data. Together these two equations form a composite expansion for the inactive streamwise Reynolds stress for flat plate boundary layers. This composite expansion for the inactive streamwise Reynolds stress can be combined with the Reynolds shear stress expansion to produce predictions for <uu>+ that agree with data. Thus a composite expansion for predicting the streamwise Reynolds stress in turbulent boundary layers is developed and shown to reproduce the correct trends, to

agree with the available data, and to explain the Reynolds Number dependence of the streamwise Reynolds stress.

Table of Contents

List of Tables

List of Figures

Chapter 1 Introduction

1.1 Background

A turbulent flow is one in which eddies over a wide range of sizes are sustained so that mixing of momentum and other properties takes place to a much greater extent than in laminar flow. Turbulence is a complex and chaotic motion of fluids, which occurs when the inertia forces are significantly larger than the viscous forces; that is at high Reynolds Numbers. In turbulent flows, fluctuating velocities are evidence of the nearly random rotating eddies that exchange energy between different sizes and from one flow direction to another. This dynamic exchange of energy between eddies and between different velocity components, does not occur in laminar (low Reynolds Number) flows. Turbulent flows have vortices throughout their structure and as a result are diffusive per the discussions of Panton (1996). Turbulent flows near walls form relatively thin complex boundary layers, which govern the significant change of momentum between the flow and wall. A thorough understanding of wall bounded turbulence is important for predicting, quantifying, and effectively using fluid flows in our energy intensive world.

A number of important parameters that describe turbulent flow and its internal structure are composed of time averaged moments of the fluctuating velocities. The important two-component moments include the Reynolds stresses, turbulence intensities (components of the turbulent kinetic energy), and the two-point velocity correlations. In this work the coordinates will be designated as x, y, and z corresponding to the velocity

fluctuations u, v, and w in the steamwise, wall normal, and cross flow directions respectively. The mean unidirectional flow velocity is U(y) and the time or ensemble average of a quantity is denoted by < >. The Reynolds shear stress <uv> for example appears in the momentum equation and has a direct relationship to momentum exchange in a flow. The streamwise Reynolds stress <uu> is an important two-component moment that has a higher magnitude and a different behavior than the other Reynolds stresses. The peak in the streamwise Reynolds stress that occurs at approximately y+ = 15 is known to be related to the turbulent kinetic energy production in a boundary layer (DeGraaff and Eaton 1999). Taken together, the Reynolds Stress tensor quantifies the structure of turbulence such that if they could be predicted, which is in general not achievable at this time, then a nearly complete description of a turbulent flow would be available.

There is an extensive and rich literature concerning turbulent flows, experimentation dealing with turbulence, and analysis and modeling of turbulent flows as discussed in Gad-e-Hak, M. and Bandyophadhyay (1994), Fernholtz and Findley (1996), and Panton (2005). Despite this history and the gains in understanding that have been made, there is still not a complete and useful analytic description of turbulence, a universally applicable and accurate model, or adequate methods for predicting the Reynolds stress distributions within turbulent boundary layers (Panton, 2005). The observed energy spectra in turbulent flow can be explained but not predicted, the

structures can be observed but not quantitatively described, and the mechanisms that sustain turbulence are still a mystery as discussed in Panton (2001).

1.2 Turbulent Wall Layers and Boundary Layers

Turbulent wall layers are present in pipes, channels, and boundary layers in most practical flow situations. Turbulent wall layers have a significant impact on the control and economics of moving fluids. Turbulent boundary layers over flat plates are one of the most fundamental; most extensively studied, and yet not fully resolved situations in turbulence.

Most boundary layers are driven by or affected by pressure gradients, which act in the direction of the dominant flow. Non- equilibrium boundary layers, which are affected by changing pressure gradients, have continuously changing values of boundary layer thickness, velocity profile, Reynolds stress profiles, and other parameters that are representative of the structure of the flow. If the pressure gradient in the flow direction is constant then the boundary layer is considered an equilibrium boundary layer and the thickness, velocity, and Reynolds stress gradients are consistent. In order to simplify the studies and the quantitative descriptions of turbulent boundary layer flows most research is conducted on equilibrium or on zero pressure gradient boundary layers, DeGraaff and Eaton (1999). Pressure gradient effects are not the same in pipe and channel flows because by nature the pressure gradient and flow profiles in closed conduits eventually come to a steady condition. A flat plate boundary layer pressure gradient is dependent on

the free stream velocity conditions and under carefully arranged conditions can result in a zero pressure gradient.

Boundary layers are measured by a number of different scales and confusion can occur when different studies or data sets use different definitions for the boundary layer thickness or other important parameters. The generally accepted velocity scales for turbulent boundary layers are the free stream or external velocity, Ue, which exist just outside the boundary layer and the friction velocity, u*, that is defined as $u^* = \sqrt{\tau/\rho}$. The extent of the turbulent boundary layer measured from the wall to the area where the velocity is the external or nearly the same as the external velocity is referred to as the physical boundary layer thickness. However, the boundary layer thickness can be taken as δ, δ99, or δ95 as shown in Figure 1-1 where some of the common boundary layer thicknesses are illustrated. The δ99 thickness for example is defined as the distance from the wall to the location where the velocity is equal to 99 percent of Ue. At experimentally high Reynolds Numbers the boundary layer thickness is typically 35 mm ± as much as 20 mm. Thus the location of δ99 in contrast to either δ or δ95 is experimentally difficult to determine without a significant uncertainty. Some definitions of the boundary layer thickness based on integrals of the velocity profiles, such as the displacement thickness, δ*, and the momentum thickness, θ, have been defined and used. However, these integral length scales are not suitable for scaling turbulent boundary layers because their relationship to the physical thickness, δ, changes as the Reynolds Number changes (Panton 2005). Another length scale suggested by Rotta (1953) and

advanced by Clauser (1956) and others to avoid the sensitivity problem is based on an integral of the velocity defect law and is defined as $\Delta_{RC} = Ue * \delta * / u *$. Osterlund (1999) has shown that velocity profile scaling with Δ_{RC}, the Rotta-Clauser thickness is consistent with δ scaling but potentially more accurate. Scaling of the outer lengths of turbulent boundary layers is generally expressed as $Y = y / \delta$ with whichever boundary layer thickness value is defined or available. An alternative outer scaling that uses the Rotta-Clauser thickness will be expanded on in a later section and used throughout this work is $\eta = y / \Delta_{RC}$. The inner length scale for turbulent boundary layers is generally accepted as $y^+ = y\ u^* / \nu$ (Panton 1997). It is important to realize that the Reynolds Number defined as $Re^* = \delta\ u^* / \nu$ is the ratio of the inner length scale, y+ to the outer length scale Y and hence the ratio of the sizes of the inner to the outer regions.

Boundary layer properties such as the mean velocity or Reynolds stresses are properly scaled when the dependence on Reynolds Number is minimized. The internal structure of turbulent boundary layer flows can be considered to be defined by the profiles of the various Reynolds stresses and thus scaling for the Reynolds stresses is essential for understanding turbulent boundary layers. Wall bounded turbulent flows in channels, pipes, and over flat plates have many similarities. In particular, the mean velocity profile for channels, pipes, and flat plates can be scaled in the same manner. Moreover, the Reynolds shear stress <uv> for channels, pipes, and the inner part of the Reynolds shear stress for flat plates can be scaled with the friction velocity, u*. It has

been demonstrated, by Panton (2005), that the inner and outer parts of the Reynolds shear stress for channel and pipe flow can be scaled with a composite expansion. The inner part of a zero pressure gradient flat plate boundary layer also shows this same scaling, however, the outer part of the Reynolds shear stress has a different outer scaling because it has a different velocity behavior at the edge of the wall layer.

However, the streamwise Reynolds stress <uu> has some unusual treads: (1) it does not scale well with the friction velocity u* as the scale unit and (2) it is roughly a factor ten times larger that the Reynolds shear stress -<uv>. The first trend was only recently confirmed by DeGraaff and Eaton (2000) and Metzger and Klewicki (2001). They claim that the streamwise Reynolds stress <uu> for flat plate boundary layers scales with a mixed scaling, Ue u*.

1.3 Active and Inactive Motions

Obtaining a proper scaling for the streamwise Reynolds stress would allow for construction of a composite expansion. As noted above, the streamwise Reynolds stress <uu> has a peak in magnitude of roughly 10 times the Reynolds shear stress <uv>, which occurs in the inner region near y+ = 15. The peak magnitude depends on Reynolds Number. One explanation of the large values of the streamwise Reynolds stress is inactive motions in the flow, an idea conceived by Townsend (1976). This idea was advanced in a period of time when it was thought that <uu> scaled with u*.

Additional works that have extended Townsend's ideas are studies by Perry et al. (1986), Marusic et al. (1997), and Marusic and Kunkel (2003).

Active motions are defined as fluctuations that make essential contributions to the Reynolds shear stress <uv>, while inactive motions, which are large in scale, do not contribute to Reynolds shear stress. Panton (2007) has suggested that active and inactive motions can be considered to scale differently and proposed that this fact can be used to separate the active part from the inactive part of the streamwise turbulent motions.

Townsend argues that although most of the eddy motions are "active" and have an effect on turbulent stresses, some of the eddy motions are "inactive" and have no apparent effects on the Reynolds shear stresses. Inactive fluctuations are envisioned to be large scale outer motions that are influenced by the outer velocities but extend to and interact with the wall. The outer layer of a turbulent boundary layer is different than the outer layer in pipes and channels because of the difference in the outer shape of the velocity profile. Hence, one would anticipate that the inactive motions in these three flows and particularly in the boundary layers flows would be different.

1.4 Composite Expansions

Composite expansions are a means by which a physical behavior that depends on two different but overlapping functions or asymptotic behaviors can be represented.

Composite expansions are the result of matched asymptotic expansions and provide a mathematical basis for representing physically important quantities. In turbulent flows the single perturbation parameter, Reynolds Number, has been used in composite expansions to describe the wall normal velocity profile and normalized Reynolds shear stress profile, $<uv>^+$.

Composite asymptotic expansions have been successfully used to develop representations and prediction methods for turbulent wall bounded velocity profiles and Reynolds stresses in pipes and channels as developed by Panton (2005 and 2007). The Reynolds shear stress will be discussed as an example of a wall layer composite expansion. The Reynolds shear stress in the outer region is

$$\frac{< uv >}{u_*^2} = G(Y) \qquad as \ \ \mathrm{Re}_* \to \infty$$

while in the inner region it is taken as

$$\frac{< uv >}{u_*^2} = g(y^+) \qquad as \ \ \mathrm{Re}_* \to \infty$$

The common part of these functions is

$$\frac{< uv >}{u_*^2} = G(Y = 0) = g\ (y^+ \to \infty) = 1$$

A composite expansion, which is good for all y, is assembled as

$$\frac{\langle \mathrm{uv} \rangle}{\mathrm{u}^{*2}} = \langle \mathrm{uv} \rangle^+ = \mathrm{g}\left(\mathrm{y}^+\right) + \mathrm{G}(\mathrm{Y}) - \text{Common Part}$$

Since $y^+ / Y = \mathrm{Re}_*$, this expression accounts for the Reynolds Number dependence of the Reynolds shear stress and can be used to plot the <uv>+ for a selected Re*.

The outer behavior of the Reynolds shear stress is different for the turbulent boundary layer than for pipe and channel flows because of the outer velocity behavior. The outer functions for the Reynolds shear stress in pipes and channels is G(Y) = 1-Y per Panton (1996, 2002, and 2005). The outer function for the Reynolds shear stress for the flat plate boundary layer must satisfy the following relationship from the momentum equation (Panton 2002).

$$\frac{dG}{dY} = -Y \frac{d}{dY}\left[\frac{U - U_e}{u^*}\right] \qquad \text{Equation 1}$$

A composite expansion for the streamwise Reynolds stress for flat plate boundary layers has not been demonstrated in published literature and there are still questions and controversy about the proper scaling of the normalized streamwise Reynolds stress, <uu>+ in a zero pressure gradient turbulent boundary layer as discussed by DeGraaff and Eaton (2000) and Marusic and Kunkel (2003). As discussed in the turbulent boundary layer background, there is a peak in the streamwise Reynolds stress for flat plate boundary layers that is much larger than the other Reynolds stresses and does not consistently scale with either the inner variable of u* and y+ or with the other variables of Ue and Y as presented by DeGraaff and Eaton (1999). It is known that the outer layer of the flat plate boundary Reynolds stresses behaves differently and in a

more complex manner than the outer layer of pipe and channel flows. Another reason that a composite expansion has not previously been developed for the streamwise Reynolds stress for a zero pressure gradient flat plate may have to do with the different contributions of the active and inactive motions in the boundary layer as suggested by Panton (2005). If an accurate composite expansion can be found for the streamwise Reynolds Stress for flat plate boundary layers it will account for Reynolds Number dependence and will add to the understanding of the structure of flat plate turbulent boundary layers.

1.5 Current Work and Objectives

The goal of the research presented in this dissertation is to develop a composite expansion for the turbulent boundary layer streamwise Reynolds stress while considering the influence of active and inactive motions in zero pressure gradient flat plate boundary layers. A proper scaling of the streamwise Reynolds stress that separates the active and inactive motions will allow predictions of the Reynolds stress profiles including the peak in amplitude and the Reynolds Number dependent changes for wall bounded flows. One requirement for this goal is to identify and use quality data that is available for evaluations of composite expansions and predictions of the streamwise Reynolds Stress.

The first step is to review and evaluate the available modern and hopefully high precision data so that the behavior of Reynolds stresses in inner and outer variables can

be plotted and compared to appropriate functions. The Reynolds shear stress is by Townsend's definition an active part of turbulence in a boundary layer. From that part of the available data that has the highest resolution Reynolds shear stress data will be examined and compared to composite expansions that represent the high Reynolds Number limits of the data. The streamwise Reynolds stress will also be examined, plotted, and compared to scaling variables. The next step using u*/Ue as a gauge function will be to remove the active part of the turbulent motions represented by the Reynolds shear stress from the streamwise Reynolds stress so that the inactive part of the streamwise Reynolds stress can be plotted. This inactive part of the streamwise Reynolds stress will then be plotted as a function of the inner length y+ and as a function of the outer length scale η. With the inner and outer behavior of the separated inactive streamwise Reynolds stress evident in several graphs of selected data, functions that have the proper asymptotic behavior and fit the shape of this data will be used to form a composite expansion for the inactive part of the streamwise Reynolds stress. If a satisfactory composite expansion that matches the inactive streamwise Reynolds stress can be constructed then the active part of turbulence can be added to the inactive part so that a complete reconstruction of the streamwise Reynolds stress can be assembled. A composite expansion of the streamwise Reynolds stress will show the Reynolds Number dependence and the proper scaling of this important parameter for Turbulent Boundary Layers.

1.5.1 Objectives

The objectives of this research are to analyze data for the Reynolds shear stress, <uv>, and streamwise Reynolds stress, <uu>, for zero pressure gradient boundary layers. The analysis for <uu> will use the concept of active and inactive motions, and recognize that they scale differently. Specific objective are:

1. Develop an outer correlation equation for the Reynolds shear stress <uv> and accept the inner correlation based on pipe and channel flows as valid for boundary layers.

2. Process data to yield the inactive component of the streamwise Reynolds stress by subtracting the active part of the Reynolds stress from the total streamwise Reynolds stress.

3. Develop an outer region correlation for the inactive component of <uu>.

4. Develop an inner correlation for the inactive motions of the streamwise Reynolds stress.

5. Form a composite expansion for the Reynolds shear stress, <uv> that displays the dependence on y and Re* found in the data.

6. Form a composite expansion for the inactive component of the streamwise Reynolds stress, <uIuI > that displays the correct dependence on y and Re*.

7. Form a composite expansion for the streamwise Reynolds stress <uu> that displays the dependence on y and Re* that agrees with the data.

Chapter 2. Experimental Data

2.1 General Data

Turbulent boundary layers are thin portions of flows next to a wall in which a lot of velocity changes and Reynolds stress activities take place. It is difficult to make high resolution measurements of the fluid velocity components within these thin boundary layers. In order to define viscous sub-layer profiles data must be taken near the walls, at y+ values of less than 10. The streamwise Reynolds stress for example requires many measurements point from y+ = 1 or 2 through 100 or 200 in order to define the amplitude and location of the peak that occurs near y+ = 15. The vast majority of data has been taken with hot wire anemometers. The size of hot wire elements is critical in terms of minimizing the loss of small scale eddy information on the accuracy of Reynolds stress parameters as confirmed by Nickels et al. (2007). The length of the hot wire normalized with the viscous length scale, that is $l+ = l\, u^*/\nu$, is an important value, which must remain relatively small in order to obtain undistorted measurements of turbulent velocity components. A hot wire anemometer cannot resolve the effect of turbulent eddies that are smaller than the wire length. As Reynolds Number increases and distance from the wall decreases more energy is contained in the smaller eddies, such that the size of the hot wire becomes more important. An important result found by Nickels et. al. (2007) is repeated in Figure 2-1, which shows the streamwise Reynolds stress measured in a constant Reynolds Number boundary layer flow with four different size hot wire anemometers. The smallest wire with an l+ = 10 data show a significant

peak at y+ = 15 as expected in this type of flow. Figure 2-1 shows that as the hot wire non-dimensional length increased, the amplitude of the streamwise Reynolds stress at points close to the wall decreased. This effect of the hot wire length on the accuracy of measurements most likely has adversely affected a significant amount of data taken over the past several decades.

The limitations of hot wire size in measuring the small eddy contributions to turbulence are normally more significant for X-wire configurations used to measurement the Reynolds shear stress and other two-component quantities. The recent work by Nickels et al. (2007) indicates that values of l+ of approximately 10 to 15 or less are required to obtain accurate Reynolds stress data. Although the sample volumes for LDA measurement are usually small the same limitation in eddy size effects are present because an LDA averages the velocities of the detected particles that pass through the measurement volume. This limitation in the measurement based on size of the sampling probe is especially important close to the wall where the velocity gradients are larger. Care should be taken when selecting data for evaluation because of this effect.

2.2 DeGraaff and Eaton

One set of fairly recent experiments was designed and conducted specifically to obtain measurements close to the wall in high Reynolds Number flat plate boundary layers and to avoid some of the limitations of the hot wire anemometer size effects. This experiment was reported on by DeGraaff and Eaton (1999 and 2000). This experiment

was conducted in a wind tunnel capable of an 8 to 1 range in Reynolds Numbers and used a specifically designed Laser Doppler Anemometer, LDA, system to measure the velocity components u and v down to wall distances of y+ = 1 at the lowest Reynolds Number and y+ = 23 at the highest Reynolds Number. The normalized measurement volume with the LDA ranges from l+ = 1 to a maximum of 16.9 such that this measurement system provides high resolution, near wall, low distortion measurements. Despite the efforts undertaken by DeGraaff and Eaton, there is a level of uncertainty for the measurement results in the DeGraaff and Eaton (1999) work that is approximately 4 percent for the streamwise Reynolds stress and 8 to 10 percent for the Reynolds shear stress values.

DeGraaff and Eaton (2000) report the mean velocity, the streamwise Reynolds stress, the wall normal Reynolds stress, and the Reynolds shear stress for five different Reynolds Numbers for steady zero pressure gradient boundary layer flows. The five Reynolds Number, Re*, values are 539, 992, 1692, 4339, and 10030. These data includes a wide Reynolds Number range from one that is somewhat low to a relatively high value that is the highest Reynolds Number in the data available for review. The log law portion of a turbulent boundary layer and hence the overlap behavior just becomes evident at Re* values of 500 or greater (Panton 2005). Thus Re*= 500 is the lowest Reynolds Number for data that is considered in this work, unless specifically stated otherwise. A summary of the important parameters for the five measurements of the flat plate turbulent boundary layer include free stream velocity, boundary layer thicknesses,

friction velocity, viscosity, and the Rotta-Clauser thickness, as reported by DeGraaff and Eaton is shown in Table 1.

Table 1. DeGraaff and Eaton Turbulent Boundary Layer Parameters

Re*	Ue	δ	δ*	u*	ν	Δ_{RC}
	m/sec	mm	mm	m/sec	μm^2/sec	mm
539	6.04	31.25	5.26	0.269	15.548	118.1
992	9.83	37.93	6.28	0.403	15.395	153.2
1692	18.95	35.87	5.71	0.727	15.412	148.8
4339	14.36	34.56	4.94	0.512	4.081	138.6
10030	17.15	35.58	17.15	0.573	2.034	139.2

Plots of the DeGraaff and Eaton Reynolds shear stress are shown in Figure 2-2 as a function of the inner length scale y+ and against the outer scale of η in Figure 2-3. The inner length scale commonly used in boundary layer literature, is defined as $y+ = y\, u^*/ \nu$, and is provided with the data by DeGraaff and Eaton (1999) as well as by most of other researchers. The outer length scale, Eta, is defined as $\eta = y/\Delta_{RC}$ where the Rotta-Clauser length scale, Δ_{RC}, is defined as, $\Delta_{RC} = \delta^* Ue / u^*$ and the factors to calculate Δ_{RC} are provided by DeGraaff and Eaton. The streamwise Reynolds stress data from DeGraaff and Eaton are shown against the same inner and outer scaling in Figure 2-4 and 2-5 respectively. It is clear in Figure 2-4 that there is a Reynolds Number dependence in the <uu>+ data for y+ values of approximately 10 and higher. Figure 2-5

also shows some Reynolds Number effects in the outer layer scaling for η values between 0.05 and 0.2 for this data which covers a nearly 20 to 1 Re* range. The DeGraaff and Eaton data is a valuable set of data for determining a proper scaling of the Reynolds stresses and the agreement of composite expansions to streamwise Reynolds stress trends.

2.3 Spalart

Another source of high resolution near wall boundary layer results is obtained from the DNS calculation by Spalart (1988) although these calculations are limited in Reynolds Number. Spalart presents the mean velocity, the Reynolds shear stress, the streamwise Reynolds stress, and many other turbulence components for the three Reynolds Numbers of Re* = 150, 325, and 650. The highest of these Reynolds Numbers is within the range of the DeGraaff and Eaton and other experimental data and so may be useful for comparison. The lowest Reynolds Number in the Spalart DNS results is clearly too low to be applicable to practical flat plate boundary layer scaling. Being numerical rather than experimental, the Spalart data is accompanied by fewer of the measured parameters that help to scale and convert the data but it is accompanied by various normalized and non-dimensional parameters. A summary of the parameters used to scale and otherwise compare the Spalart results is shown in Table 2. Spalart does report the y+ values and sufficient information to calculate η from 0.25* y+/Re*. The values of u*/ Ue and of u* itself shown in Table 2 are calculated from other non-dimensional parameters provided by Spalart and from the Reδ* = δ* Ue / ν parameter.

A plot of Spalart Reynolds shear stress vs. the inner y+ variable is shown in Figure 2-6 and the same data as a function of a calculated η variable is shown in Figure 2-7. Plots of the streamwise Reynolds stress from Spalart calculations are shown in Figure 2-8 as a function of the inner y+ and in Figure 2-9 vs. the outer length scale, η. Although of limited Re* range, the Spalart data, and particularly the highest Re* data provide a solid basis for comparison with some of the other data.

Table 2. Spalart Turbulent Boundary Layer Parameters

Re*	Ue	Reδ*	u*/Ue	u*
150	18.5	500	0.05354	0.9905
325	20.3	1000	0.04781	0.9705
650	22.0	2000	0.04551	1.0013

2.4 *Osterlund*

Another set of carefully documented data that has been referenced in several studies of turbulent boundary layers (Panton 2005) and is useful for this analysis are the zero pressure gradient data taken in the large wind tunnel at KTH, Stockholm and presented by Osterlund (1999). A large number of measurements were taken at different locations along the 7 meter length of the flat plate in the wind tunnel test section so that the development of the boundary layer could be tracked and documented. The data available for evaluation of zero pressure gradient turbulent boundary layers were taken near the downstream end of the test section, at X = 5.5 m, and consist of data at seven

(7) Reynolds Number between Re* = 1676 and Re* = 5156. A summary of the parameters that describe the data that are reported by Osterlund is presented in Table 3.

Table 3. Osterlund Turbulent Boundary Layer Parameters

Re*	Ue	δ_{95}	δ^*	U*	Δ_{RC}
1676	10.38	0.0633	0.0132	0.3833	0.3581
2310	15.78	0.0594	0.0121	0.5633	0.3391
2919	21.18	0.0572	0.0114	0.7398	0.3270
3497	26.49	0.0557	0.0110	0.9115	0.3184
4061	31.79	0.0545	0.0106	1.081	0.3117
4609	37.03	0.0536	0.0103	1.247	0.3063
5156	42.33	0.0529	0.0101	1.414	0.3016

The Osterlund data were taken with hot wire anemometers using single wire probes for the mean velocity and the streamwise Reynolds stress and "X" wires probes for the Reynolds shear stress and other normal and cross stream Reynolds stress components. The non-dimensional wire lengths for the single wire measurements varied from $l^+ = 6.55$ to $l^+ = 59.8$ per Osterlund's calculations for the various Reynolds Number data sets. The average non-dimensional wire length for the Osterlund data is 22.9 wall units such that the data are marginal in terms of providing undistorted measurements particularly near the wall. For this reason Osterlund has been reluctant to publish these data. The "X" wire lengths are similar to the single wire lengths and the separation

between wires causes an increased opportunity for distortion of the measurement due to the hot wire geometry. The Osterlund Reynolds shear stress data display some unexpected trends in the overlap region and a little beyond, from y+ of 50 to 1000, and do not included measurements at small y+ values of 10 or less. As a result of these inconsistencies and the limited inner range of the data the Reynolds shear stress data from Osterlund are not used in this study.

The streamwise Reynolds stress data from Osterlund are also limited in terms of the near wall information to y+ values from 11.1 for the smallest Re* data to y+ = 36.7 for the largest Reynolds number data. However, the streamwise Reynolds stress data in the outer region seem to be consistent and to display the expected Reynolds Number dependence such that it should be useful for comparing to suggested composite expansions for the streamwise Reynolds stress in the outer boundary layer. A plot of the Osterlund streamwise Reynolds stress as a function of the inner scale y+ is shown in Figure 2-10, where the behavior around the peak near y+ = 15 out to y+ of approximately 80 may be questionable or is at least unclear but the behavior for y+ > 100 is consistent with other data in this study. Streamwise Reynolds stress data recorded by Osterlund as a function of length scale η is shown in Figure 2-11, which reflects a consistent essentially Reynolds Number independent outer behavior.

2.5 Carlier and Stanislas

Recent measurements of the structure of a turbulent boundary layer in which PIV measurements were used to quantify the vortices and visualize the structure of the boundary layer and hot wire anemometer measurements were made to determine turbulent quantities including Reynolds stresses have been completed by Carlier and Stanislas (2005). Carlier and Stanislas acquired mean velocity, each component of the turbulence intensity (including streamwise Reynolds stress), Reynolds shear stress, and other quantities at four different Reynolds Numbers. The Reynolds Numbers for these wind tunnel experiments ranged from Re* = 2517 to Re* = 6779. A summary of the parameters that represent the turbulent boundary layer study by Carlier and Stanislas are show in Table 4.

Table 4. Carlier and Stanislas Turbulent Boundary Layer Parameters

Re*	Ue	δ	δ*	u*	Δ_{RC}
	m/sec	m	m	m/sec	M
2517	3.0	0.350	0.055	0.108	1.528
3785	5.0	0.319	0.0442	0.178	1.242
4822	7.0	0.298	0.0395	0.243	1.138
6779	10.0	0.304	0.0397	0.335	1.185

The turbulence quantities from the boundary layer studies by Carlier and Stanislas are measured using hot wire anemometers with non-dimensional lengths of

approximately $l^+ = 4$ to $l^+ = 12$. These relative small hot wires are capable of accurate undistorted measurements at locations relatively close to the wall; that is, at $y+ < 10$. The hot wire probes used for the Reynolds shear stress measurements are X - wires and are larger in effective length and slightly more susceptible to distortions or adverse influences than single wire probes. The Reynolds shear stress data from the Carlier and Stanislas experiments are plotted against the inner y+ scale in Figure 2-12 and as a function of the outer η scale in Figure 2-13. The minimum y+ values in the Reynolds shear stress data are between $y+ = 7$ and $y+ = 14$. There is however, some apparent distortion or offset in the geometric position of this Reynolds shear stress data, which can be seen when these data are compared to other data such as the DeGraaff and Eaton data. There also appears to be some offset or expansion of the Reynolds shear stress data beyond $\eta = 0.25$ when plotted on the outer scale. Although these data are available for comparison they will not be used for fitting composite expansions during this study because they appears to be offset or at least different than other data of this type.

The streamwise Reynolds stress data from the Carlier and Stanislas experiments are plotted vs. the determined y+ values in Figure 2-14 and as a function of the η outer scale in Figure 2-15. These streamwise Reynolds stress data that were taken with a small hot wire anemometer is smooth in its appearance, has a peak between y+ of 13 and 16 and has a Reynolds Number dependence at the high y+ values and a consistent behavior in the outer η range. The Carlier and Stanislas streamwise Reynolds stress data should provide useful information for fitting or evaluating a composite expansion.

2.6 Castillo and Johansson

In recent years Professor Luciano Castillo and various colleges have published several works on zero pressure gradient turbulent boundary layers. The first of these by Castillo and Johansson (2002) presented some data taken with an LDA system that has been part of the baseline data for several other studies. Other works that use and discuss these data include Castillo and Walker (2002), Seo et al. (2004), Cal et al. (2006) and the 2007 paper on "Inner and outer scaling in rough surface zero pressure gradient turbulent boundary layers" (Brzek et al. 2007). Although the most recent paper in this group (Brzek et al. 2007) is focused on the effects of rough surfaces on turbulent boundary layers it shows that the baseline smooth wall data is of high quality. This smooth wall data was provided for this research project by private communication (Castillo and Brzek 2007).

The zero pressure gradient turbulent boundary layer data provided by Professor Castillo was taken with a Laser Doppler Anemometer in the wind tunnel at Chalmers University of Technology in Gothenburg, Sweden. The measurement volume of this LDA is 58 μm long, which is similar to the DeGraaff and Eaton LDA system, and results in viscous length scales, l+, of approximately 0.81 to 4.14 depending on the Reynolds Number of the experiment. The estimated uncertainties for these measurements according to Brzek et al. (2007) is less than ± 1 percent for the averaged mean velocity and approximately ± 2 percent for the averaged Reynolds stress

components. The Reynolds Number range covered by the smooth wall baseline testing is from Re* = 682 to Re* = 1584, which is just over 2.3 to one and is much less of a range than covered by the DeGraaff and Eaton data. This Castillo and Johansson data do agree well with the results obtained by DeGraaff and Eaton and are a valuable source of data for fitting and evaluating composite expansions for Reynolds shear stress and streamwise Reynolds stress. A summary of the parameters for the 8 different Reynolds Numbers evaluated from these data is shown in Table 5. The raw experimental wall distance values are included in these data and the scaling of y+ and η as well as other parameters are calculated from the basic experimental variables.

The Reynolds shear stress, <uv>+, data from Castillo and Johansson (2002) are plotted as a function of y+ in Figure 2-16, which shows the expected behavior at both small and large y+ values. There appears to be a grouping of the Reynolds shear stress data into two levels between y+ = 7 and y+ of approximately 40 that is not consistent with Reynolds Number. One group of the data passes through the magnitude of 0.4 at a y+ very close to 11 and the other group passes through the Reynolds shear stress level of 0.4 at y+ values near 14. There is a gap between these lines on the plot (Figure 2-16) such that the data appear to be in two groups that are not based on Reynolds Number. The lowest Reynolds Number data are lowest on the graph (a high y+ at 0.4) as expected based on similar data (DeGraaff and Eaton, Spalart, etc.) but so are two of the highest Reynolds Number shear stress data lines. There are also some of the moderate to low Reynolds Number shear stress data lines higher on the graph (crossing the 0.4 magnitude

at a low y+) where we would expect the high Reynolds Number results to be located. The DeGraaff and Eaton data for example are more consistent with the low Reynolds Number results being lower on the plot (Figure 2-2) and the high Reynolds Number data appearing higher on the plot (passing through 0.4 at a lower y+ value). The DeGraaff and Eaton data that cover a much wider Reynolds Number range than the Castillo and Johansson data, passes through the Reynolds Shear stress magnitude of 0.4 between y+ = 8 and y+ = 12 in the inner region of the turbulent boundary layer. Despite this small inconsistency in the data from Castillo and Johansson, the resolution, repeatability, and apparent accuracy of these data will serve well for fitting and evaluating composite expansions of both the Reynolds shear stress and the streamwise Reynolds stress. These same Reynolds shear stress data from Castillo and Johansson are plotted as a function of the outer length scale, η, in Figure 2-17. In the outer scale plot these data display a mostly consistent and an expected trend.

The streamwise Reynolds stress from the same experiment by Castillo and Johansson is plotted as a function of y+ in Figure 2-18 and of η, in Figure 2-19. These plots of the streamwise Reynolds stress data demonstrate a high repeatability of the data with only small changes due to small changes in Re* and consistent trends with Reynolds Number. These streamwise Reynolds stress data will be shown to be very useful for fitting and evaluating turbulent boundary layer composite expansions.

Table 5. Castillo and Johansson Turbulent Boundary Layer Parameters

Re*	Ue	δ	δ*	u*	Δ_{RC}
	m/sec	m	m	m/sec	M
682	10.137	0.0240	0.00409	0.4263	0.09724
788	10.07	0.0285	0.00496	0.4147	0.1204
876	9.963	0.0324	0.00556	0.4054	0.1366
927	9.99	0.0345	0.00598	0.4032	0.1483
973	10.00	0.0364	0.00635	0.4009	0.1584
1320	19.87	0.0258	0.00446	0.7696	0.1152
1553	20.1	0.0305	0.00517	0.7650	0.1359
1584	20.06	0.0313	0.00547	0.7589	0.1445

2.7 Hutchins and Marusic

Data taken with hot wire anemometers in large scale turbulent boundary layers at the University of Minnesota have recently been reported by Hutchins and Marusic (2007). Other data similar to the Hutchins and Marusic investigations were taken at the University of Melbourne in Australia but are not shown here. The purpose of the Hutchins and Marusic data is to evaluate the large scale streamwise features in the log region of turbulent boundary layers. Various other types of data including PIV measurements were made during the same experiments. In addition to the mean velocity and the steamwise Reynolds stress, two-point velocity correlations and various spectra

of the flow were taken. However, no Reynolds shear stress data were taken during the Hutchins and Marusic testing. The Reynolds Number range covered by the Hutchins and Marusic data plotted in this work is from Re* = 1014 to Re* = 2635 and only three sets of data are considered. The parameters of free stream and friction velocity, boundary layer and displacement thickness, and the Rotta-Clauser thickness for these data are summarized in Table 6. The streamwise Reynolds stress from the Hutchins and Marusic testing are plotted as functions of y+ in Figure 2-20 and as functions of η in Figure 2-21. These data represent useful streamwise Reynolds stress data taken with hot wire anemometers with non-dimensional lengths that ranged form l+ = 14 for the lowest Reynolds Number to l+ = 45 for the highest Reynolds Number.

Table 6. Hutchins and Marusic Turbulent Boundary Layer Parameters

Re*	Ue	δ	u*	Δ_{RC}
1014	5.2	0.070	0.2217	1.64
1911	12.1	0.064	0.4686	1.65
2635	16.9	0.066	0.6190	1.80

Chapter 3 Composite Expansions

3.1 Composite Expansions for Reynolds Shear Stress on Turbulent Boundary Layers

Composite expansions are based on matching expansions that represent the asymptotic behavior of the variable being studied in the limit of a controlling parameter, Reynolds Number in this case. Composite expansions absorb and account for Reynolds Number effects in the quantities that they represent such as the Reynolds shear stress (Panton 1997). Composite expansions consist of a wall law or inner function and a wake law with the wake law made up of an outer function and a common part, per developments shown by Panton (2002 and 2005) and earlier researchers. Thus for the extensively studied Reynolds shear stress a proper composite expansion is represented as a wall law and a wake law as shown in Equation 2,

$$\frac{<uv>}{u_*^2} = g_o\left(y^+\right) + W_{uv}(Y) = g_o\left(y^+\right) + G_o(Y) - G_{cp}(Y) \quad \text{Equation 2.}$$

where $g_o(y+)$ is the wall or inner law, Wuv(Y) is the wake law, $G_o(Y)$ is the outer function and G_{cp} is the common part that is normally included with the outer function. The behavior of the inner Reynolds shear stress has been studied extensively and it has been shown through asymptotic analysis and fitting of data that the form of the inner $g_o(y+)$ function is as shown in Equation 3 (Panton 2007).

$$g_o(y+) = \frac{2}{\pi}\,\mathrm{Arctan}\left(\frac{2\,k\,y^+}{\pi}\right)\left[1 - \mathrm{Exp}\left(\frac{-y^+}{C^+}\right)\right]^2 \quad \text{Equation 3.}$$

This expression can be properly and accurately used to represent the inner behavior of wall turbulence for pipes and channels per work by Panton (1997) and can also be used to represent the inner behavior of the Reynolds shear stress in boundary layers (Panton 2005). There are two constants in this empirical expression, the von Karman constant, k, and the inner scaling constant, C+. Both of these constants are related to the law of the wall for the mean velocity as well as to the behavior of the inner portion of the Reynolds shear stress as shown by Panton (2007). Therefore it is possible to select or determine one of these constants from other studies and analyses.

There have been many evaluations of the von Karman constant, k, both over years of past research and recently using high quality modern data. The most commonly published and advocated values of the von Karman constant for turbulent wall layers range from 0.38 to 0.41, with the more recent modern values for boundary layers being on the low side of this range (Panton 2005). In order to have a consistent value of the von Karman constant that is applicable to the boundary layer data being evaluated and in agreement with other recent turbulent boundary layer work, a k = 0.39 value has been chosen for use throughout this analysis.

Having selected a von Karman constant, k = 0.39, the C+ constant in the inner Reynolds shear stress function, $g_o(y+)$, remains to be determined by fitting to data. However, to determine the best C+ constant for the inner Reynolds shear stress function, a wake or outer function and common part must be available so that the inner portion of

Reynolds shear stress data can be separated and then used to evaluate the inner function constant. It is known that the outer function for the Reynolds Shear stress in pipe and channel flows is Go(Y) = 1 - Y and that the common part is 1.0 as shown by Panton (2001). The outer Reynolds shear stress function for turbulent boundary layers is different than for pipes and channels because the velocity profile behavior at the outer edge of a boundary is different than the velocity profile at the centerline of a pipe or channel. The asymptotic behavior of the required outer function for the Reynolds shear stress is such that Go(y) should be 1.0 at Y = 0 and should approach zero at the outer edge of the boundary layer. Furthermore, the Go(y) function should satisfy Equation 1, which is derived from the momentum equations (Panton 2005). An expression for the outer Reynolds shear stress function, Go(y), can be obtained by substituting the Coles - Lewkowicz wake law into Equation 1 and integrating. The Lewkowicz corner correction to the Coles velocity wake law contains terms for Y^4, Y^3, Y^2 and a constant. In addition the Coles wake law contains the Coles wake coefficient, Π. Thus integrating the Coles -Lewkowicz wake function in Equation 1 results in the Go(y) function with terms for Y^5, Y^4, Y^3 and Y, as shown in Equation 4, that is suggested as an outer Reynolds shear stress function for turbulent boundary layers.

$$G_o(Y) = 1 + \left(\frac{1}{1+\Pi}\right)\left(\frac{8}{5}Y^5 + \left(\frac{12\Pi - 9}{4}\right)Y^4 + \left(\frac{2 - 12\Pi}{3}\right)Y^3 - Y\right) \quad \text{Equation 4}$$

The wake parameter, Π, used in this outer Reynolds shear stress function is directly related to the Coles wake coefficient used in typical boundary layer wake law equations. Equation 4 satisfies the expected asymptotic limits, as it approaches 1.0 as Y approaches

0 and approaches 0 as Y approaches 1. The G_{cp} that goes with this outer function is 1.0 as it is for pipes and channels. The acceptability of the above equation for the outer Reynolds shear stress will be demonstrated by matching data in the following analysis and by the fact that when combined with the inner function, Equation 3, it will produce a calculated Reynolds shear stress that agrees with the available high quality data.

One additional variable or in this case scale parameter that must be addressed and defined in order to be evaluated and match the plotted data is the η outer scale that is used rather than the Y scale. The outer boundary layer length scale Eta (η) is dependent on the Rotta-Clauser boundary layer dimension, Δ_{RC}, that is, $\eta = y/\Delta_{RC}$. The Rotta-Clauser thickness is determined from other boundary layer parameters as follows; $\Delta_{RC} = \delta^* Ue / \nu$. There is, of course, a relationship between the maximum of Y and of η, which is the same as the relationship between δ and Δ_{RC}. When the ratio of Δ_{RC} / δ is calculated from experimental quantities the ratio of these lengths typically varies from approximately 3.7 to 4.3 or more. In one set of experimental results available for this analysis, the different Reynolds Number cases have calculated Δ_{RC} / δ values that range form 4.05 to 4.62 from the same test apparatus. This type of variation causes a distortion in the data when plotted as a function of η. There is also a relationship between the ratio of Δ_{RC} to boundary layer thickness δ and the Coles wake coefficient, Π, as well as the von Karman coefficient that was shown by Panton (2005) to be such that Δ_{RC} / δ is approximately equal to $(1+ \Pi)/ k$. In all of the data that follows the η value was either provided by the researchers, or Δ_{RC} was provided with the data and used

to calculate the η, or the ratio of η relative to Y (the ratio Δ_{RC} / δ) was forced to be 4.0 in order to avoid distortions in the outer scale direction of the plots. In the data sets which required adjustment in of Δ_{RC} / δ ratio including the Castillo and Johansson data this relationship may have an influence on the Π parameter that is a best fit for the outer Reynolds shear stress function.

The first step in developing, and confirming a composite expansion for the Reynolds shear stress is to prepare plots of the inner portion of selected Reynolds shear stress data and compare that data to the inner function, Equation 3, to determine the best value for C+. However, in order to separate the inner part from the total Reynolds shear stress, the suggested outer function must be plotted on an outer representation of the Reynolds shear stress data and then subtracted from the total data. The resulting inner Reynolds shear stress data is then plotted as a function of y+. The first set of data to be evaluated in this manner is the DeGraaff and Eaton data. The DeGraaff and Eaton Reynolds shear stress as a function of η is plotted in Figure 3-1 where the outer Reynolds shear stress function, Equation 4, is plotted for a selected Coles wake constant of Π = 0.56. The η scale for the DeGraaff and Eaton data are calculated from the given Δ_{RC} values. The outer function magnitude and position in Figure 3-1 is largely insensitive to small changes in the Coles wake constant, Π. Values of the Coles wake constant for turbulent boundary layers have been reported to vary from 0.55 to 0.64 for recent flat plate zero pressure gradient data such that the value selected here, 0.56, is consistent with other works including Panton (1997), Osterlund (1999), Panton (2002),

Brzek (2007), and Perry and Marusic (1995). The Coles wake constant can change significantly if a pressure gradient is present in the boundary layer (Perry and Marusic 1995). The relationship presented earlier between the Rotta-Clauser thickness and the difficult to determine normal boundary layer thickness and the Coles wake coefficient, $\Delta_{RC} / \delta \sim (1+ \Pi)/ k$, along with the von Karman constant, implies a value of $\Pi = 0.56$, which is one of the reasons this value has been selected for the present work. The difference between the Reynolds shear stress data and the outer function, $G_o(\eta)$, for the outer parts of plots ($\eta > 0.05$) such as Figure 3-1 could be used to determine the best fit for Π. However, there is less sensitivity to the Coles wake constant than to the C+ parameter so that the above preferred $\Pi = 0.56$, value is selected for this analysis. The next step is to calculate the inner part of the Reynolds shear stress and to determine the best C+ value.

In order to continue the analysis, the outer function minus the common part, $G_o(\eta)-1$, is subtracted from the Reynolds shear stress (both shown in Figure 3-1) and the result is plotted as a function of y+ as shown in Figure 3-2 for the DeGraaff and Eaton data. The inner part of the Reynolds shear stress rises from zero very near the wall to 1.0 past the overlap region and well away from the wall. The inner function, g(y+), is also plotted in Figure 3-2. The difference between the g(y+) inner function and the inner part of the Reynolds shear stress data in Figure 3-2 can be used to determine the best value of C+. With the preferred value of the Coles wake constant, $\Pi = 0.56$, the best fit C+ for the DeGraaff and Eaton data is 7.61 using the data shown in Figure 3-2. If the

Coles wake constant is changed to a different but acceptable value within the normal range, that is to $\Pi = 0.64$, Figure 3-1 would appear essentially the same and the best value for C+ for the DeGraaff and Eaton data would be 7.66. It can be shown by this work that the C+ parameters for any given data set has a low sensitivity to the Coles wake constant.

The same process of plotting the outer Reynolds shear stress function, Equation 4, with the Reynolds shear stress and then taking the difference between data and $G_o(\eta)$-1 can be used to determine the inner part of the Reynolds shear stress data. The inner part of the data is then compare to the inner function from Equation 3 in order to find the best fit value for the wall law constant, C+. Using the selected von Karman coefficient, $k = 0.39$, and the preferred Coles wake coefficient, $\Pi = 0.56$, a process of minimizing the difference between the inner portion of the Reynolds shear stress data and the inner function can be used to determine the best fit value for the C+ parameter. The minimization of the difference between the inner data and the inner function is performed over the range from $y+ = 1$ to $y+ = 200$ so that the outer layer of the g(y+) data, which are all near 1.0, do not have an unnecessary influence on the wall law constant. A plot of the Reynolds shear stress data from the Spalart (1988) DNS work and the outer, $G_o(\eta)$, function is shown in Figure 3-3. Derived from Figure 3-3, the inner part of the Reynolds Shear stress data and the inner, g(y+) function are plotted in Figure 3-4. With the preferred Coles wake coefficient, $\Pi = 0.56$, the best value for C+ is 5.24 using only the two higher Reynolds Number data sets from Spalart. The lowest

Reynolds Number, Re* = 150, in the Spalart DNS work is too low to represent a turbulent boundary layer with an overlap region.

The most recent set of high resolution data with accurate near wall values is that from the Castillo and Johansson and the Reynolds shear stress data from eight of the Castillo and Johansson tests along with the outer, G_o, function are plotted in Figure 3-5. The value of the Coles wake coefficient in Figure 3-5 is $\Pi = 0.56$, although a change to $\Pi = 0.64$ does not make a marked difference and is just noticeable in the plot and in the resulting C+ value. The difference between the Reynolds Shear stress data in Figure 3-5 and the outer G_o function minus the common part is plotted in Figure 3-6 along with the inner g(y+) function. The best fit for the C+ parameter, so that g(y+) approximates the inner ($y+ < 200$) behavior for all eight of the Reynolds Number data sets in Figure 3-6, is C+ = 9.35, although this curve does not agree closely with all of the data sets. The effect of the two groupings of the <uv>+ data in the Castillo and Johansson results discussed in Chapter 2 can be seen in Figure 3-6 as well. If the Reynolds Number data sets that rise at lower y+ values, the data that are higher on the plot and reaches <uv>+ = 0.4 at a lower y+ (approximately 11) value, are fit for the best C+, then the result is very close to 7.61, which is the best value for the similar DeGraaff and Eaton data.

The results of separating the inner Reynolds shear stress data using the outer G_o function from Equation 4 and then matching the inner part of the Reynolds shear stress data to the inner, g(y+) function from Equation 3, not only determines the best values for

the Π and C+ constants but also shows that the G_o function (Equation 4) is a proper asymptotic representation of the outer behavior of the Reynolds shear stress. The plots of the Reynolds shear stress data with the outer functions for the three selected quality turbulent boundary layer data sets are shown in Figures 3-1, 3-3, and 3-5. A summary of the best fit C+ values for the selected DeGraaff and Eaton, Spalart, and Castillo and Johansson data are shown in Table 7, where values of C+ are given for Coles wake coefficient of the preferred value of Π = 0.56 and for the other acceptable value of Π = 0.64 to show the trends in C+. The numerical average of the C+ coefficient shown in Table 7 is 7.4 for Π = 0.56 and 7.56 for Π = 0.64. However, since the Spalart data is known to be at low Reynolds Numbers and the Castillo and Johansson data has the divided inner Reynolds shear stress behavior, the selected wall law constant C+ value for this analysis will be that of the DeGraaff and Eaton results, that is 7.61 with Π = 0.56. These values of C+ are all within the range of values that are typical for zero pressure gradient turbulent boundary layers as shown in Panton (2005).

Table 7. Data Fits for Reynolds Shear Stress using Outer Go and Inner g Functions

Data Set	Coles Wake Coeff. Π	Inner <uv>+ Coeff. C+
DeGraaff and Eaton	0.56	7.61
DeGraaff and Eaton	0.64	7.66
Spalart	0.56	5.24
Spalart	0.64	5.54
Castillo and Johansson	0.56	9.35
Castillo and Johansson	0.64	9.48

The fact that the outer G_o function in Equation 4 agrees with this data on the outer scaling of η from 0.05 to 0.25 and that the resulting difference agrees with the known inner g(y+) function (Equation 3) indicates that Equation 4 is a proper representation for the outer Reynolds shear stress behavior. For the remainder of this analysis, the Reynolds shear stress will be represented by the sum of the inner g(y+) function and the outer $G_o(\eta)$ function less the common part, $G_{cp} = 1.0$ with the parameters of $k = 0.39$, $\Pi = 0.56$, and $C+ = 7.61$.

In order to confirm this representation of the Reynolds shear stress, the sum of the inner g(y+) function, the outer $G_o(\eta)$ function, and the common part with the parameters of $k = 0.39$, $\Pi = 0.56$, and $C+ = 7.6$ are plotted and compared to some of the select data. Figure 3-7 is a comparison of the constructed Reynolds shear stress to the

DeGraaff and Eaton data. These representations include the effects of the Reynolds Number because of the scaling between the inner y+ and the outer η. The same comparison for the highest Spalart Reynolds Number curve using the selected average best overall coefficients is show in Figure 3-8, which indicates that agreement to the generalized Reynolds shear stress prediction is good at low and high y+ values, although somewhat low compared to the Spalart data in the overlap range. A plot of the Castillo and Johansson Reynolds shear stress data with four different calculated results between the lowest and the highest Reynolds Numbers is shown in Figure 3-9. The apparent agreement to the Castillo and Johansson data is generally good particularly considering that the best fit C+ value is much higher (9.35) than the accepted average values of 7.61. The three plots in Figures 3-7 through 3-9 show that the chosen mathematical representation of the Reynolds shear stress is a consistent and reasonable prediction as a function of Reynolds Number. This composite expansion for the turbulent boundary layer Reynolds shear stress can be used for predicting levels in other zero pressure gradient turbulent boundary layers.

3.2 Separation of Active and Inactive Streamwise Reynolds Stresses

The goal of this research is to develop a composite expansion for the streamwise Reynolds stress in turbulent boundary layers so that predictions can be made for boundary layers where there are no data. There is a Reynolds Number dependence in the available streamwise Reynolds stress data that does not scale with the typical inner or outer parameters which has made it difficult to develop a proper composite expansion

for this variable (Marusic and Kunkel 2003). The most likely reason that the streamwise Reynolds stress is difficult to scale is that it is influenced by both active and inactive motions as defined by Townsend (1976). Therefore, an approach that can separate the inactive and active motions would be of benefit and should allow development of a composite expansion for the parts and then the complete streamwise Reynolds stress.

The approach of separating the streamwise Reynolds stress into active and inactive parts was suggested by the work of Townsend (1976) and others who have followed that line of reasoning (Perry et. all 1986, Perry and Li 1990, Marusic et. al. 1997, and Marusic and Kunkel 2003) and was developed mathematically and specifically for channel flows by Panton (2007). If the velocity is taken as the sum of an active part and an inactive part, $u = u_A + uI$, it can be shown that Equation 5 follows.

$$\langle uu \rangle^+ = \langle uIuI \rangle^+ - 2\langle u_A \rangle^{+2} + \langle u_A u_A \rangle^+ \qquad \text{Equation 5}$$

In order to develop a matched asymptotic expansion for this streamwise Reynolds stress relationship it is necessary that each term in the equation be scaled so as to be of order 1 in the limit as $Re^* \rightarrow \infty$. Based on the assumption that the active part of the motion scales the same as the Reynolds shear stress on u*, the following relationships can be developed.

- <uu># = <uu>+ (u*/Ue), where # denotes an order one scaling,
- <uIuI># = <uIuI>+ (u*/Ue), and
- (-2< u_A>+^2 + < u_A u_A>+) # = (-2< u_A>+^2 +< u_A u_A>+) (u*/Ue).

Panton (2007) also showed that the active terms behave like the Reynolds shear stress and should be able to be replaced by <uv>+. Furthermore, this analysis and more general analyses by Panton suggest the (u*/Ue) term as a gauge function for a Poincare expansion for the streamwise Reynolds stress. One of the assumptions in the analysis that leads to an expression for the inactive streamwise Reynolds stress is based on the definition of the active motion as that part of the turbulence that contributes to the Reynolds shear stress and is that the active part of the streamwise motion scales in the same manner as the Reynolds shear stress. Substitution of the above expression and assumptions into Equation 5 yields Equation 6 for the inactive part of the streamwise Reynolds stress.

$$\langle uIuI \rangle \# = \langle uu \rangle^{+} \frac{u^{*}}{Ue} + \langle uv \rangle^{+} \frac{u^{*}}{Ue} \qquad \text{Equation 6}$$

The first step in developing or evaluating a composite expansion for the streamwise Reynolds stress is to separate the inactive part by applying Equation 6 to the data. For the following analysis the <uv>+ term in Equation 6 will be calculated in accordance with the composite expansion for the Reynolds shear stress developed in section 3.1 using Equations 3 and 4, the Gcp common part, and the parameters k = 0.39, $\Pi = 0.56$, and C+ = 7.61. The u*/ Ue ratio for each of the data sets will also be used and the data will be plotted as a function of the inner y+ scaling and the outer η scaling.

The inactive streamwise Reynolds stress from the DeGraaff and Eaton data is shown on an inner y+ scale in Figure 3-10 and on an outer η scale in Figure 3-11. It can be seen in Figure 3-10 that there is still a Reynolds Number dependence of the data at

large y+ values but that the dependence at the peak Streamwise Reynolds stress at y+ near 15 has been reduced. There is a greatly reduced Reynolds Number dependence of the outer part of the inactive streamwise Reynolds stress shown in Figure 3-11 compared to the out part of the streamwise Reynolds stress from the same DeGraaff and Eaton data shown in Figure 2-5. Figure 3-11 shows not only a reduced Reynolds Number dependence in the outer region of the data on the η scale but also a function that fits the outer behavior. This outer equation for the inactive streamwise Reynolds stress will be discussed in the next section of this analysis.

The inactive streamwise Reynolds stress can also be separated form the Spalart DNS data in the same manner as used for the DeGraaff and Eaton turbulent boundary layer data by using Equation 6 with the calculated <uv>+ values (plotted in Figure 3-8) and the (u*/Ue) ratio. The inactive parts of the streamwise Reynolds stress extracted from the Spalart results are shown in Figure 3-12 where the reduction in Reynolds Number dependence near the peak in <uIuI># compared to the effects of Reynolds Number on the peaks in <uu>+ data in Figure 2-7 can be observed. The same Spalart inactive streamwise Reynolds stress results are plotted as function of η in Figure 3-13. An outer inactive streamwise Reynolds stress equation is shown in Figure 3-13, which indicates a fairly good agreement to the two higher Reynolds Number inactive streamwise Reynolds stress curves. The source and use of this outer inactive streamwise Reynolds stress equation will be discussed in the next section of this analysis.

The same process for separating out the inactive part of the streamwise Reynolds stress using Equation 6 and calculated values of the Reynolds shear stress, based on Equations 3 and 4, is followed for the Osterlund data. In this process the calculated Reynolds shear stress is used to represent the active part of the streamwise Reynolds stress. According to Townsend definitions the active part of the streamwise Reynolds stress contributes to the Reynolds shear stress and is reasonable expected to scale in the same manner. The inactive streamwise Reynolds stress from data provided by Osterlund at seven (7) different Reynolds Numbers is plotted as a function of y+ in Figure 3-14, where there are no data for y+ less than 11 and not much for y+ less than 20. There is a clear Reynolds Number dependence for the data at y+ greater than 100. These same data plotted as a function of η are shown in Figure 3-15, where a well behaved outer trend for all the different Reynolds Numbers is indicated.

As discussed in Chapter 2, the Osterlund data are limited in the low y+ range and do not contain sufficient data approaching the wall to represent the peak in streamwise Reynolds stress. As a result of not having sufficient data to fit composite expansion equations or coefficients to the inner or overlap portion of the inactive streamwise stress from the Osterlund experiments, no outer inactive equation is shown with the inactive streamwise Reynolds stress in Figure 3-15.

The process of separating the inactive streamwise Reynolds stress from the total streamwise Reynolds stress is repeated for the Carlier and Stanislas data. The results of

the streamwise Reynolds stress as a function of the inner y+ scale are shown in Figure 3-16. The Carlier and Stanislas inactive streamwise Reynolds stress shows an extremely good collapse of the data for the region of y+< 100 for all of the Reynolds Numbers tested. The same Carlier and Stanislas inactive streamwise Reynolds stress data are shown as a function of the outer scale η in Figure 3-17. A reasonable good collapse of this data in the outer region is shown and an outer inactive streamwise Reynolds stress equation to be discussed in the next section of this chapter is also shown in Figure 3-17.

The extensive and high resolution zero pressure gradient smooth wall boundary layer data from Castillo and Johansson can also have the inactive portion of the streamwise Reynolds stress separated or isolated in the same manner used for the other data. The Reynolds shear stress values are calculated using Equation 3 and 4, the common part, and the accepted constants of k = 0.39, Π = 0.56, and C+ = 7.61. Both the streamwise Reynolds stress and the Reynolds shear stress are then scaled with the gauge function u*/Ue and the difference is taken per Equation 6 to yield the inactive streamwise Reynolds stress. The result for the Castillo and Johansson data is shown as a function of y+ in Figure 3-18 and as a function of the outer scale η in Figure 3-19. The collapse of the inner (y+ < approx. 50) inactive streamwise Reynolds stress data is clearly indicated in Figure 3-17. The collapse of the Reynolds Number dependence of the outer Castillo and Johansson inactive Reynolds stress data is also shown in Figure 3-19 where an outer equation that fits this trend is shown. The development and use of

this outer inactive streamwise Reynolds stress equation will be presented in the next section of this chapter.

The Hutchins and Marusic data, although limited in Reynolds Number range and in wall resolution by hot wire non-dimensional lengths, can have the inactive part of the streamwise Reynolds stress separated from the rest of the streamwise Reynolds stress data. The process is the same as for the other experimental data evaluated in this study and although Hutchins and Marusic did not take any shear stress data the Reynolds shear stress can be calculated from Equations 3 and 4 in the same manner as for the other data. The inactive streamwise Reynolds stress from the Hutchins and Marusic data as a function of y+ is shown in Figure 3-20. The inactive streamwise Reynolds stress in Figure 3-20 does not appear to be Reynolds Number independent at the peak amplitude near y+ = 15, which is in contrast to most of the other data sets. One explanation for this result may be a consequence of the hot wire lengths and the fact that the basic streamwise Reynolds stress data in Figure 2-20 appear to have the same peak amplitude for all of the Reynolds Numbers tested although this is not the normal trend. The same Hutchins and Marusic streamwise Reynolds stress data are plotted as a function of the outer η scale in Figure 3-21. The collapse of the outer inactive streamwise Reynolds stress data from the different Reynolds Numbers appears to be clear particularly if compared to the total streamwise Reynolds stress data in Figure 2-21. An outer streamwise Reynolds stress equation is not shown with this data.

3.3 Composite Expansion for the Inactive Streamwise Reynolds Stress

It was recognized by Panton (2007) that the inactive part of streamwise turbulent boundary layer motions will scale differently than the active part of this motion, which scale as the Reynolds shear stress. Thus with the inactive part of the streamwise Reynolds stress separated from the rest of the streamwise Reynolds stress an attempt can be made to develop a composite expansion for the inactive part separately. The composite expansion for the inactive streamwise Reynolds stress will take the form shown in Equation 7 that combines an inner and outer parts and a common part.

$$\langle uIuI\rangle\# = \langle uIuI\rangle\#\,\mathrm{Inner}\left(y^{+}\right) + \langle uIuI\rangle\#\,\mathrm{Outer}(\eta) - C_{CP} \qquad \text{Equation 7}$$

The outer behavior of the inactive streamwise Reynolds stress from the four relatively consistent and high resolution data sets of DeGraaff and Eaton, Spalart, Calier and Stanislas, and Castillo and Johansson have been plotted in Figures 3-11, 3-13, 3-17, and 3-19 respectively. These four sets of data are used to evaluate the equations that constitute a composite expansion for the inactive streamwise Reynolds stress in this analysis.

Using asymptotic analysis and channel flow data, Panton suggested and used a relationship of the form of Equation 8 to match the outer part of the inactive streamwise Reynolds stress in geometries with centerline velocities as follows;

$$< uIuI >\#\,\mathrm{Outer} = (C_{cp} - C_{min}) * (1 - 4 * \eta)^{1.5} + C_{min} \qquad \text{Equation 8}$$

where C_{cp} is the common part of the inactive streamwise Reynolds stress and C_{min} is the minimum or centerline magnitude for channels (or pipes). The 4 η term is the full boundary layer thickness and is the same as Y for a well behaved boundary layer. The common part of the inactive streamwise Reynolds stress is the value that is approached at η= 0 without considering the details of the inner behavior and at the same time the value that the inner part approaches at large y+ values. The common part, $C_{cp,}$ of the inactive streamwise Reynolds stress can be judged from plots of the data such as the four referenced above (Figures 3-11, 3-13, 3-17, and 3-19) and as will be shown can be confirmed by later evaluation of the inner part of the streamwise Reynolds stress. The centerline magnitude for a channel or a pipe flow is different than for a boundary layer where the velocity, including the inactive part of the velocity, is expected to approach a minimum value. The minimum value, C_{min}, for the streamwise Reynolds stress can be estimated from the same plots of data referred to above and may be associated with the free stream turbulence and should be small for a boundary layer.

Equation 8 is not satisfactory for turbulent boundary layer data as evaluated in this analysis and is found to be always low in the region between η of approximately 0.05 and 0.20. Because the velocity profile and gradients are different in a boundary layer than in a channel or pipe flow it was determined that an additional term is required in order for Equation 8 to match the outer inactive streamwise Reynolds stress. A modification of Equation 8 was considered and the form in Equation 9 has been used in the remainder of this analysis of zero pressure gradient turbulent boundary layers.

$$< uIuI >\#Outer = (C_{cp} - C_{min}) * (1 - 4 * \eta)^{1.5} + A_{Out}\ Exp(- C_{Out} (4 * \eta - 0.5)^2) + C_{min}$$

Equation 9

As indicated in the above discussion, C_{cp} and C_{min} are values that can be estimated from the data and confirmed by agreement with the selected levels or trends in the data such that they are not arbitrary fitting coefficients. The two parameters, A_{Out} and C_{Out} are coefficients that can be used to fit Equation 9, the outer streamwise Reynolds stress equation, to a selected data set for which C_{cp} and C_{min} have been correctly selected. The A_{Out} coefficient influences the magnitude of the adjustment in the central portion of Equation 9 and C_{Out} affects the width of that influence between small values of η and larger values of η.

The inactive streamwise Reynolds stress from the DeGraaff and Eaton data is shown in the previously presented Figure 3-11 where Equation 9 has been fit to that data. The agreement is reasonably good and the values used are C_{cp} = 0.235, C_{min} = 0.019, A_{Out} = 0.018 and C_{Out} = 35. It will be shown in the evaluation of the inner equation for the inactive streamwise Reynolds stress that this 0.235 value for the common part is a good representation of these data. The sensitivity of the best fit of the outer equation to the data is such that the C_{Out} width coefficient can be changed by 10% with only a small change in the difference between the data and the equation. On the other hand, a change of just 5% in the A_{Out} amplitude coefficient causes a significant difference in fit of the equation to the data. In general, each of the variables, $C_{min,}$ A_{Out},

and C_{Out} can be adjusted by small amounts while the agreement of the outer inactive streamwise Reynolds stress equation to the data can be minimized if one of the other values is increased or decreased a small amount to compensate.

The inactive streamwise Reynolds stress from the Spalart DNS results is shown in Figure 3-13 as identified in the above discussion. This DNS data is slightly different than the other data sets primarily because it is a low Reynolds Number result but a reasonably good agreement is achieved using slightly different coefficients. Only the higher two Reynolds Numbers are considered in fitting of the outer inactive streamwise Reynolds stress equation. The Carlier and Stanislas data processed to separate the inactive streamwise Reynolds stress is shown in Figure 3-17 where Equation 9, is also plotted and the coefficients are adjusted to minimize the difference between the equation and the data over the range of $\eta = 0.05$ and 0.25. Equation 9 and the inactive part of the streamwise Reynolds stress data provided by Castillo and Johansson are shown in Figure 3-19. The agreement of the outer inactive streamwise Reynolds stress equation to the Castillo and Johansson data in Figure 3-19 appears to be a close representation. A summary of the coefficients used to fit Equation 9 to the inactive streamwise Reynolds stress data including the common part, the minimum or boundary layer edge values, the magnitude adjustment coefficient A_{Out} and the width or extent adjustment coefficient C_{Out}, are shown in Table 8.

Table 8. Coefficients for the Outer Inactive Streamwise Reynolds Stress Equation

Data	C_{cp}	C_{min}	A_{Out}	C_{Out}
DeGraaff/Eaton	0.235	0.019	0.018	35
Spalart	0.265	0.002	0.022	16
Carlier/Stanislas	0.235	0.008	0.010	33
Castillo/Johansson	0.230	0.010	0.015	32
Selected	0.235	0.010	0.017	32

An inner equation is needed for the inactive streamwise Reynolds stress if a complete composite expansion is to be developed. The inner behavior of the inactive streamwise Reynolds stress can be displayed by subtracting the outer inactive streamwise Reynolds stress equation from the inactive data, adding the common part, and plotting the result as a function of the inner scale y+ variable. Starting with the DeGraaff and Eaton data in Figure 3-11, the outer equation, Equation 9 using the best fit DeGraaff and Eaton coefficient from Table 8 was subtracted from the data, the common part was added, and the results are shown in Figure 3-22. Figure 3-22 shows the inner inactive streamwise Reynolds stress data for 5 different DeGraaff and Eaton Reynolds Number tests and shows an inner inactive streamwise Reynolds stress equation.

The inner inactive streamwise Reynolds stress has a somewhat complex behavior on the inner scale including an approximately exponential increase approaching a peak value, a peak at y+ of approximately 15, a decreasing value from the peak to y+ of

approximately 100, and then a level magnitude at a value that is the common part of the asymptotic limit between the inner and outer expansions. In order to fit this complex behavior and have the correct limits as y+ approaches 0 and also large values an equation with several terms, at least some of which have exponential trends, is required. In his similar work with channel flow data Panton (2007) approximated the inner inactive streamwise Reynolds stress behavior with an equation with two exponential terms. A different equation has been selected for turbulent boundary layers, however, it is an equation with two exponential terms, one for the increasing trend and one for the decreasing trend, and three coefficients to adjust locations and magnitudes as required to match the data. The selected inner inactive streamwise Reynolds stress equation approaches zero from above as y+ approaches zero and has the correct order (1) for both terms. The proposed equation is shown as Equation 10;

$$< \text{uIuI} >\#\,\text{Inner} = \text{InCo}\left[1 - \text{Exp}\left(-\frac{y^+}{\text{InC1}}\right)\right]^2 - \left(\text{InCo} - C_{Cp}\right)\left[1 - \text{Exp}\left(-\frac{y^+}{\text{InC2}}\right)\right]^2$$

Equation 10

where InCo, InC1, and InC2 are coefficients for fitting this inner equation to the data. The coefficient of the first exponential term, InC1, determines where in terms of y+ the increase in the inner inactive streamwise Reynolds stress occurs and InC2 determines where in terms of y+ the decrease occurs and thus the y+ location of the peak. The amplitude coefficient, InCo, along with the common part, Ccp, affects the amplitude of the resulting inner inactive streamwise Reynolds stress function. Equation 10 is used to fit, that is minimize the difference between, the data in Figure 3-22 and the function, for

the inner behavior of the inactive streamwise Reynolds stress and the result is the red curve in Figure 3-22. The resulting best fit coefficients for the DeGraaff and Eaton data are InCo = 0.55, InC1 = 5.6, InC2 = 14 with the same common part as shown in Table 8.

The inner inactive streamwise Reynolds stress data from the Spalart DNS results are obtained by subtracting the outer equation from the outer inactive streamwise Reynolds stress data in Figure 3-13 and adding the common part with the resulting <uIuI>#Inner data shown in Figure 3-23 as a function of y+. The inner inactive streamwise Reynolds stress function, Equation 10, has been fit to the Spalart data and is shown as the red curve in Figure 3-23. The common part for the Spalart data is somewhat higher than for the other data sets evaluated but the inner plot in Figure 3-23 is able to confirm this. If a lower common part value were assumed the inner inactive equation line would be below the data for y+ values greater than 100. When the coefficients are properly selected such that Equation 10 fits the inner inactive streamwise Reynolds stress then the peak appears to occur at the correct location as well and the correct magnitude.

The process of subtracting the outer inactive streamwise Reynolds stress function, Equation 9, adding the common part, and correctly fitting the inactive streamwise data to produce the inner inactive streamwise Reynolds stress function is repeated for the Carlier and Stanislas data to produce the result in Figure 3-24. The inner inactive streamwise Reynolds stress equation is also shown in Figure 3-24 as the

red line which indicates a good fit of the proposed inner expansion function, Equation 10, to the Carlier and Stanislas data. This analysis of the inactive streamwise Reynolds stress data to determine the inner part from the separated inactive data using the outer equation is repeated for the data from Castillo and Johansson and the results are shown in Figure 3-25. Equation 10 is then fit to this inner inactive streamwise Reynolds stress data so that an inner equation for the composite expansion can be demonstrated and confirmed. Figure 3-25 shows that the selected Equation 10 function can be reasonably fit to this very recent modern data set.

The best fit coefficient for each of the four data set which are used for evaluation of the inactive streamwise Reynolds stress are shown in Table 9. These coefficients include a repeat of the common part, Ccp, the amplitude coefficient, InCo, the exponential rise coefficient, InC1, and the exponential drop coefficient, InC2. The common part is the same as shown in Table 8 and is confirmed by the high y+ end of the curves in Figures 3-22, 3-23, 3-24, and 3-25. The best fit coefficients for each of the 4 evaluated data sets minimize the difference between the Equation 10 function and the inner inactive streamwise Reynolds stress data over the entire y+ range. The choice of coefficients for fitting the inner part of the inactive streamwise Reynolds stress are not extremely sensitive. For example a choice of InCo = 0.54 with InC1 = 5.5 produces nearly the same degree of agreement as the best combination of InCo = 0.54 with InC1 = 5.6 for the DeGraaff and Eaton data. However, for this example a change in InC2 from

14 to 15 or a change in only one of the other coefficients without a corresponding adjustment in the others will result in a disagreement in the fit that is evident.

Table 9 also shows the selected values for each of these coefficients that can be used to create a generalized composite expansion representing the inactive streamwise Reynolds stress of the turbulent boundary layer.

Table 9. Coefficients for the Inner Inactive Steamwise Reynolds Stress Equation

Data	C_{cp}	InCo	InC1	InC2
DeGraaff/Eaton	0.235	0.55	5.6	14
Spalart	0.265	0.54	5.2	16
Carlier/Stanislas	0.235	0.54	5.2	14
Castillo/Johansson	0.230	0.53	5.6	15.5
Selected	0.235	0.54	5.4	15

Chapter 4 Results and Predictions

4.1 Reassembly of the Composite Expansion for Inactive Streamwise Reynolds Stress

With Equations 9 and 10 for the outer and inner parts of the inactive streamwise Reynolds stress, the selected coefficients for Tables 8 and 9, and the common part the complete inactive streamwise Reynolds stress can be assembled for any identified Reynolds Number. The approach to representing the inactive streamwise Reynolds stress with the composite expansion made-up of Equations 9 and 10 minus the common part is to assign a range of y+ values and calculate the inner inactive streamwise Reynolds stress for these y+ values from Equation 10 and the selected coefficients in Table 9. Then with the assigned Reynolds Number, corresponding outer scale, η, values can be calculated and the outer inactive streamwise Reynolds stress can be calculated from Equation 9 and the selected coefficients in Table 8. The inactive streamwise Reynolds stress is then the sum of the inner part and the outer part minus the common part. Notice that the common part here is the inactive streamwise common part and is not the same as the common part in the velocity or the Reynolds shear stress composite expansions.

As an example of predicting the inactive streamwise Reynolds stress some of the data from which the composite expansion was developed will be compared to the predictions using the selected coefficients. An inactive streamwise Reynolds stress plot of the DeGraaff and Eaton data are shown in Figure 4-1 where predictions for three of

the five DeGraaff and Eaton Reynolds Numbers including Re*=539, 1692, and 10030 are presented. The predictions of <uIuI># are abbreviated as "InAc" on the plots. Both the trends and the magnitude show good agreement to the data for the inactive streamwise Reynolds stress. At the very lowest y+ values the predicted <uIuI># values are slightly above the data. The same inactive streamwise Reynolds stress prediction are shown in comparison to the DeGraaff and Eaton data plotted as a function of the outer scale, η, in Figure 4-2. The agreement is also good in this plot except that the predictions using the selected coefficients do not approach the boundary layer edge in the same manner as the data in the region of $\eta = 0.20$. This may be because the data has widely spaced points in this area. However, the DeGraaff and Eaton inactive streamwise Reynolds stress data is higher near $\eta = 0.2$ than the other reference data. Equation 9 does fit most of the available data properly in the central area of the outer scale.

As a demonstration of predicting the inactive streamwise Reynolds stress the above process is accomplished for two of the Reynolds Numbers for which there is data from Hutchins and Marusic (2007), which are shown in Figure 3-20 and 3-21. The Hutchins and Marusic data was not used to develop the composite expansions or coefficients in Tables 8 and 9. The inactive streamwise Reynolds stress was calculated for the highest and lowest Hutchins and Marusic Reynolds Numbers, 1014 and 2635, with the selected coefficients from Tables 8 and 9. The results are shown on Figure 4-3, which indicates that although there is agreement in shape and trends of the curves and

location of the peak that the magnitude of the predicted inactive streamwise Reynolds stress is larger than measured by Hutchins and Marusic. A closer look at the inner and outer components of the Hutchins and Marusic data indicates that the common part of the inactive streamwise Reynolds stress in their data is lower than most of the other data evaluated above. An adjustment in the calculation for the common part of the Hutchins and Marusic data being 0.21 rather than 0.235 with no other changes in coefficient produces the result shown in Figure 4-4. With an adjusted common part that agrees with specific Hutchins and Marusic data the agreement of the calculated inactive streamwise Reynolds stress is an acceptable representation. The reason that the Hutchins and Marusic data has a different common part for the inactive streamwise Reynolds stress is not known but may have to do with the hot wire sizes used for the testing or with some other characteristic of their boundary layer flow.

Another example of the application of the inactive streamwise Reynolds stress composite expansion with the selected coefficients is shown in Figure 4-5 where the calculated or predicted values are compared to the data from Osterlund (1999). It was recognized at the beginning of this analysis that there are limitations in the Osterlund data in terms of y+ range and resolution based on the hot wire anemometer measurements. Although the agreement to the data in detail in Figure 4-5 is not good, the agreement in overall trends is visible and it could be considered that the predicted inactive streamwise Reynolds stress represents what would be expected from the data. It should be noted that the peak amplitude in almost all of the inactive streamwise

Reynolds stress is approximately 0.35, while the apparent amplitude in the Osterlund data is significantly lower than that expected value. A lower peak in the streamwise Reynolds stresses is a typical result for data taken with all but the smallest hot wire anemometers. The composite expansion for the inactive streamwise Reynolds stress may provide a means of evaluating turbulent boundary layer data. A plot of the same inactive streamwise Reynolds stress data on an outer scale is shown in Figure 4-6. There is generally good agreement to the inactive Osterlund data in the outer region.

Predictions of inactive streamwise Reynolds stress do agree with the other reference data such as the Carlier and Stanislas data and the Castillo and Johansson data. The Spalart data are known to have a different, somewhat higher common part of the inactive streamwise Reynolds stress such that it would be slightly off-set from a prediction with the selected universal coefficients. The composite expansion presented in this section can be used to produce an entire Reynolds Number range of expected values for the inactive streamwise Reynolds stress.

4.2 Composite Expansions for the Streamwise Reynolds Stress

In order to implement the composite expansion for streamwise Reynolds stress, the predicted Reynolds shear stress (section 3.1 above) must be added to the inactive streamwise Reynolds stress (section 3.3) and the gauge function, the ratio of u*/Ue, must be used to amplify the magnitude of the inactive streamwise Reynolds stress. The

equation for combining the inactive streamwise Reynolds stress with the calculated Reynolds shear stress to predict the streamwise Reynolds stress is given as Equation 11.

$$\langle uu \rangle^{+} = \frac{\langle uIuI \rangle^{\#}}{u^{*}/Ue} - \langle uv \rangle^{+} \qquad \text{Equation 11}$$

With the inactive streamwise Reynolds stress calculated for three of the DeGraaff and Eaton Reynolds Numbers and the Reynolds shear stress for DeGraaff and Eaton shown in Figure 3-7, the full streamwise Reynolds stress can be predicted. The active and inactive parts are combined using the gauge function as indicated in Equation 11 and the results are plotted as a function of y+ in Figure 4-7. The results of the composite expansion predictions are shown as "CmpEx" on the plots. The shape of the streamwise Reynolds stress curves, the trends in the results, and the magnitudes agreement are good and within the experimental uncertainty of the data in most areas of Figure 4-7. The low y+ increase in the streamwise Reynolds stress is one area were the prediction and data do not entirely agree. The predicted streamwise Reynolds stress is also plotted in comparison to the DeGraaff and Eaton data on an outer, η scale as shown in Figure 4-8. An important result is shown in Figure 4-8 where there is a predicted Reynolds Number dependence in the outer portion of the streamwise Reynolds stress that is in general agreement with the data. Only the DeGraaff and Eaton data with its large Reynolds Number range shows a clear separation of streamwise Reynolds stress data based on Reynolds Number on the outer scale as η decreases from 0.2 towards the

wall. From the DeGraaff and Eaton experiment the higher Reynolds Numbers have larger <uu>+ values on the outer scale throughout most of the boundary layer. The predictions of the streamwise Reynolds stress using the composite expansion suggested in this work shows a separation in the streamwise Reynolds stress starting near $\eta = 0.2$ and increasing as η is reduced with the higher Reynolds Numbers having higher levels in Figure 4-8.

Predictions of the streamwise Reynolds stress for a data set that was not used to develop the composite expansion is shown for the Hutchins and Marusic data in which the inactive results shown in Figure 4-4 are converted from inactive streamwise Reynolds stress to streamwise Reynolds stress as shown in Figure 4-9. This data does include the adjusted common part of the inactive streamwise Reynolds stress but uses the general composite expansion for the Reynolds shear stress and the accepted constants of $k = 0.39$, $\Pi = 0.56$, and $C+ = 7.61$. The experimental values for the u*/Ue ratio from the data are used in this case. The results of the calculated streamwise Reynolds stress compared to the Hutchins and Marusic data on an inner y+ scale are shown in Figure 4-9. The agreement of this prediction to the Hutchins and Marusic data is good for $y+ > 100$ but shows a different trend than the data near the peak in the streamwise Reynolds stress and at low y+ values. Most of the data examined for this analysis have increasing peak amplitudes in the streamwise Reynolds stress as Reynolds Number increases similar to that shown by the predictions. By comparison to other data and the predictions, the lack of a Reynolds Number dependence in the peak amplitude of

the streamwise Reynolds stress in the Hutchins and Marusic data appears to be a weakness in the data.

The same predictions for the Hutchins and Marusic streamwise Reynolds stress are plotted in comparison to the data on an outer, η, scale in Figure 4-10. The agreement to the different <uu>+ levels for the highest and lowest Reynolds Numbers is clearly acceptable. In this case, the composite expansion confirms the trends in the outer behavior of the streamwise Reynolds stress data.

Calculations were also made for the streamwise Reynolds stress of three of the Reynolds Numbers within the range of the Osterlund data. The Osterlund data was not used to develop the composite expansion. Figure 4-11 shows the predicted streamwise Reynolds stress for three of the seven Osterlund Reynolds Numbers along with the data as a function of y+. There is only a general agreement in this plot as the amplitude of the data for $y+ < 100$ is apparently affected by the hot wire measurement technique and there also appears to be an off-set in the data on the y+ scale. The same predictions and data are plotted as a function of η in Figure 4-12, where the agreement on the outer scale is much better and the Reynolds Number trends in the data for $\eta < 0.2$ are in agreement with the data and the composite expansion.

To show a more general prediction of the streamwise Reynolds stress, expected values are calculated for a number of cases from $Re^* = 500$ to 100,000 using the

suggested coefficients in Tables 8 and 9 with the inactive streamwise Reynolds stress composite expansion consisting of Equations 9, 10, the common part, and Equation 11 plus the Reynolds shear stress composite expansion consisting of Equations 2, 3, and 4 with the selected constant and its common part. The calculated inactive streamwise Reynolds stress and Reynolds shear stress are assembled in accordance with Equation 11 and the one additional parameter that is needed is the ratio u*/Ue as a function of the Reynolds Number. The gauge function ratio, u*/Ue is expected to be a function of Reynolds Number for turbulent boundary layers and to approach the limit of zero as Reynolds Number approaches infinity. Over 30 experimental values of u*/Ue for the different Reynolds Numbers are evaluated as part of this analysis. The high Reynolds Number data from Hutchins and Marusic (2007) that were taken in the experimental facilities in Melbourne but were not available for this composite expansion development were used for this u*/Ue vs. Re* correlation. The correlation equation to this data shows that the relationship u*/Ue = 0.06462 - 0.00350 * Ln (Re*) can be used to estimate the u*/Ue ratio with reasonable accuracy (± 5 % or better) for a wide range of Reynolds Numbers. A plot of the predicted streamwise Reynolds stress from the composite expansion developed here is shown in Figure 4-13 for the range of Re* = 500 to Re* = 100,000.

Published trends in the magnitude of the streamwise Reynolds stress include a plot of data by Nickels et al. (2007) in their Figure 4 for the level of <uu>+ at y+ = 300 as a function of Reynolds Number. The Nickels line that fits the data they presented is

repeated on Figure 4-14 and the values for streamwise Reynolds stress at y+ = 300 taken from Figure 4-13 are also plotted in Figure 4-14. The general magnitude of the streamwise Reynolds stress as a function of Reynolds Number presented here is close to that suggested by Nickels et al.. A summation of the amplitude of the peak in the streamwise Reynolds stress is provided by Panton (2007) in Figure 7 of his paper where a line is fit through the data that includes channel, pipe, and boundary layer flows. The line representing the peak amplitude of the streamwise Reynolds stress from the Panton (2007) work in repeated as the upper heavy line in Figure 4-14. Values taken from Figure 4-13 for the amplitude of the predicted peak as a function of Reynolds Number are also shown in Figure 4-14. The agreement of the peak amplitude predicted from the composite expansion in this analysis and the trend of the data found by Panton (2007) is extremely good and indicates that the composite expansion developed in this work provides a reasonable estimation of the streamwise Reynolds stress that agrees well with the limited data that is available. The equations and coefficients identified in this work allow the magnitude and trends in the streamwise Reynolds stress and also the Reynolds shear stress for turbulent flat plate boundary layers to be predicted with reasonable accuracy.

Chapter 5 Conclusions

In this study turbulent boundary layer data from six sources are scaled, plotted, and quantitatively evaluated. Composite expansions for the Reynolds shear stress, <uv>+, and the streamwise Reynolds stress, <uu>+, are developed. Active and inactive motions in the streamwise Reynolds stress are separated; and a composite expansion that accurately represents the streamwise Reynolds stress in turbulent boundary layers is developed and demonstrated.

Turbulent Reynolds stress data from 2 LDA experiments, one DNS calculation, and three sets of hot wire anemometer based measurements are plotted, evaluated, and compared. Although some of this data has limitations in terms of near wall resolution, Reynolds Number range, and hot wire sensitivity to small eddy distortions, all of this information is useful for composite expansion development or comparison.

An outer layer Reynolds shear stress equation that meets the requirements for matched asymptotic expansions and fits the shape of the outer Reynolds shear stress is presented as Equation 4. Along with the previously proven (Panton 2005) inner equation, a common part, and the accepted coefficients, $k = 0.39$, $\Pi = 0.56$, and $C+ = 7.61$, Equations 2, 3, and 4 constitute a composite expansion for boundary layer Reynolds shear stress (see Figures 3-7, 3-8, and 3-9). With this new composite expansion, the common part, and identified coefficients, the Reynolds shear stress appropriate for any selected Reynolds Number can be predicted.

Because the active motions in a turbulent boundary layer only contribute to the Reynolds shear stress, per Townsend's (1976) hypothesis, they are assumed to be proportional to the active streamwise Reynolds shear stress. With this assumption the inactive part of streamwise Reynolds stress can be separated from the total streamwise Reynolds stress. Figure 3-10 through 3-21 provide profiles of the inactive streamwise Reynolds stress.

In this analysis an inactive Reynolds stress correlation equation for the outer region is developed. Starting with an equation that fits the outer behavior of the inactive streamwise Reynolds stress for channel flows, Equation 8 (Panton 2007), and adding an additional term representing the different shape of the flat plate boundary layer, an outer equation is also developed. Equation 9 is an effective representation of the asymptotic behavior of the outer part of the inactive streamwise Reynolds stress.

The inner behavior of the inactive streamwise Reynolds stress can be identified by subtracting the outer function, Equation 9, and adding the common part to the inactive streamwise Reynolds stress data. The shape of the inner inactive streamwise Reynolds stress includes an increase at low y+ values, a decrease following a peak at approximately y+ = 15, and a constant common part at y+ values above approximately 100. An equation with two exponential terms to account for the increasing and then decreasing behavior with three fitting coefficients and a common part is selected to

match the behavior of the inner inactive streamwise Reynolds stress. The equation selected for the inner inactive streamwise Reynolds stress function, Equation 10, has the correct asymptotic behavior and can be fit closely to the data using the selected coefficients in Table 9 (see Figure 3-22 through 3-25).

A composite expansion, based on combining Equations 9 and 10 with the common part and the selected coefficients from Tables 8 and 9, demonstrates the correct behavior and matches the majority of the inactive streamwise Reynolds stress data in both the inner and outer regions (see Figure 4-1 through 4-6). The selected coefficients are weighted averages of the best fit values for the different data sets considered.

Predictions for the streamwise Reynolds stress are demonstrated by combining the composite expansions for the inactive streamwise Reynolds stress with the composite expansion results for the Reynolds shear stress and using the gauge function, u*/Ue, to weight the <uIuI># term as shown in Equation 11. These composite expansion predictions of the streamwise Reynolds stress agree with the available data (see Figure 4-7 through 4-12), within the experimental uncertainty of the data and demonstrate the expected behavior of <uu>+. The final resulting composite expansion for <uu>+ shows the regions where there is Reynolds Number dependence in the streamwise Reynolds stress and how this dependence can be predicted.

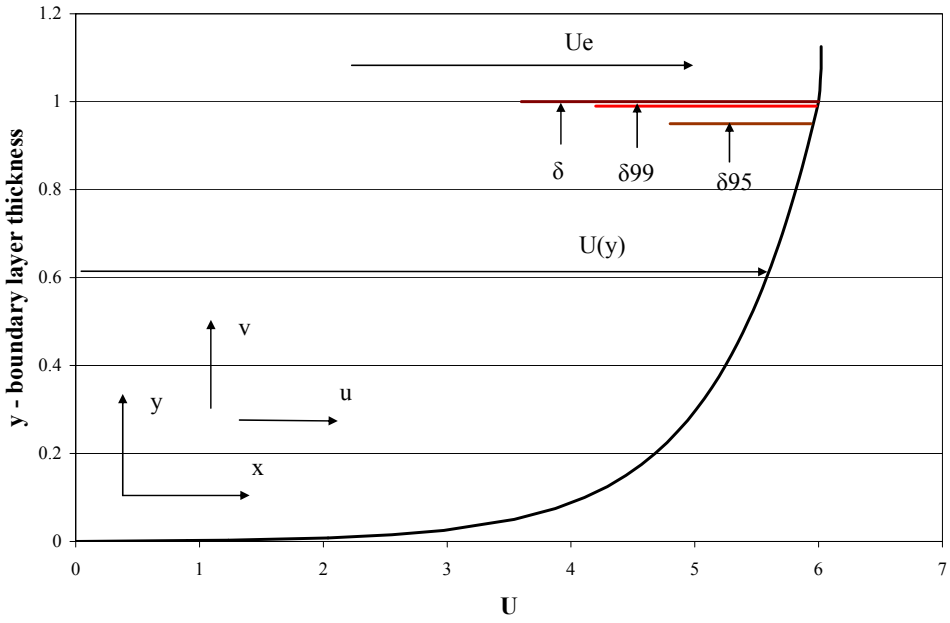

Figure 1-1. Turbulent Boundary Layer Coordinates, Mean Velocity, and Thicknesses

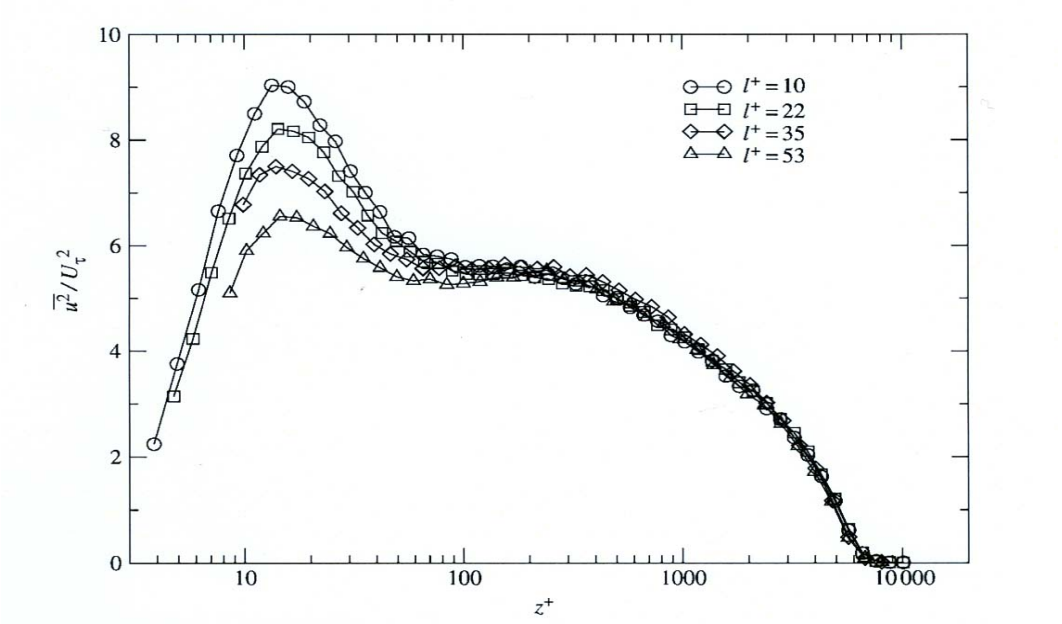

Figure 2-1. Streamwise Reynolds Stress at Constant Reynolds Number with Different Hot Wire Length which shows the Distortion from Eddy Averaging

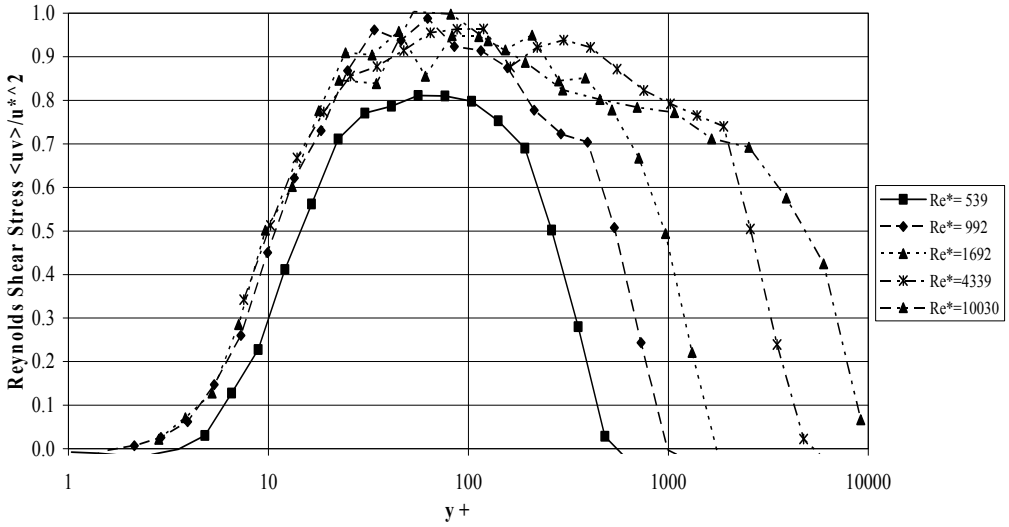

Figure 2-2. DeGraaff and Eaton Reynolds Shear Stress <uv>+ vs. y+

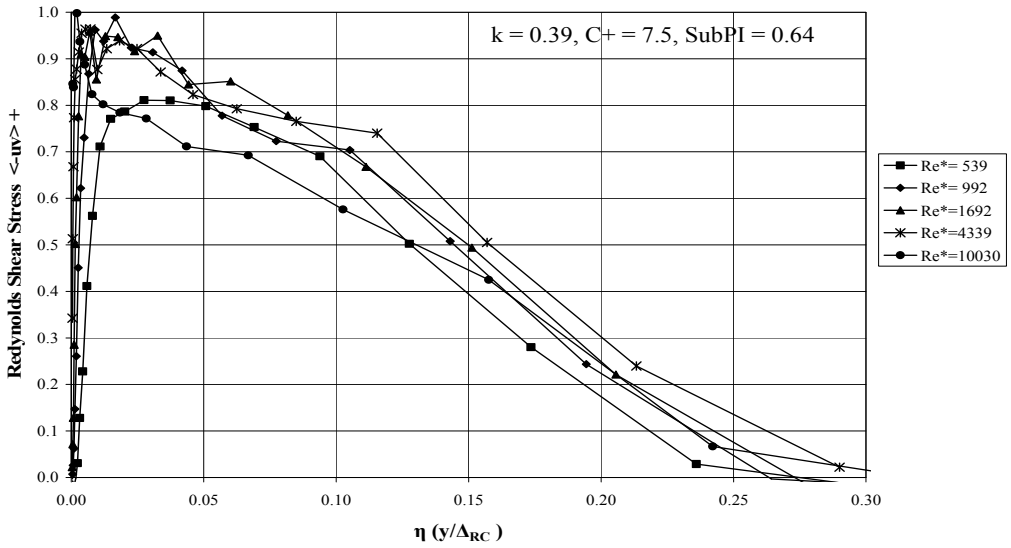

Figure 2-3. DeGraaff and Eaton Reynolds Shear Stress <uv>+ vs. η

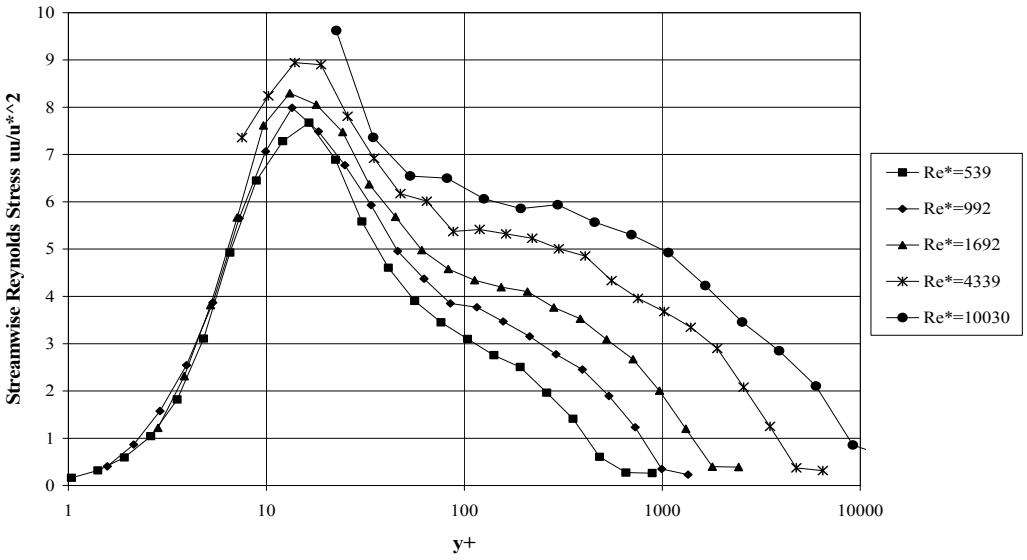

Figure 2-4. DeGraaff and Eaton Streamwise Reynolds Stress <uu>+ vs. y+

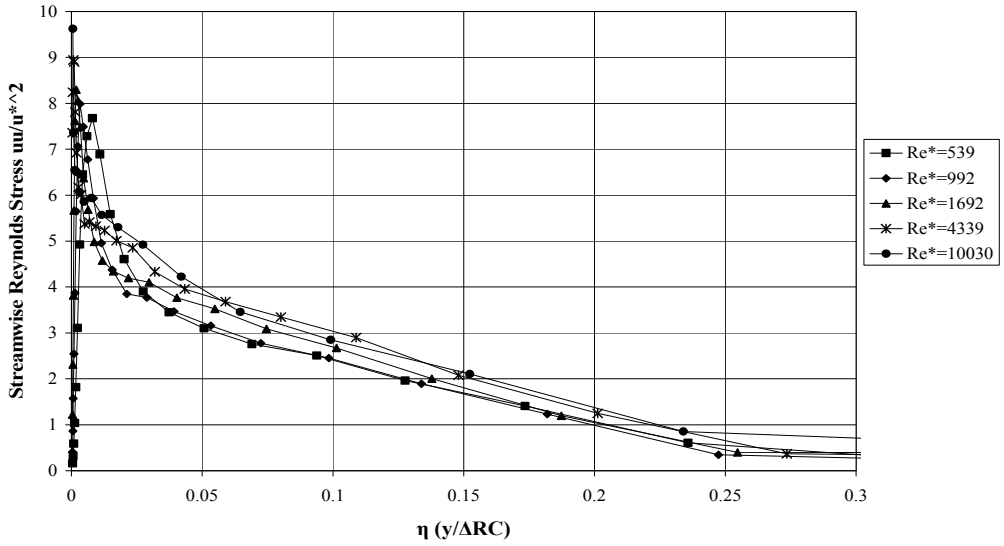

Figure 2-5. DeGraaff and Eaton Streamwise Reynolds Stress <uu>+ vs. η

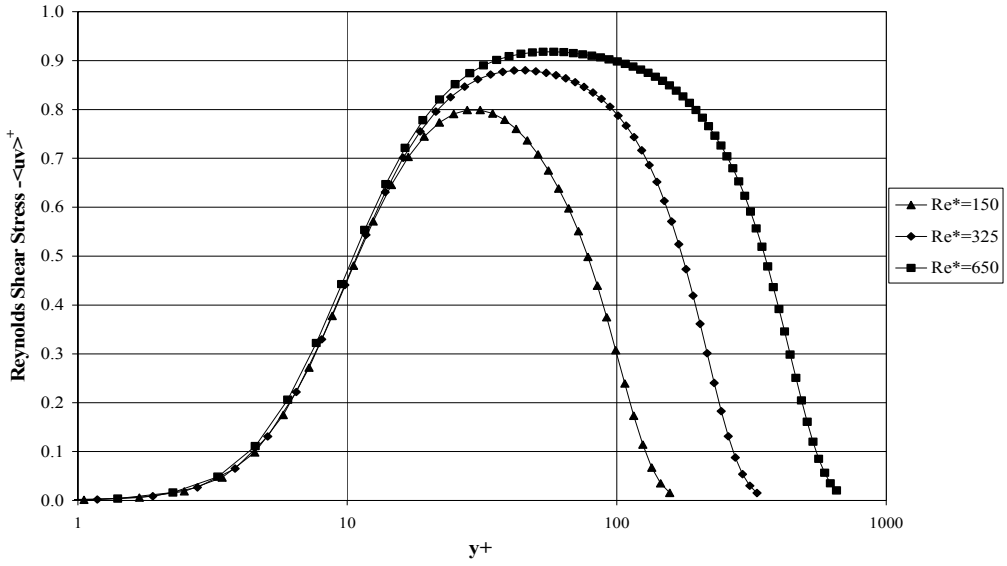

Figure 2-6. Spalart's DNS Reynolds Shear Stress <uv>+ vs. y+

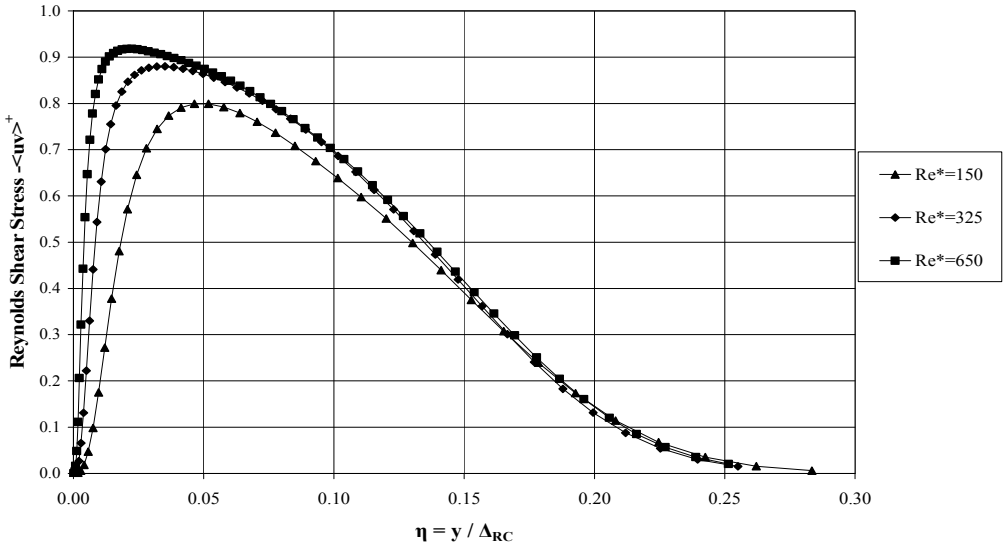

Figure 2-7. Spalart's DNS Reynolds Shear Stress <uv>+ vs. $\eta = y/\Delta_{RC}$

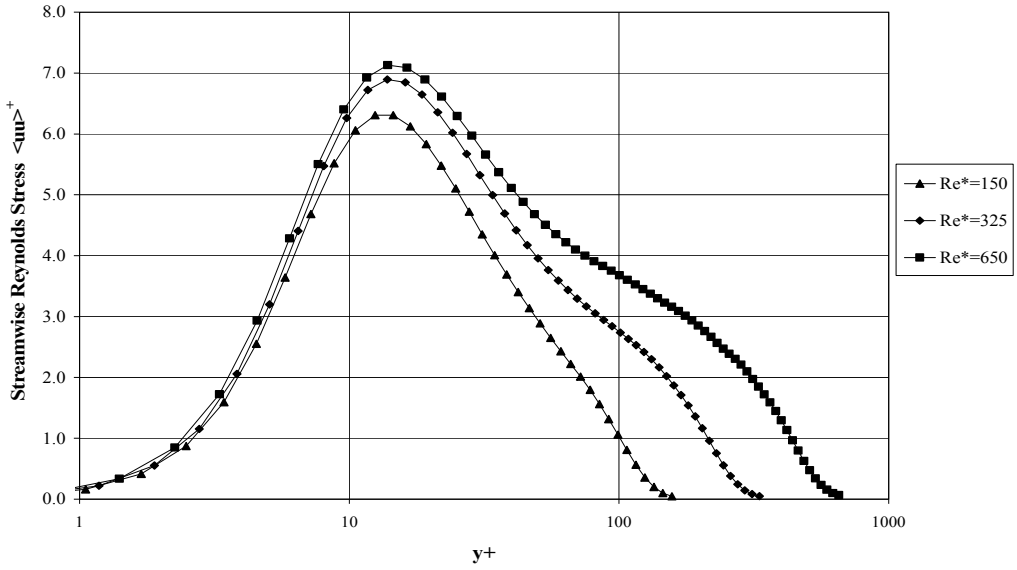

Figure 2-8. Spalart's DNS Streamwise Reynolds Stress <uu>+ vs. y+

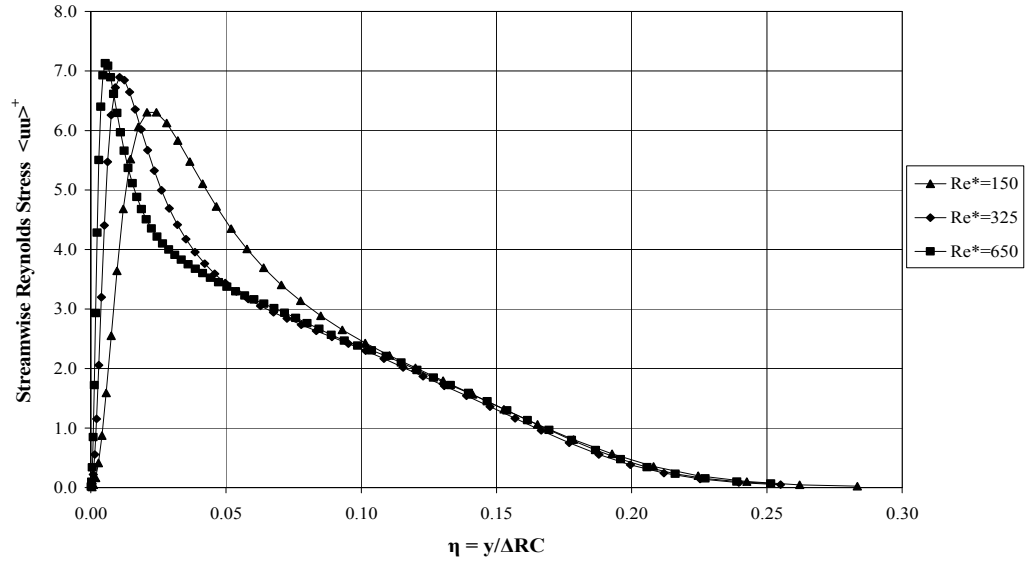

Figure 2-9. Spalart's DNS Streamwise Reynolds Stress <uu>+ vs. $\eta = y/\Delta_{RC}$

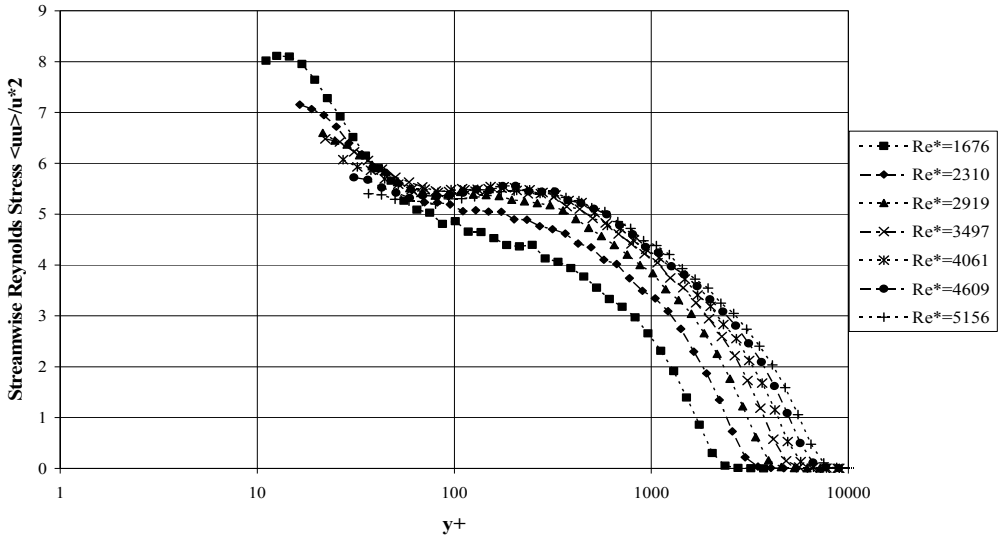

Figure 2-10. Osterlund's Streamwise Reynolds Stress <uu>+ vs. y+

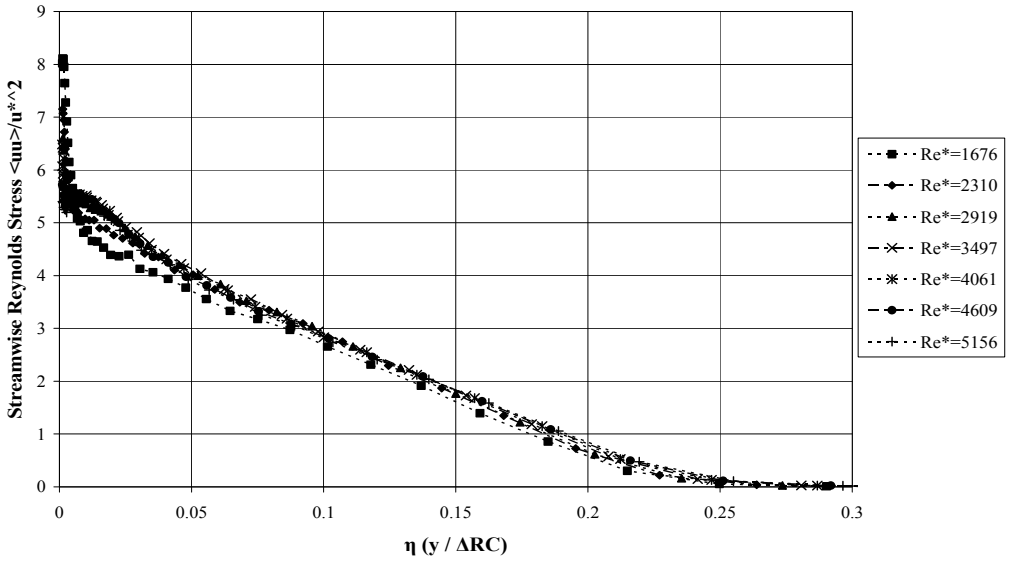

Figure 2-11. Osterlund's Streamwise Reynolds Stress <uu>+ vs. η

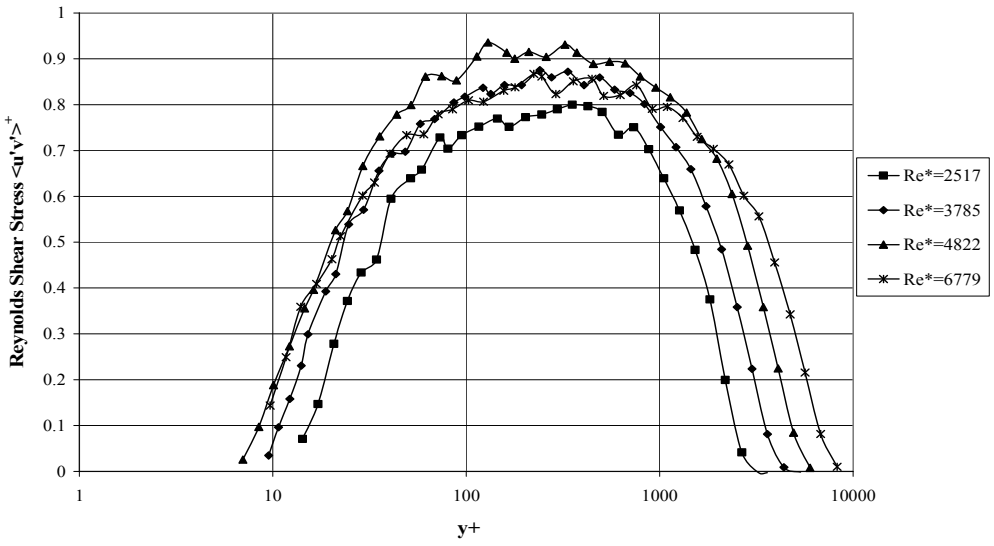

Figure 2-12. Carlier and Stanislas Reynolds Shear Stress <uv>+ vs. y+

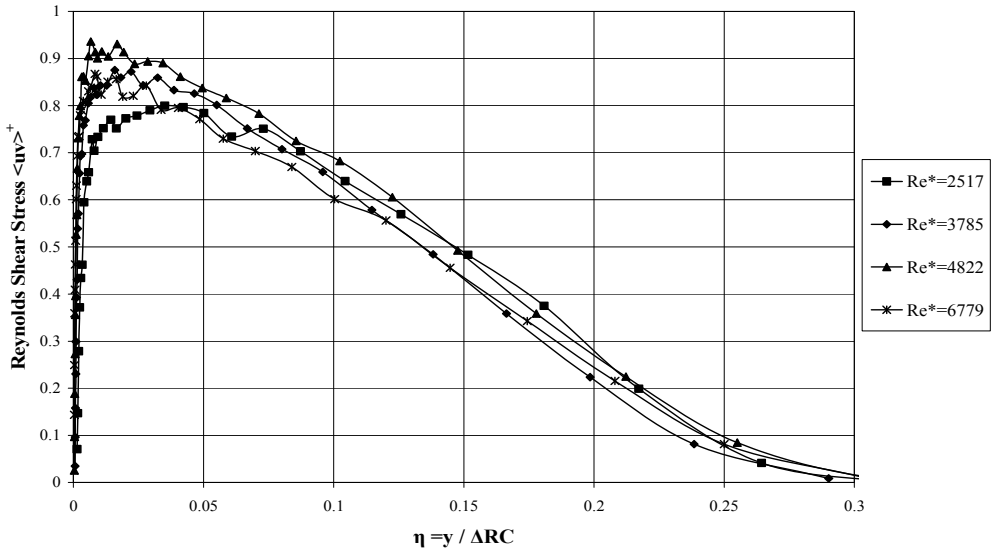

Figure 2-13. Carlier and Stanislas Reynolds Shear Stress <uv>+ vs. $\eta = y/\Delta_{RC}$

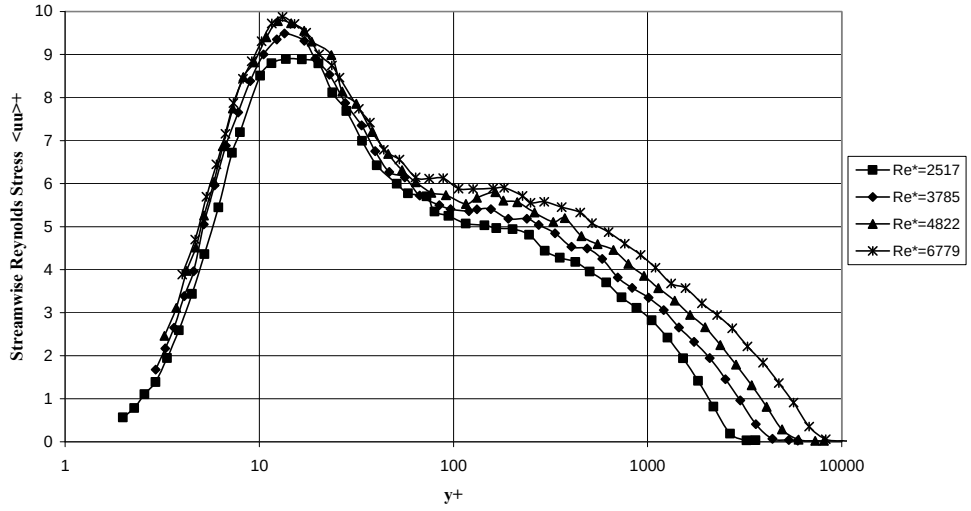

Figure 2-14. Carlier and Stanislas Streamwise Reynolds Stress <uu>+ vs. y+

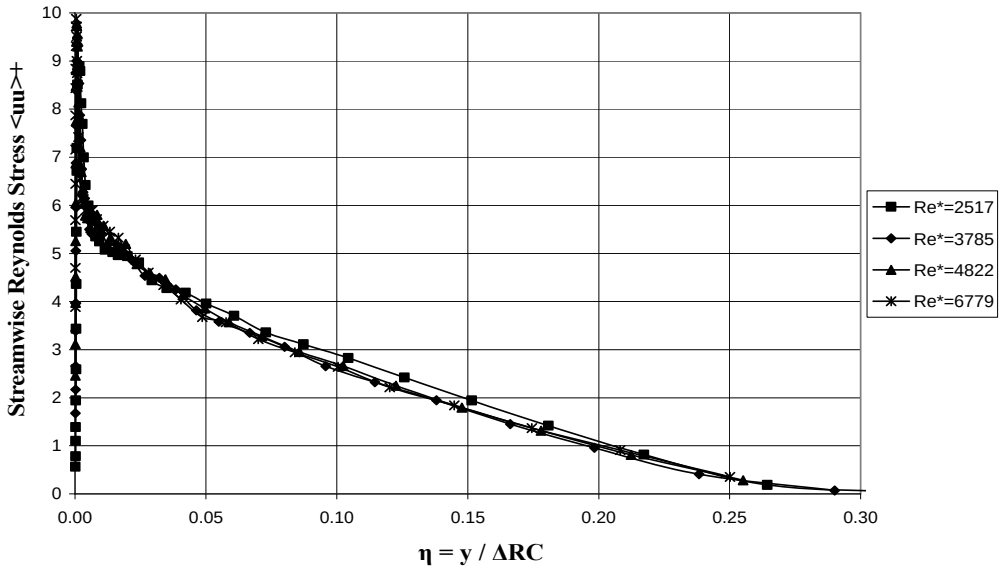

Figure 2-15. Carlier and Stanislas Streamwise Reynolds Stress <uu>+ vs. $\eta = y/\Delta RC$

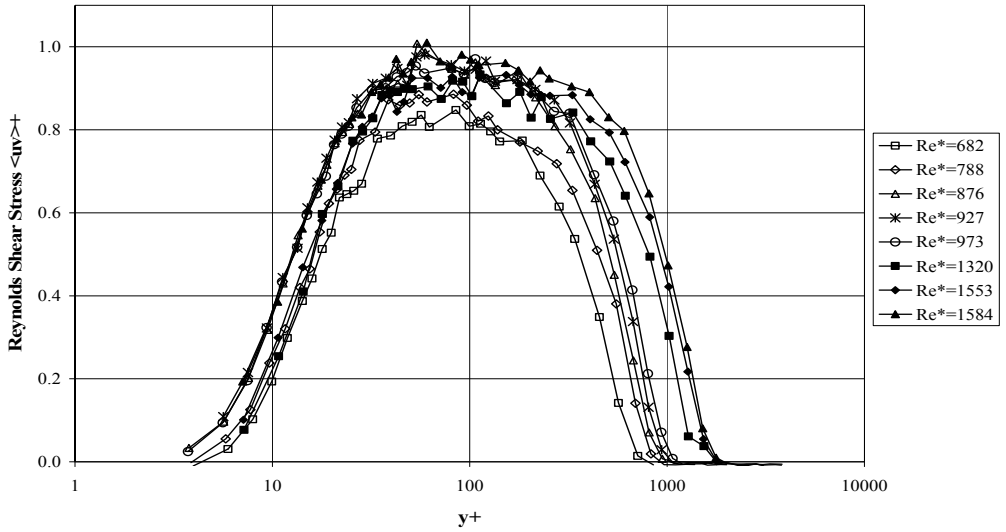

Figure 2-16. Castillo and Johansson Reynolds Shear Stress for a ZPG BL vs. y+

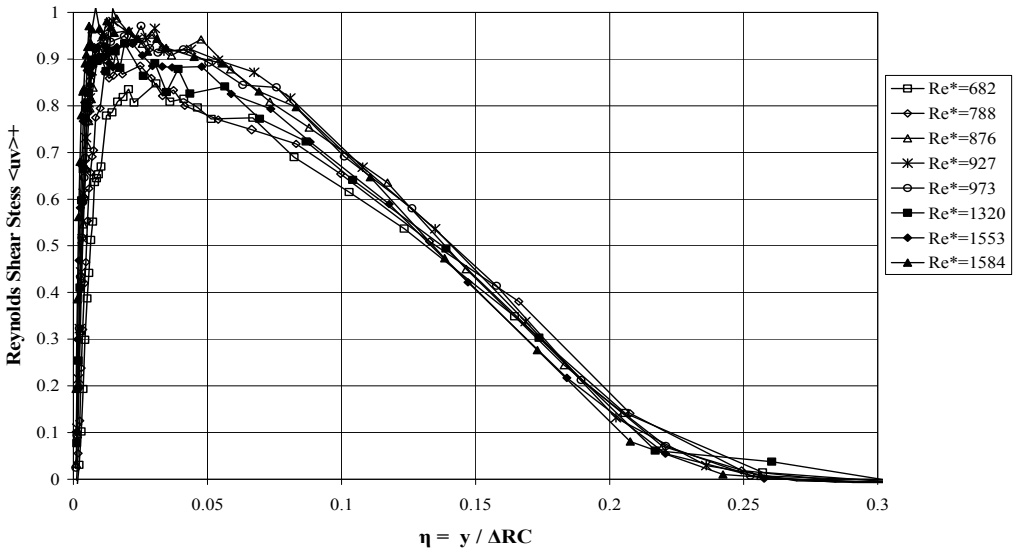

Figure 2-17. Castillo and Johansson Reynolds Shear Stress for a ZPG BL vs. η

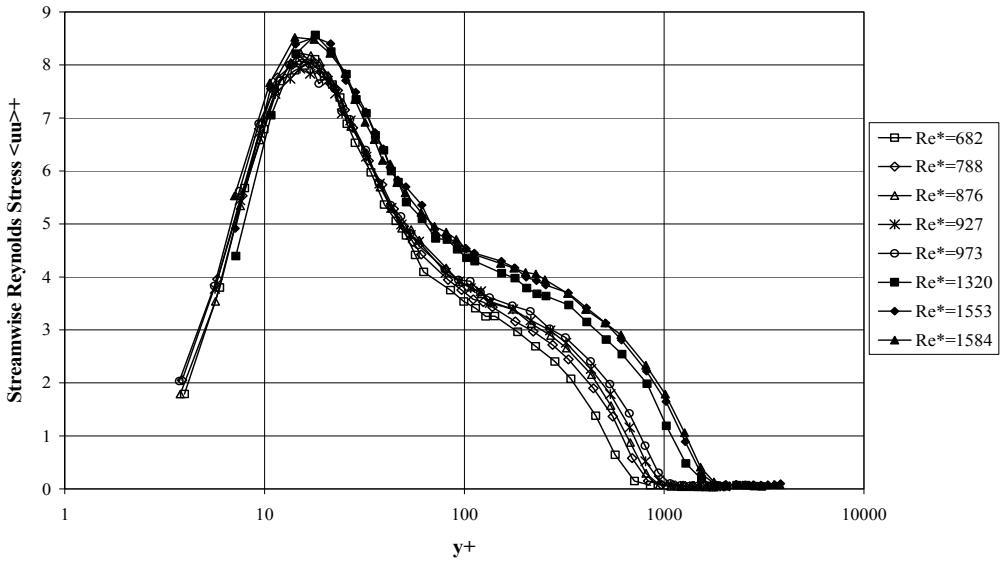

Figure 2-18. Castillo and Johansson Streamwise Reynolds Stress for a ZPG BL vs. y+

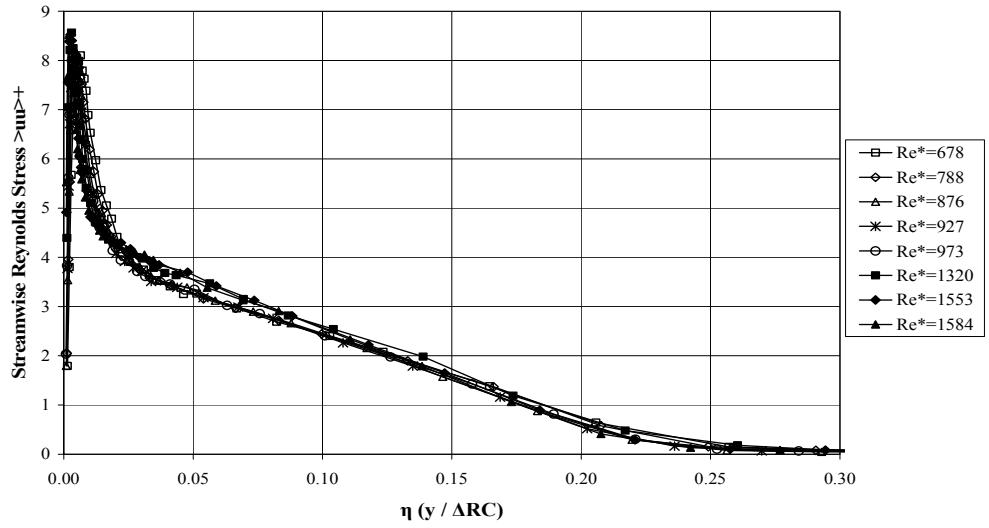

Figure 2-19. Castillo and Johansson Streamwise Reynolds Stress for a ZPG BL vs. η

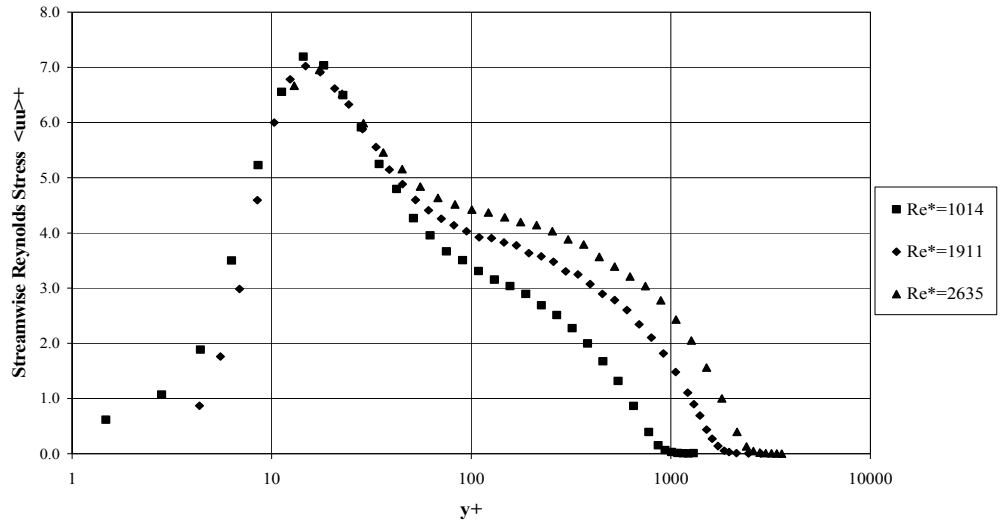

Figure 2-20. Hutchins and Marusic Streamwise Reynolds Stress <uu>+ vs. y+

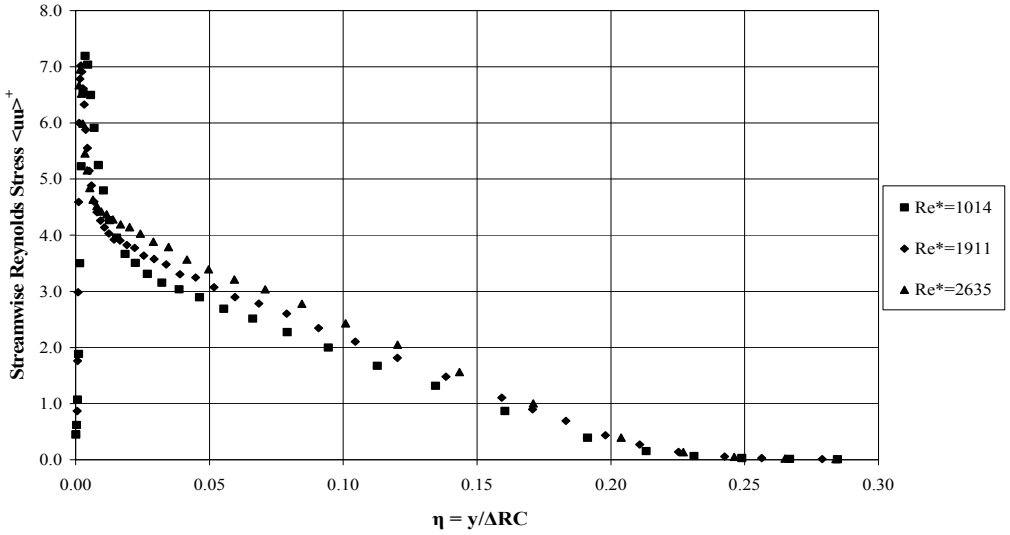

Figure 2-21. Hutchins and Marusic Streamwise Reynolds Stress <uu>+ vs. η

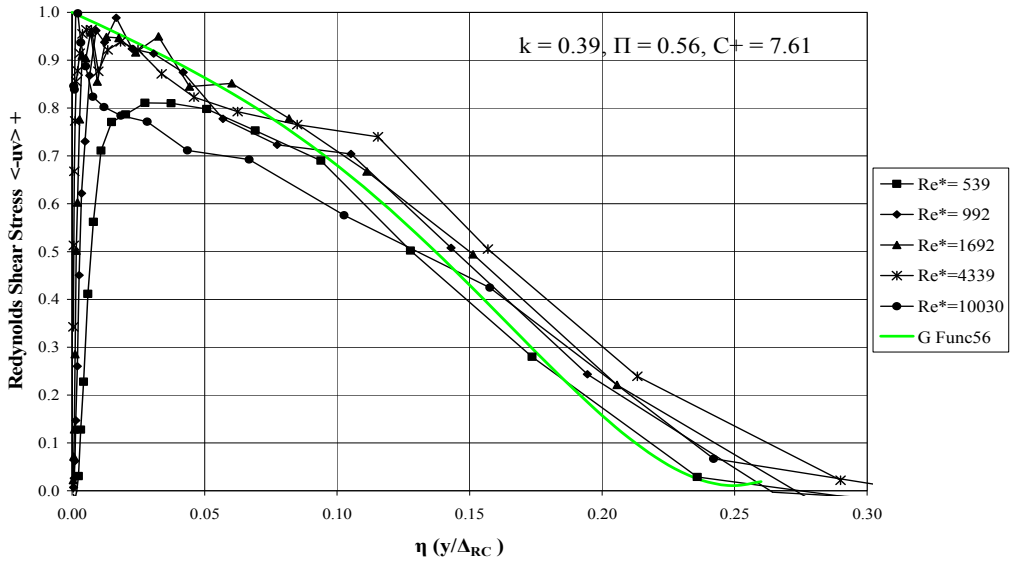

Figure 3-1. DeGraaff and Eaton Reynolds Shear Stress and G_o vs. $\eta = y/\Delta_{RC}$

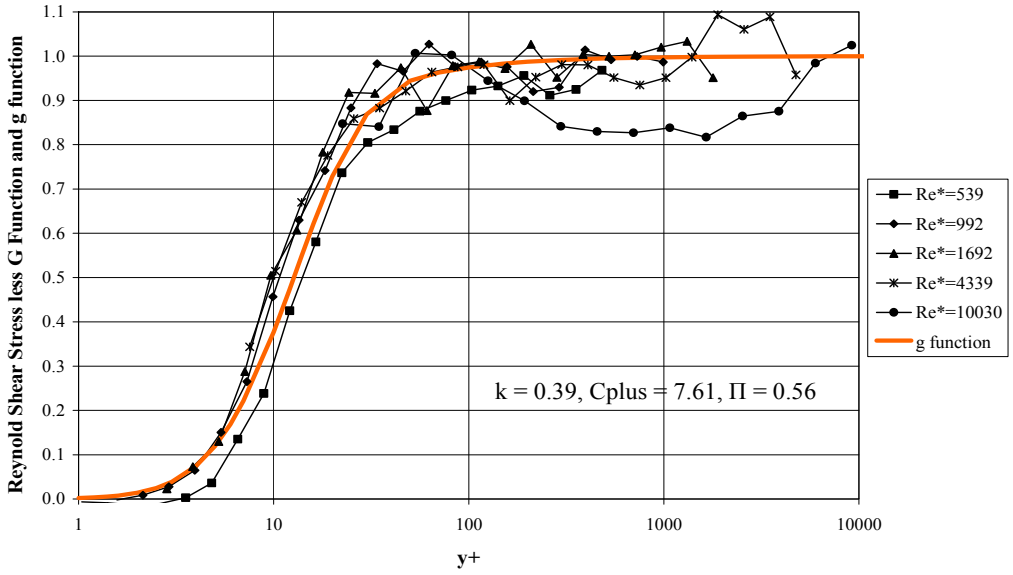

Figure 3-2. DeGraaff and Eaton Inner Reynolds Shear Stress and g(y+) vs. y+

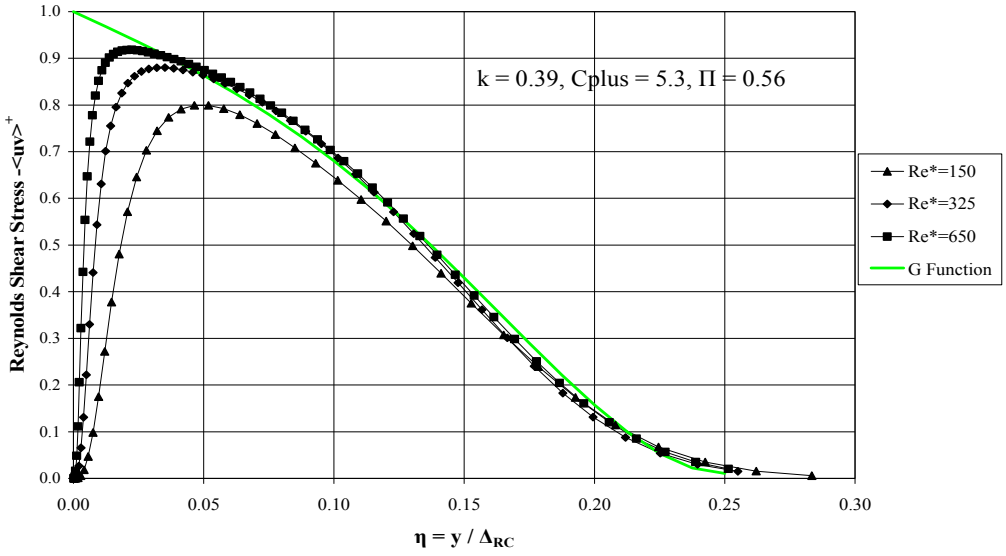

Figure 3-3. Spalart DNS Reynolds Shear Stress and G_o vs. $\eta = y/\Delta_{RC}$

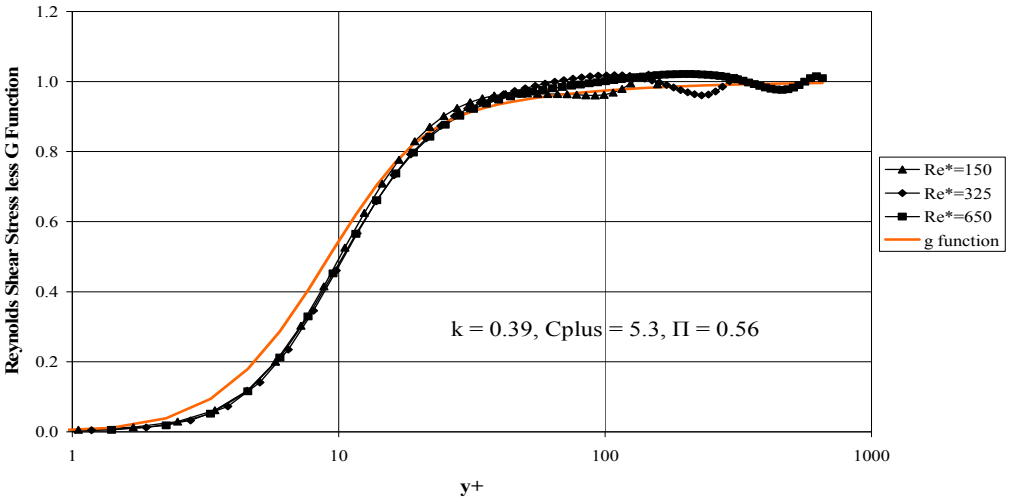

Figure 3-4. Spalart DNS Inner Reynolds Shear Stress and g(y+) vs. y+

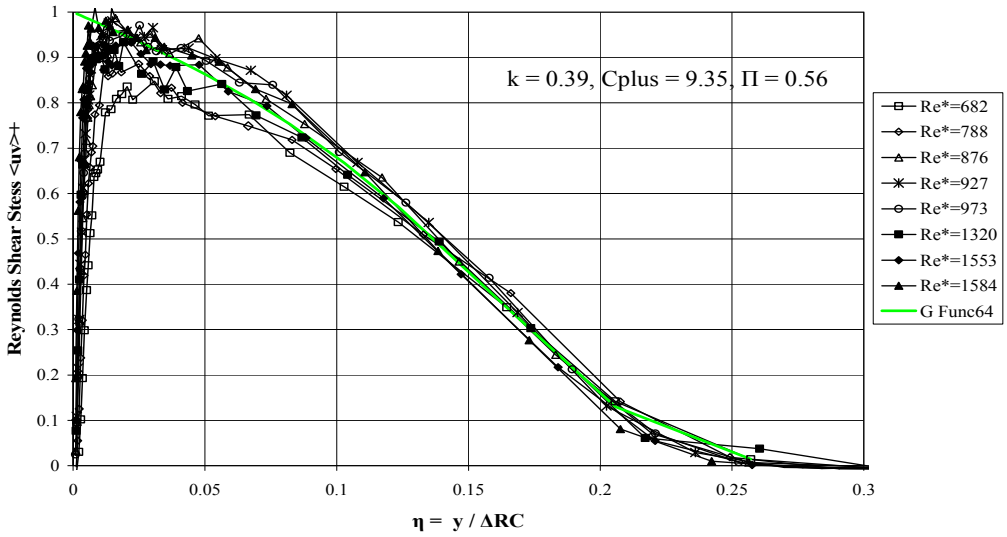

Figure 3-5. Castillo and Johansson Reynolds Shear Stress for a ZPG BL and G_o vs. η

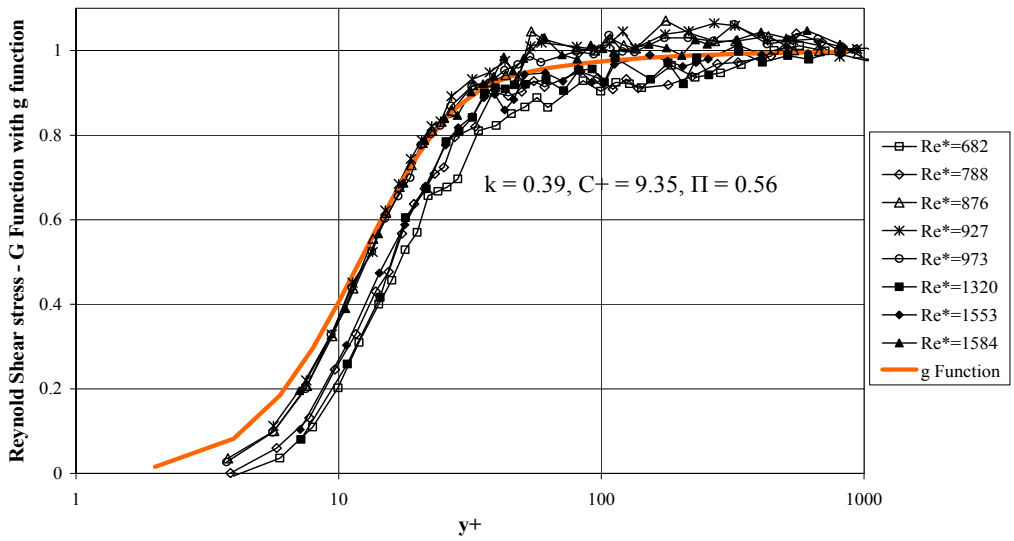

Figure 3-6. Castillo and Johansson Inner Reynolds Shear Stress and g(y+) vs. y+

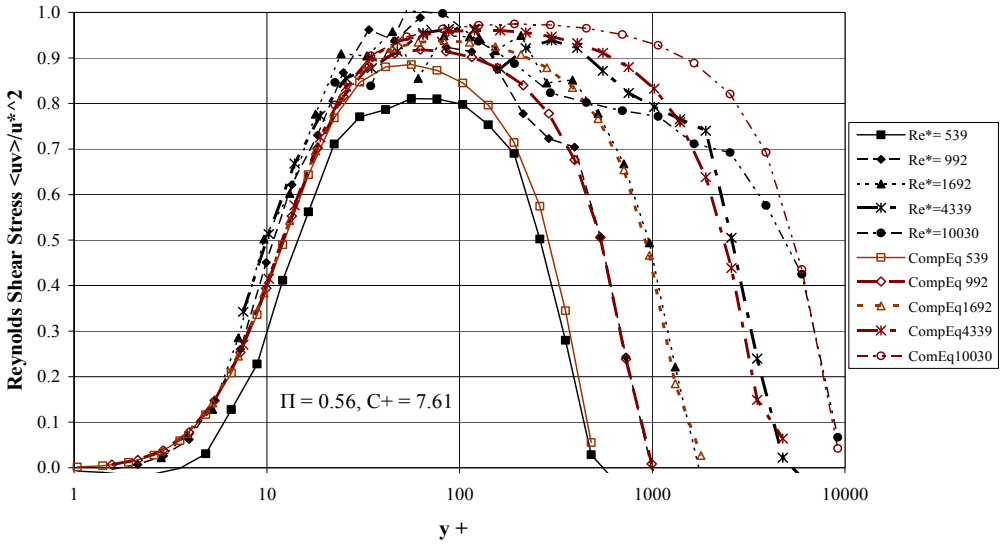

Figure 3-7. DeGraaff and Eaton Reynolds Shear Stress with Composite Expansions

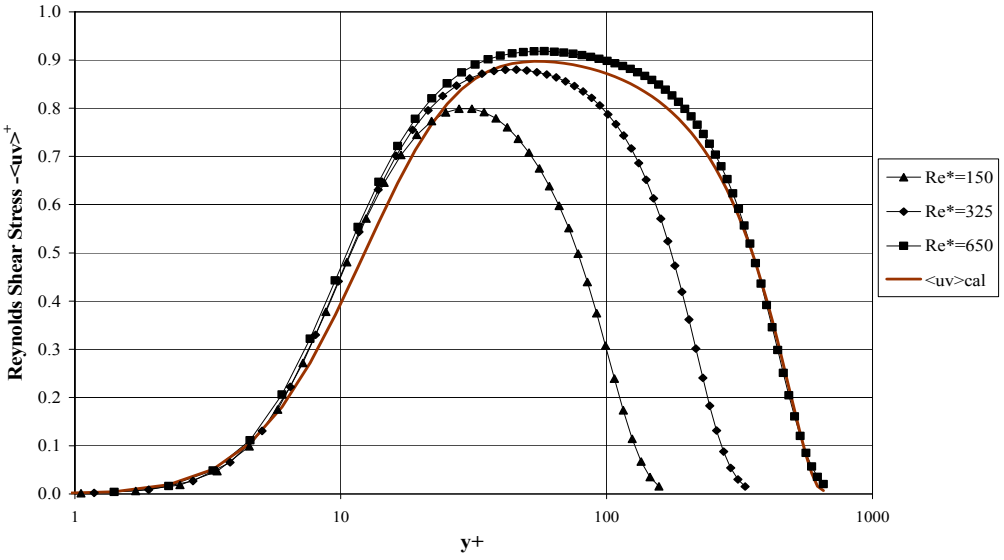

Figure 3-8. Spalart's DNS Reynolds Shear Stress with Composite Expansion

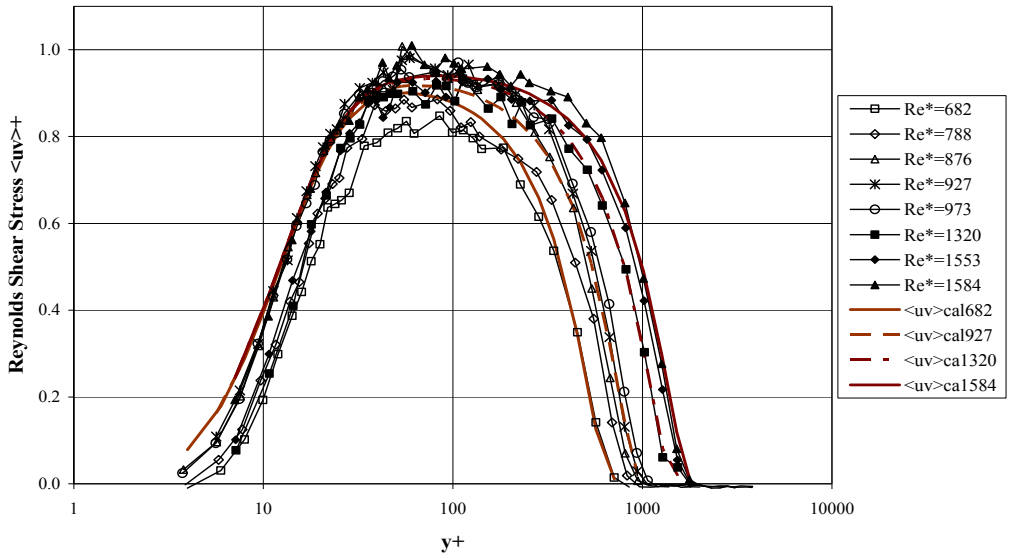

Figure 3-9. Castillo and Johansson Reynolds Shear Stress for a ZPG BL with Composite Expansions vs. y+

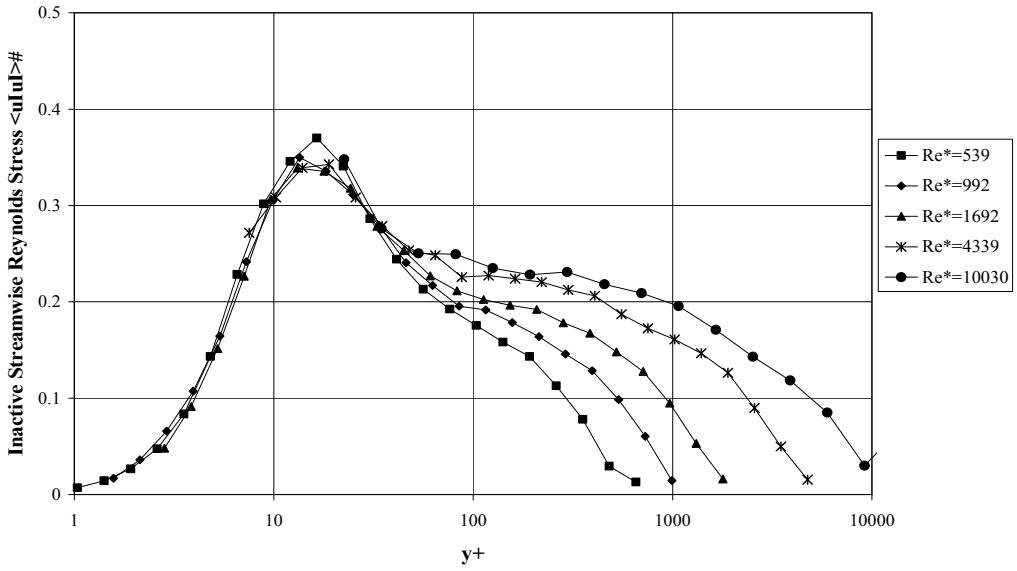

Figure 3-10. DeGraaff and Eaton Inactive Streamwise Reynolds Stress <uIuI># vs. y+

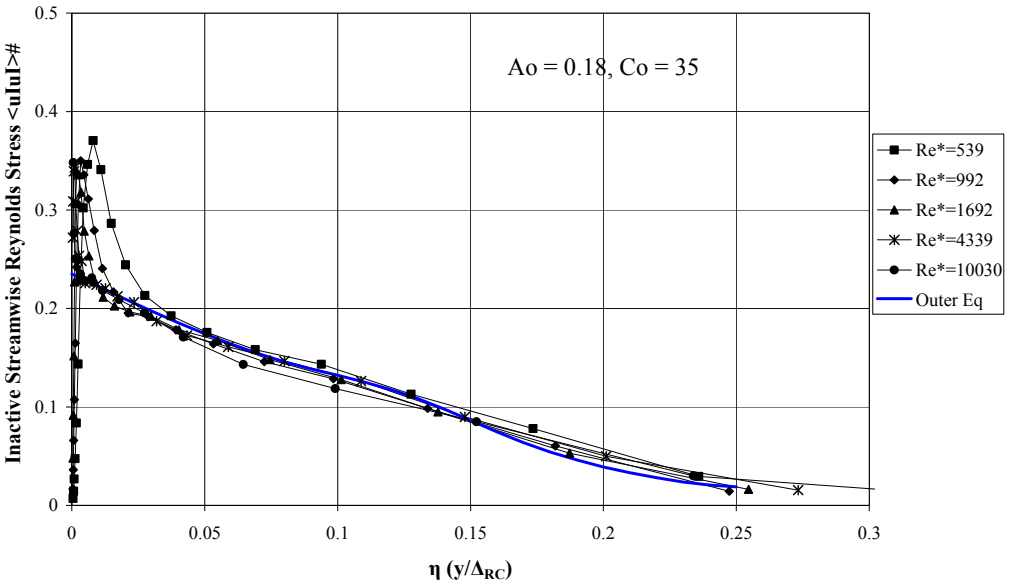

Figure 3-11. DeGraaff and Eaton Inactive Streamwise Reynolds Stress <uIuI># vs. η

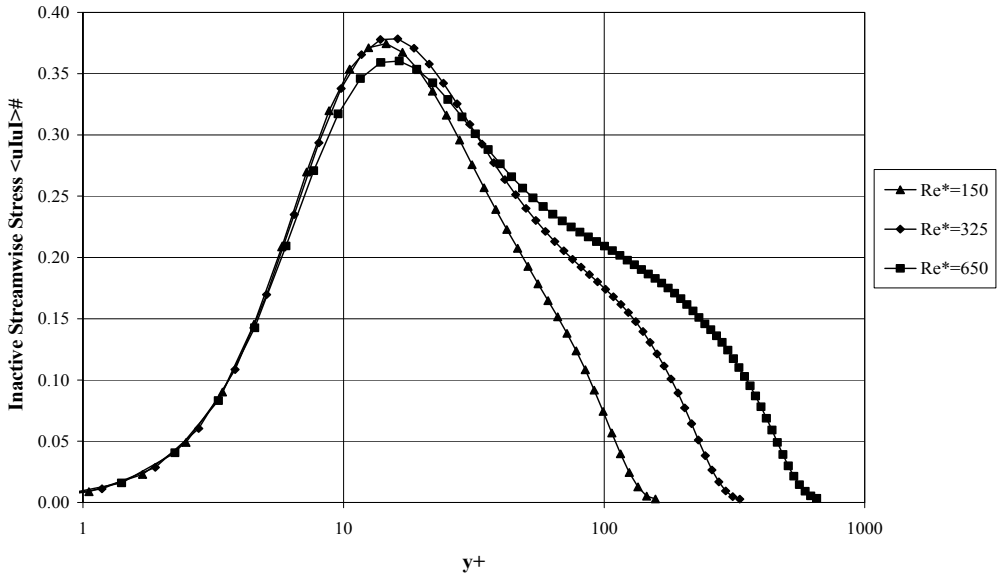

Figure 3-12 Spalart Inactive Streamwise Reynolds Stress <uIuI># vs. y+

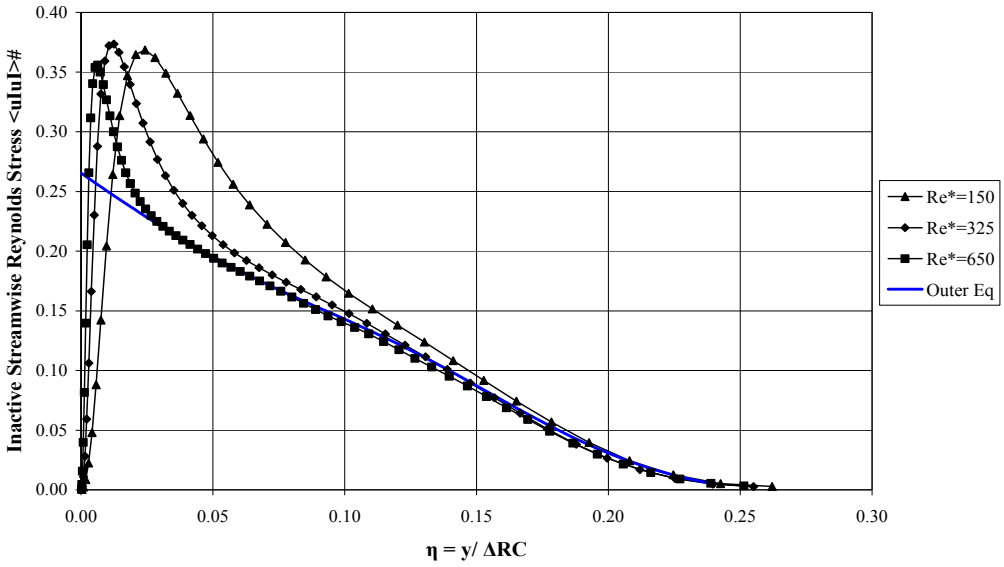

Figure 3-13. Spalart Inactive Streamwise Reynolds Stress <uIuI># vs. η

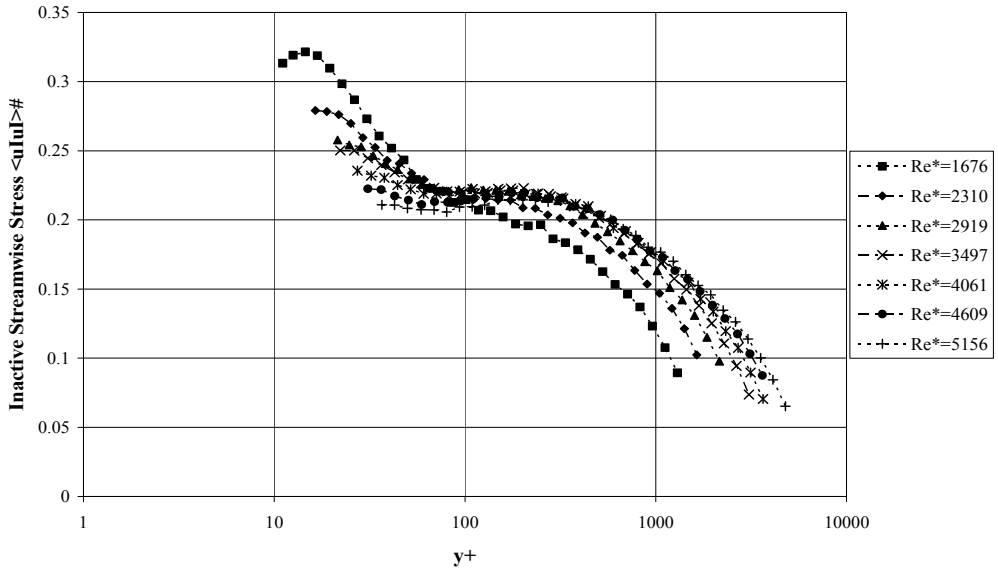

Figure 3-14. Osterlund Inactive Streamwise Reynolds Stress <uIuI># vs. y+

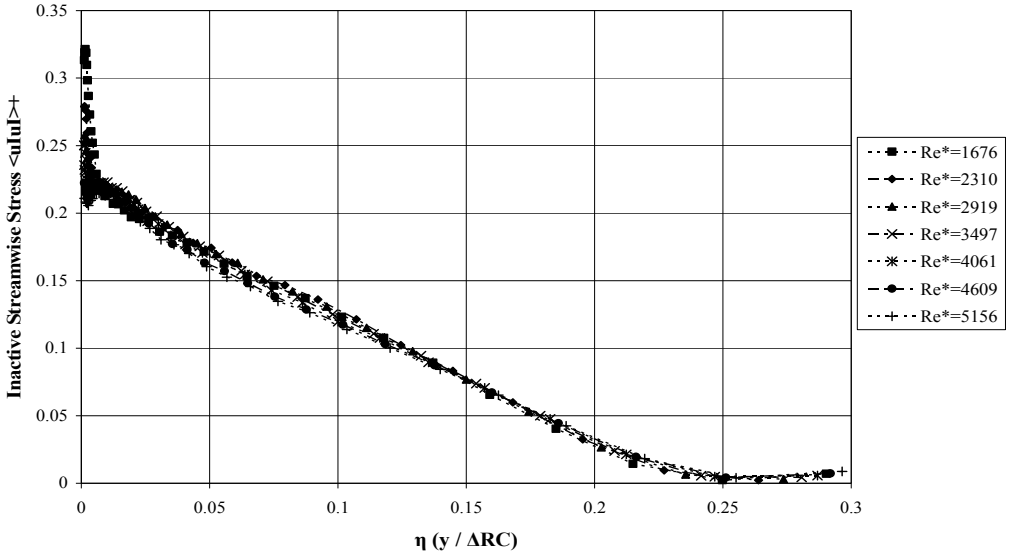

Figure 3-15. Osterlund Inactive Streamwise Reynolds Stress <uIuI># vs. η

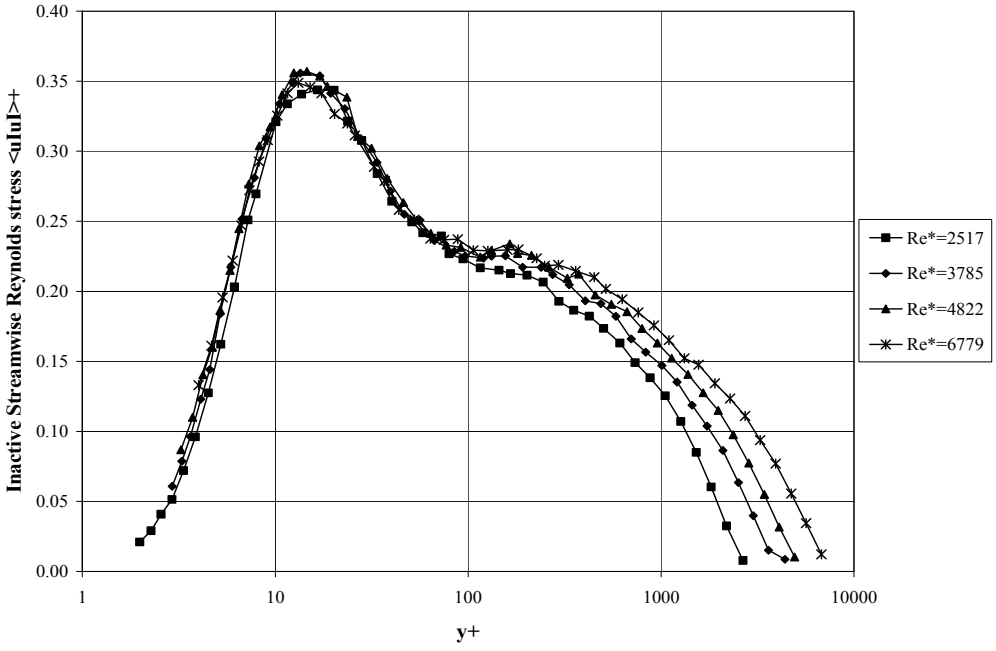

Figure 3-16. Carlier and Stanislas Streamwise Reynolds Stress <uIuI># vs. y+

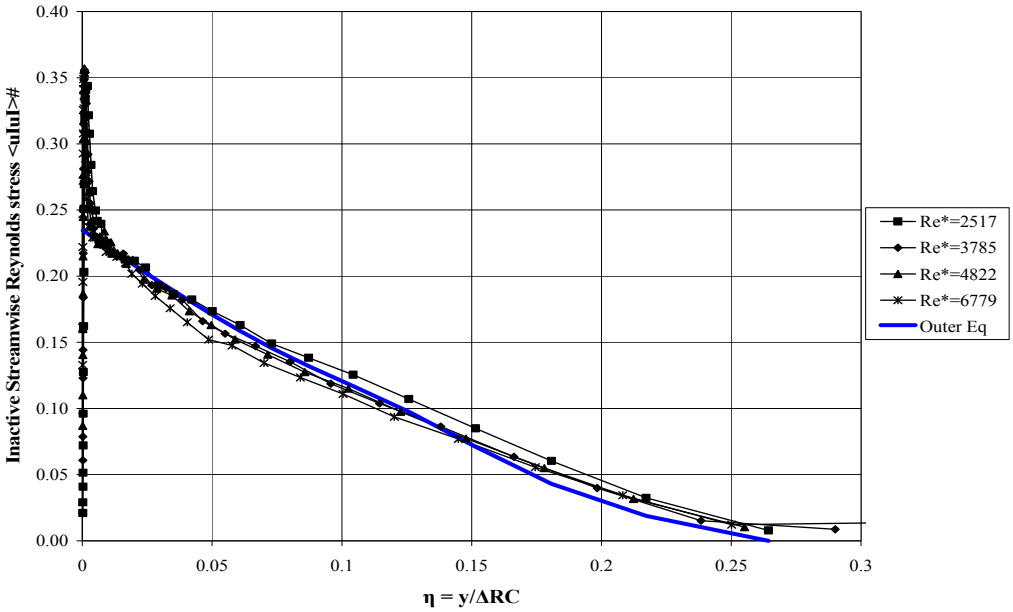

Figure 3-17. Carlier and Stanislas Streamwise Reynolds Stress <uIuI># vs. η

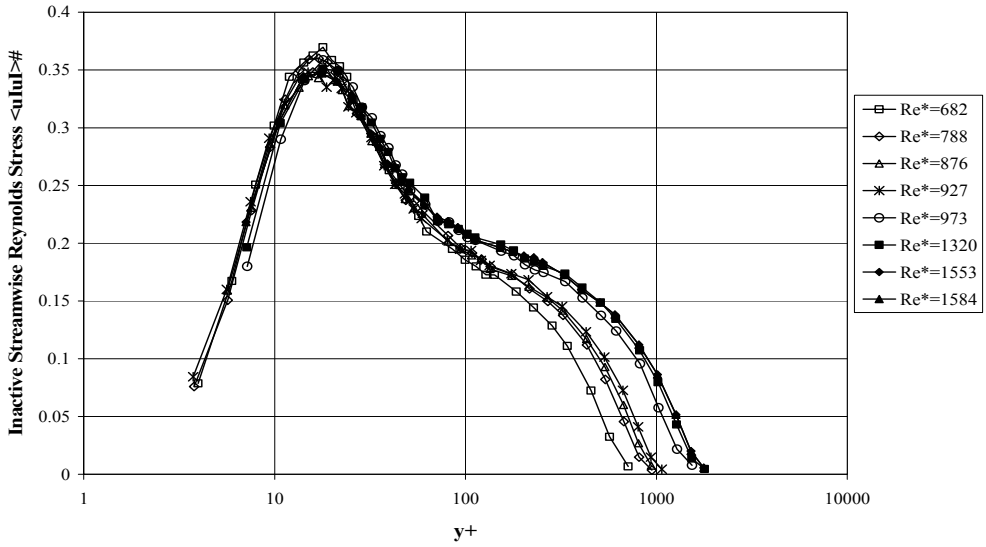

Figure 3-18. Castillo and Johansson Inactive Streamwise Reynolds Stress <uIuI># vs. y+

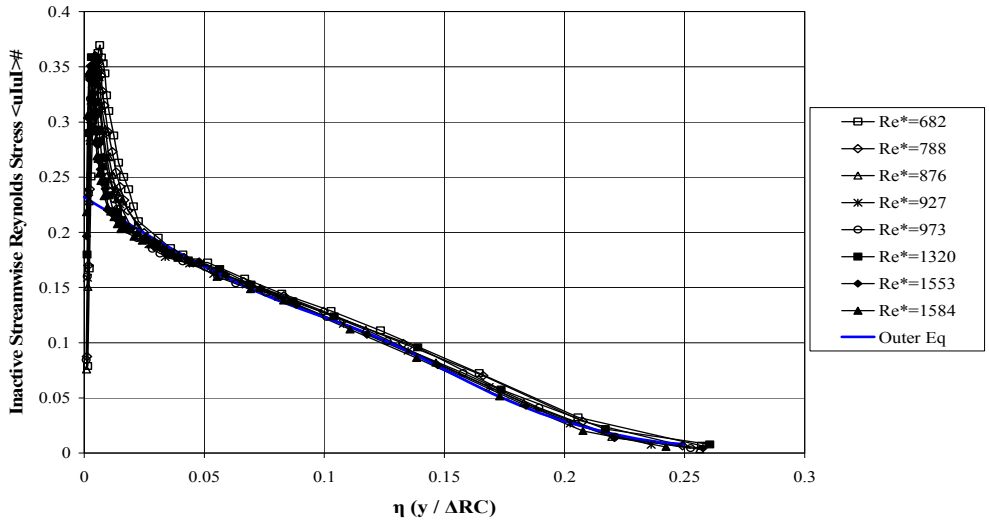

Figure 3-19. Castillo and Johansson Inactive Streamwise Reynolds Stress <uIuI># vs. η

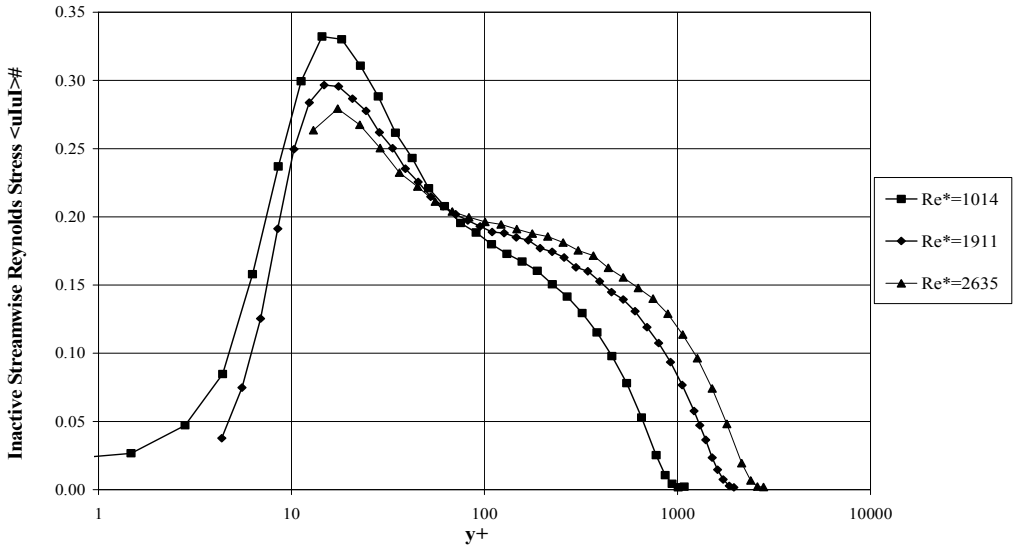

Figure 3-20. Hutchins and Marusic Inactive Streamwise Reynolds Stress <uIuI># vs. y+

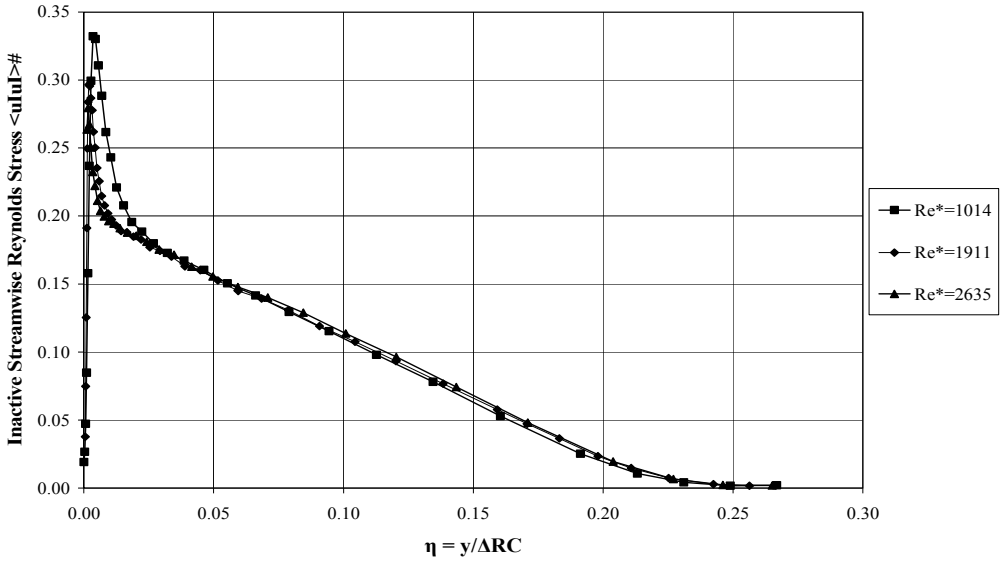

Figure 3-21. Hutchins and Marusic Inactive Streamwise Reynolds Stress <uIuI># vs. η

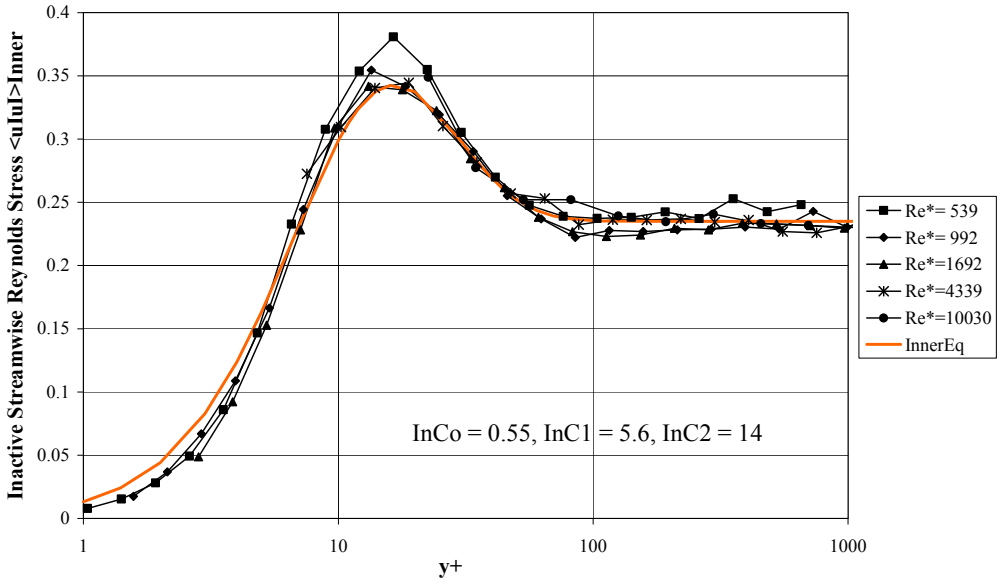

Figure 3 - 22. DeGraaff and Eaton Inner Inactive Streamwise Reynolds Stress vs. y+

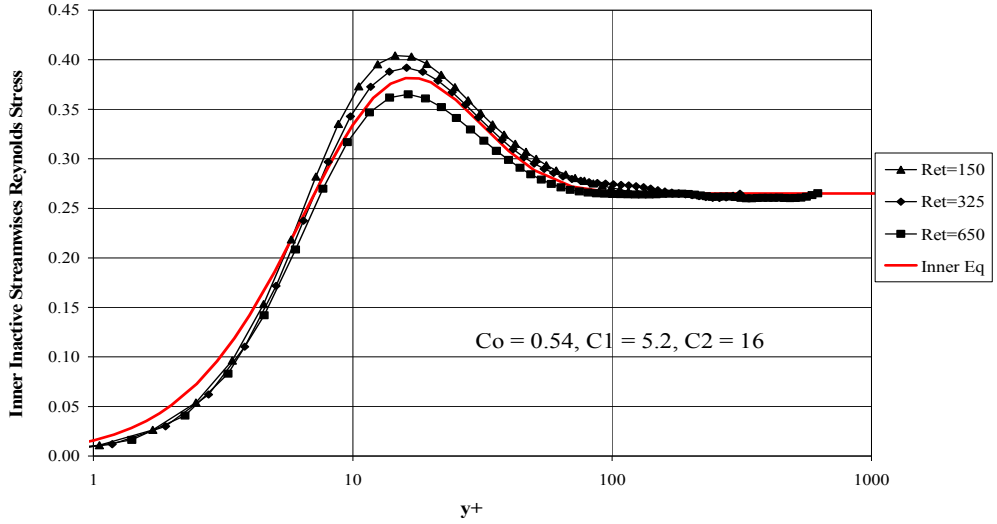

Figure 3-23. Spalart Inner Inactive Streamwise Reynolds Stress vs. y+

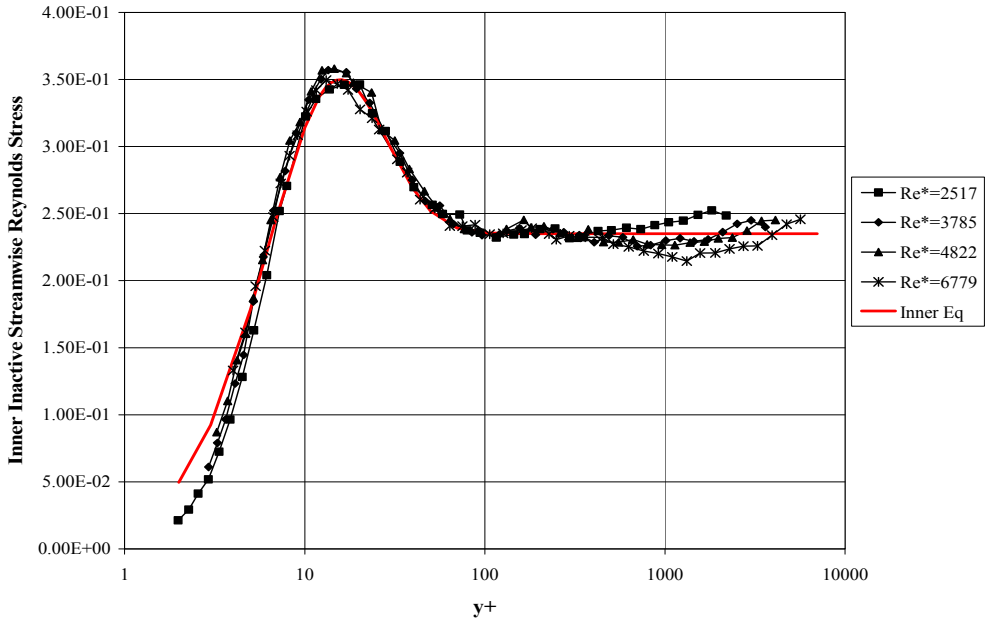

Figure 3-24. Carlier and Stanislas Inner Streamwise Reynolds Stress vs. y+

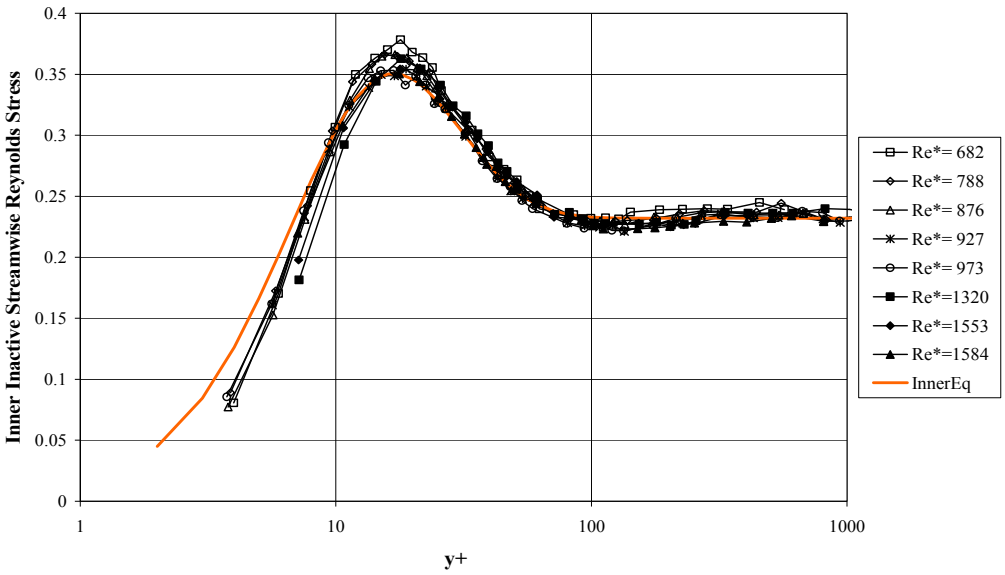

Figure 3-25. Castillo and Johansson Inner Streamwise Reynolds Stress vs. y+

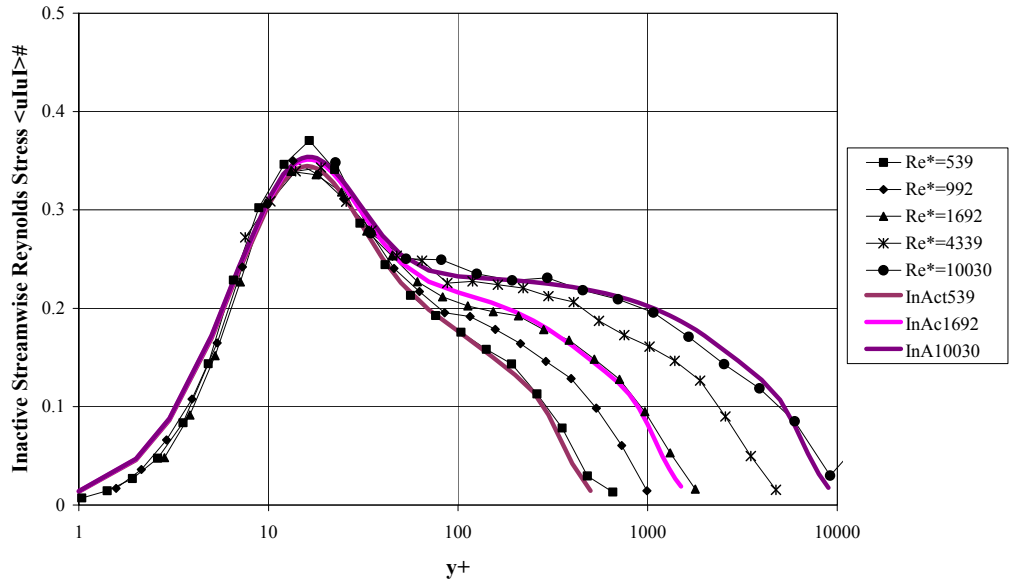

Figure 4-1. Predicted Inactive Streamwise Reynolds Stress Compared to DeGraaff and Eaton Data with Selected Coefficients vs. y+

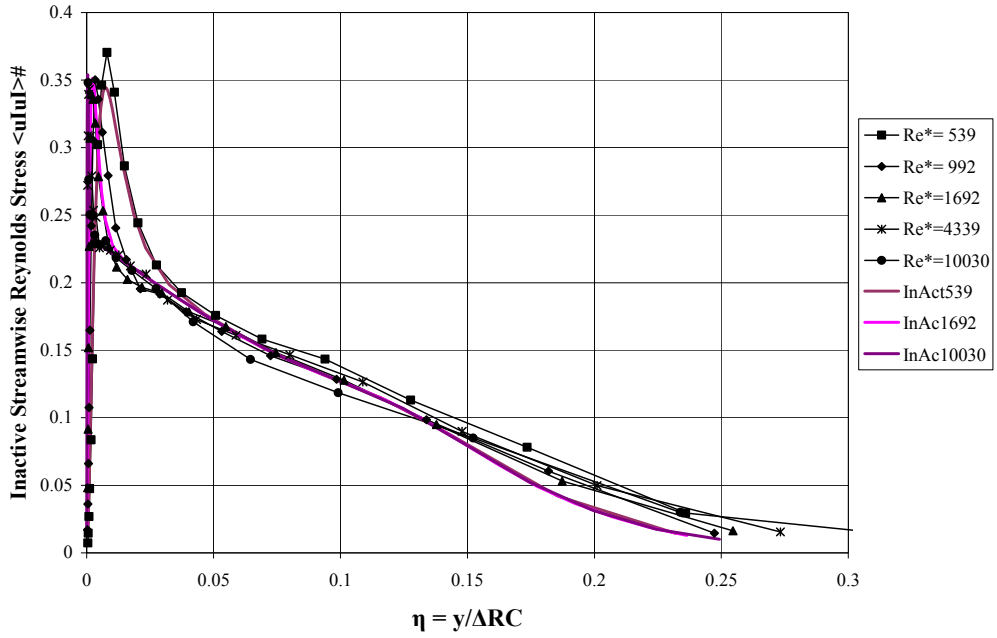

Figure 4-2. Predicted Inactive Streamwise Reynolds Stress Compared to DeGraaff and Eaton Data with Selected Coefficients from vs. η

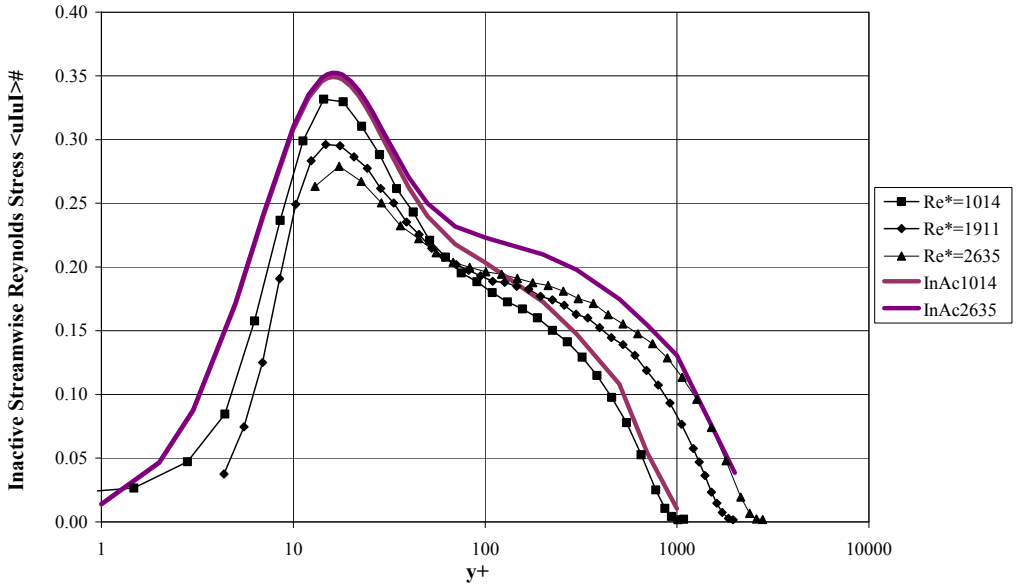

Figure 4-3. Predicted Inactive Streamwise Reynolds Stress Compared to Hutchins and Marusic Data with Selected Coefficients vs. y+

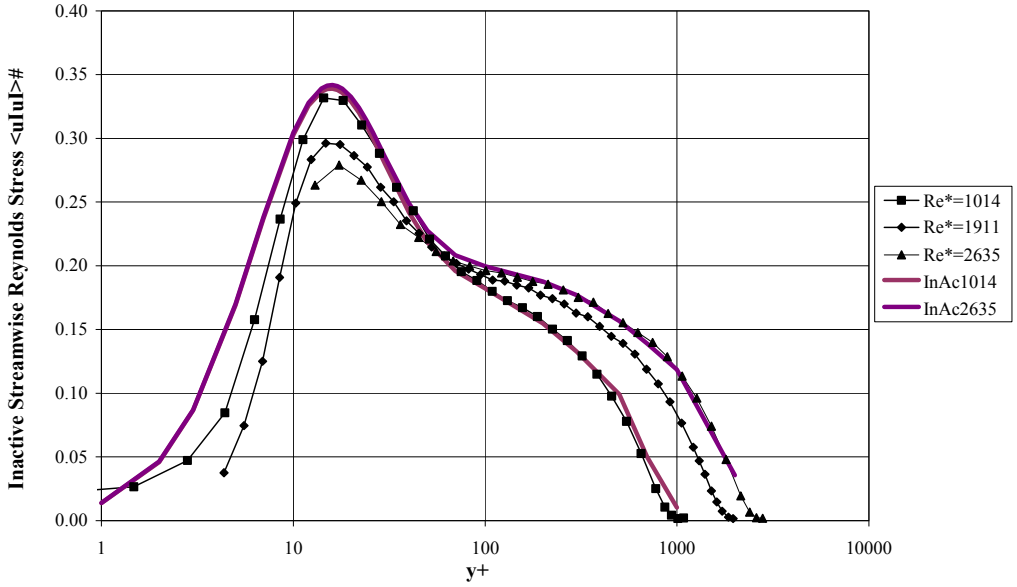

Figure 4-4. Predicted Inactive Streamwise Reynolds Stress Compared to Hutchins and Marusic Data with an Adjustment to the Common Part and Selected Coefficients vs. y+

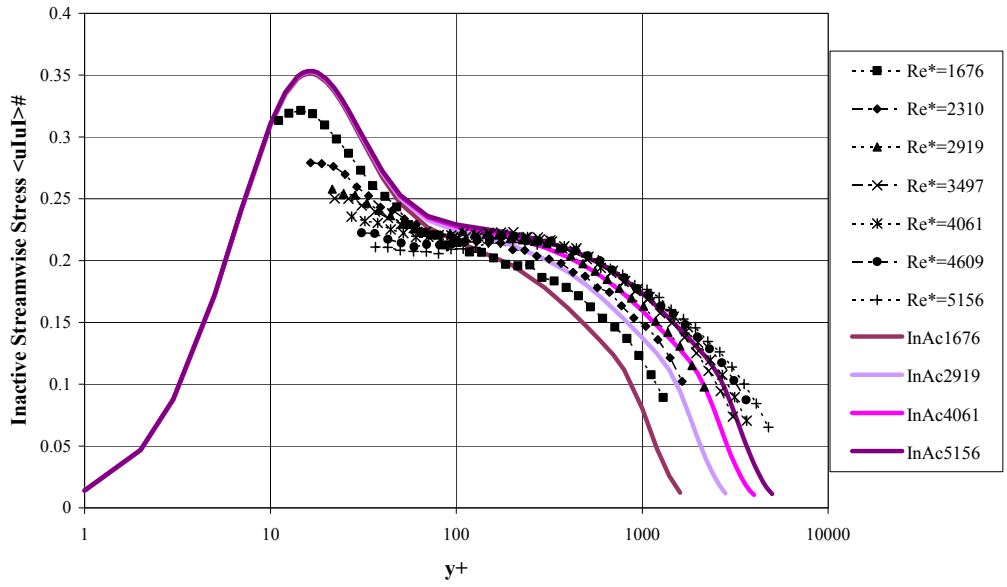

Figure 4-5. Predicted Inactive Streamwise Reynolds Stress Compared to Osterlund Data with Selected Coefficients vs. y+

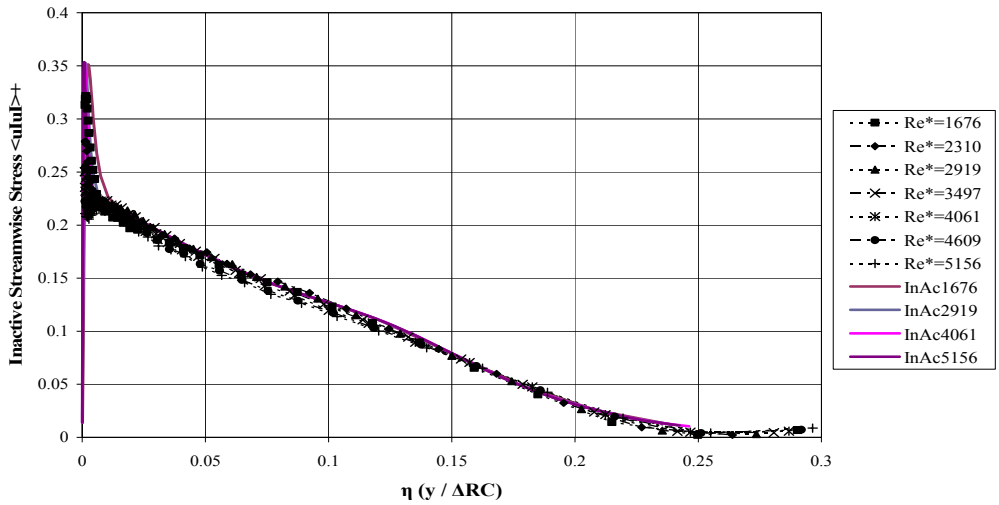

Figure 4-6. Predicted Inactive Streamwise Reynolds Stress Compared to Osterlund Data with Selected Coefficient vs. η

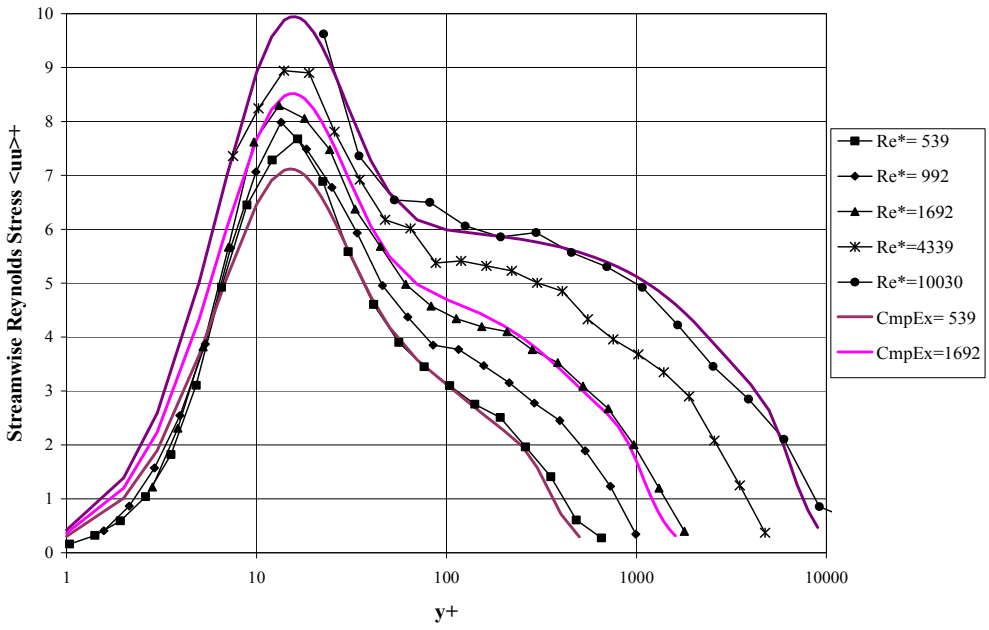

Figure 4-7. Predicted Streamwise Reynolds Stress Derived from Composite Expansions Compared to DeGraaff and Eaton Data vs. y+

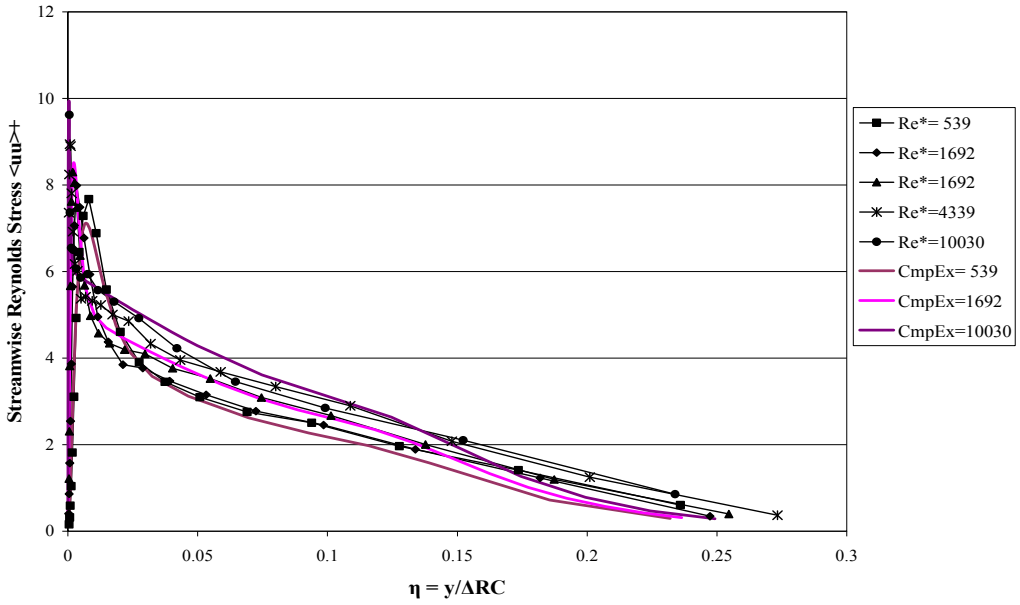

Figure 4-8. Predicted Streamwise Reynolds Stress Derived from Composite Expansions Compared to DeGraaff and Eaton Data vs. η

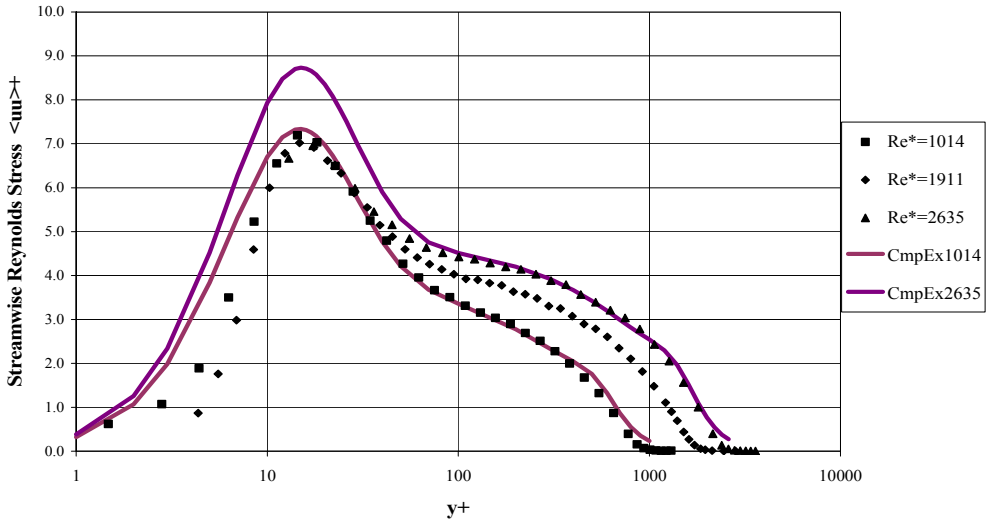

Figure 4-9. Predicted Streamwise Reynolds Stress Derived from Composite Expansions as Compared to Hutchins and Marusic Data vs. y+

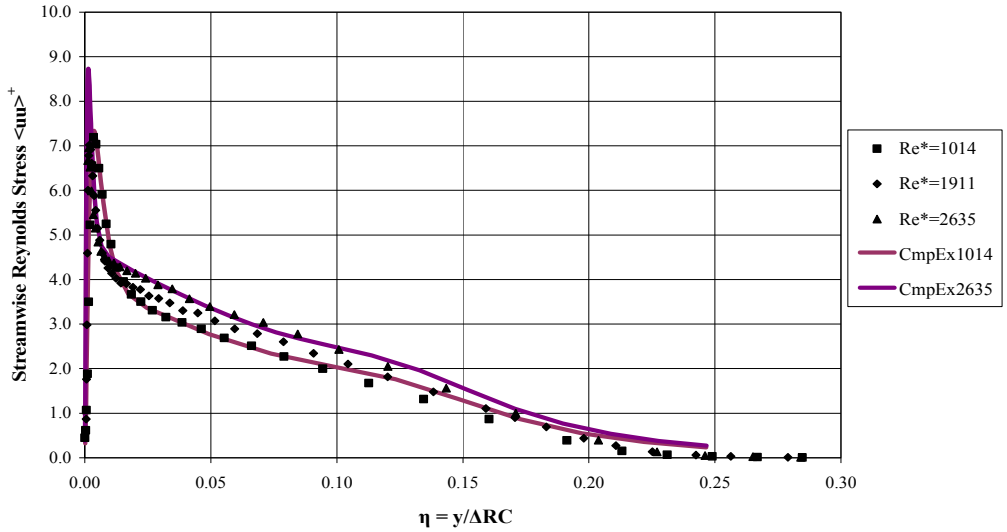

Figure 4-10. Predicted Streamwise Reynolds Stress Derived from Composite Expansions as Compared to Hutchins and Marusic Data vs. η

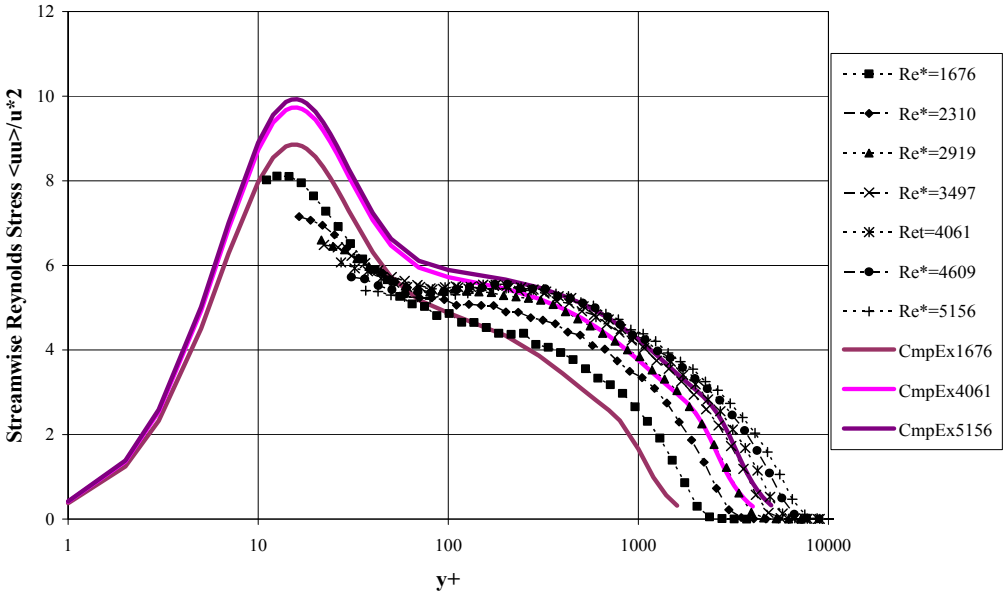

Figure 4-11. Predicted Streamwise Reynolds Stress Derived from Composite Expansions as Compared to Osterlund Data vs. y+

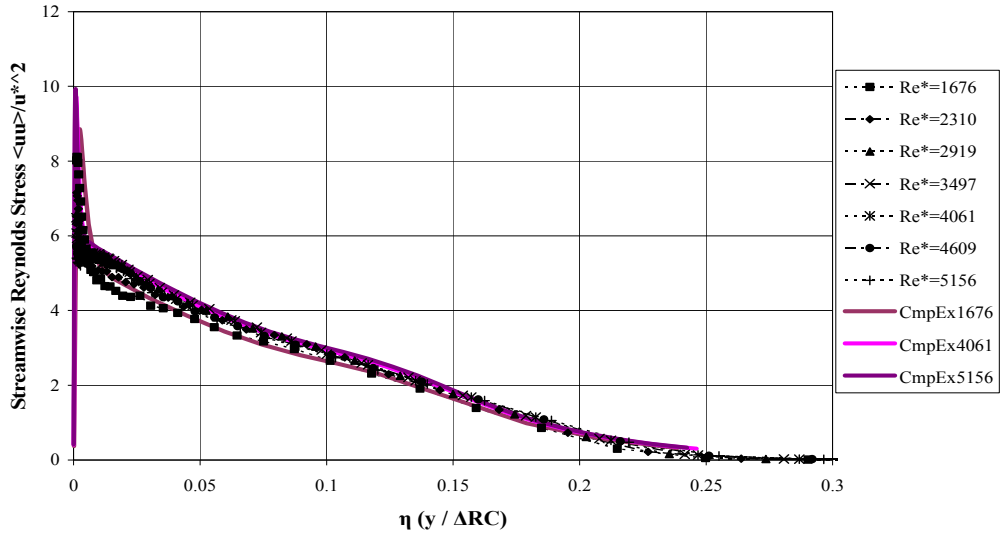

Figure 4-12. Predicted Streamwise Reynolds Stress Derived from Composite Expansions as Compared to Osterlund Data vs. η

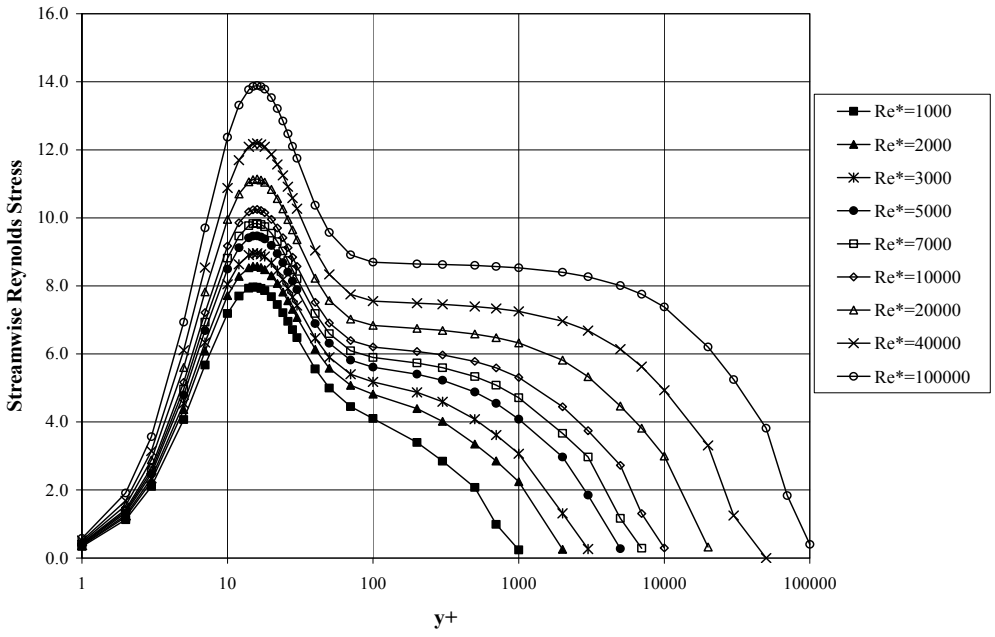

Figure 4-13. Predicted Streamwise Reynolds Stress from Composite Expansions for a Range of Reynolds Numbers from Re* = 500 to Re* = 100,000.

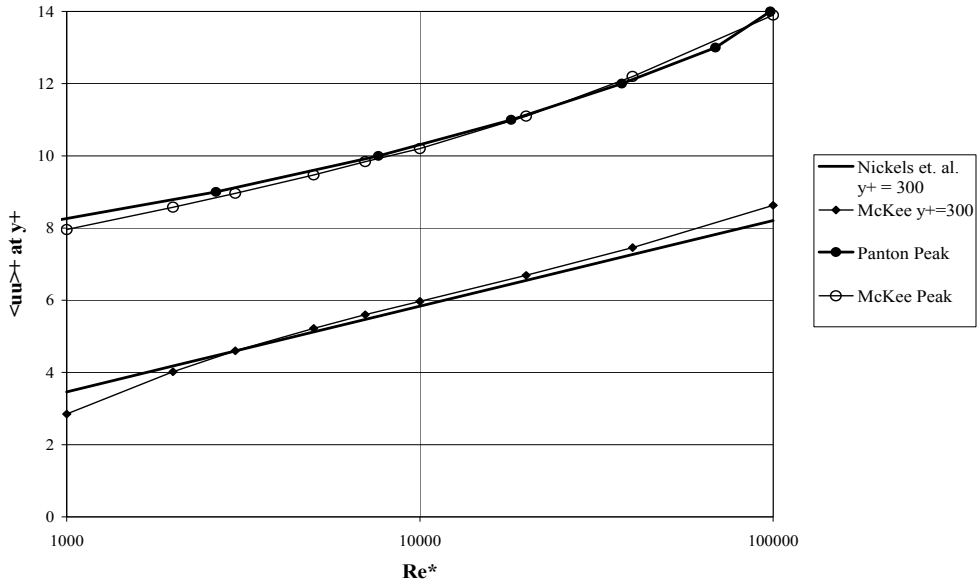

Figure 4-14. Predicted Amplitude at y+ = 300 and at the Peak Streamwise Reynolds Stress as a Function of Reynolds Number Compared to Data Fits by Nickels et al. (2007) Figure 4, and by Panton (2007) Figure 7.

Nomenclature

A_{Out} = Outer inactive streamwise Reynolds stress amplitude coefficient
C+ = Inner Reynolds shear stress scaling constant
C_{CP} = Inactive streamwise Reynolds stress common part
C_{min} = Inactive streamwise Reynolds stress minimum part
C_{Out} = Outer inactive streamwise Reynolds stress width (extent) coefficient
G(Y) = $G_o(Y)$ = Outer Reynolds shear stress function
G_{CP} = Common part for Reynolds shear stress
g(y+) = Inner Reynolds shear stress function
InCo = Inner inactive streamwise Reynolds stress amplitude coefficient
InC1 = Inner inactive streamwise Reynolds stress increase coefficient
InC2 = Inner inactive streamwise Reynolds stress decrease coefficient
k = Von Karman constant
l = Hot wire or measurement volume length
l+ = l u*/ν = Normalized hot wire (measurement volume) length
Re* = δ u*/ν = Reynolds Number (boundary layer friction velocity)
U(y) = Mean velocity, dependent on y
Ue = External or free stream velocity
u = Streamwise velocity
u* = $\sqrt{\tau_w/\rho}$ = Friction velocity
u_A = Active streamwise velocity component
uI = Inactive streamwise velocity component
v = Wall normal velocity
W(Y) = Wake function
x = Streamwise distance
Y = y/δ = Normalized distance from the wall
y = Distance from the wall
<uu> = Streamwise Reynolds stress
<uu>+ = <uu> /u*^2 = Normalized streamwise Reynolds stress
$<u_A u_A>+$ = Normalized active streamwise Reynolds stress
<uIuI>+ = Normalized inactive streamwise Reynolds stress
<uIuI># = Inactive streamwise Reynolds stress of Order 1
<uv> = Reynolds shear stress
<uv>+ = <uv> /u*^2 = Normalized Reynolds shear stress
Δ_{RC} = Ue δ* /ν = Rotta-Clauser boundary layer thickness
δ = Boundary layer thickness
δ* = boundary layer displacement thickness
δ99 or δ95 = Measures of the boundary layer thickness where U(y)/Ue = 99% or 95%
η = y/Δ_{RC} = Normalized boundary layer thickness based on Δ_{RC}
Π = Cole's wake coefficient
ρ = Fluid density
τ_w = Wall shear stress
ν = Fluid viscosity

Bibliography

Brzek, B., Cal, R.B., Johansson, G., and Castillo, L. 2007, "Inner and outer scaling in rough surface zero pressure gradient turbulent boundary layers", *Phy. Fluids* 19. 2007.

Cal, R. B., Johansson, G., and Castillo, L., 2006, "Upstream Condition Effects on Turbulent Boundary Layers Subject to Favorable Pressure Gradients", AIAA Journal, Vol. 44, No. 11, November 2006.

Carlier, J. and Stanislas, M., 2005, "Experimental study of eddy structures in a turbulent boundary layer using particle image velocimetry", J. Fluid Mech. Vol. 535, pp 143-188, 2005.

Castillo, L. and Johansson, G., 2002, "The effects of the upstream condition on a low Reynolds number turbulent boundary layer with zero pressure gradient", J. Turbul. 3, 031, August 2002.

Castillo, L. and Walker, D. 2002, "Effect of Upstream Conditions on the Outer Flow of Trubulent Boundary Layers", AIAA Journal, Vol. 40, No. 7, July 2002.

Clauser, F. H., 1956, "The Turbulent Boundary Layer," Adv. Appl. Mech., 4, pp. 1-51.

DeGraaff, D. B. and Eaton, J. K. 1999, "Reynolds Number Scaling of the Turbulent Boundary Layer on a Flat Plate and on Swept and Unswept Bumps", Report No. TSD-118, Stanford University, Stanford, Calif., January 1999.

DeGraff , D. B., & J. K. Eaton 2000 "Reynolds number scaling of the flat plate turbulent boundary layer," *J. Fluid Mech.* 422, pp 319-346.

Fernholtz, H.H., and Findley, J.P., 1996, "The Incompressible Zero Pressure Gradient Turbulent Boundary Layer: An Assessment of the Data", Prog. Aerosp. Sci., 32, pp 245.

Gad-el-Hak, M. and Bandeyophadhyay, P., 1996, " Reynolds Number Effects in the Wall-Bounded Turbulent Flow", Appl. Mech. Rev., 47, p. 307.

Hutchins, N. and Marusic, I., 2007, "Evidence of very long meandering features in the logarithmic region of turbulent boundary layers", J. Fluid. Mech, Vol. 579, pp 1-28. 2007.

Marusic , I. & Kunkel, G. J. 2003 "Streamwise turbulent intensity formulation for flat plate boundary layers," *Phys. Fluids* 15, pp 2461-2464.

Maursic , I. Uddin, A. & Perry, A. 1997 "Similarity law for the streamwise turbulence intensity in zero-pressure-gradient turbulent boundary layers," *Phys Fluids* 9 p. 3718.

Metzger. M. M., & Klewicki 2001 "A comparative study on near-wall turbulence in high and low Reynolds number boundary layers ," *Phys. Fluids*, 13, pp 692-701.

Nickels, T.B., Marusic, I., Hafez, S., Hutchins, N. and Chong, M.S., 2007, "Some predictions of the attached eddy model for a high Reynolds number boundary layer", *Phil.Trans. Royal. Soc*. Series A, Vol. 365, pp 807-822. January 2007.

Österlund, J. M., 1999 "Experimental studies of zero-pressure-gradient turbulent boundary layer flows," Doctoral Thesis, Royal Institute of Technology, Stockholm.

Panton, Ronald L. (1996), "Incompressible Flow", John Wiley & Sons, Inc.,1996.

Panton, R. L., 1997 , "A Reynolds stress function for wall layers," Journal of Fluid Engineering, 119, pp 325.

Panton, Ronald L. 2001, "Overview of the self-sustaining mechanisms of wall turbulence", Progress in Aerospace Sciences Vol. 37, 2001, pp 341-383.

Panton, R. L. 2002 "Reynolds Number Effect for the Reynolds Stress in a Boundary Layer," AIAA 2002-1105.

Panton, R. L., 2005, "Review of wall turbulence as described by composite expansions", Appl. Mech. Rev., 58, pp 1-36.

Panton, R. L., 2007 "Composite asymptotic expansions and scaling wall turbulence," Phil. Trans. Royal Soc. Series A, Vol. 365, 733-754. January 2007.

Perry, A. E., Henbest, S. & Chong, M. S. 1986 "A theoretical and experimental study of wall turbulence, *J. Fluid Mech.*, 165, pp163-199.

Perry, A. E. and Li, J.D. (1990) "Experimental support for the attached-eddy hypothesis in zero-pressure-gradient turbulent boundary layers," J. Fluid Mech., 218, pp 405-438.

Perry, A.E. and Marusic, I., 1995, "A wall-wake model for the turbulence structure of boundary layers. Part 1, Extension of the attached eddy hypothesis". J. Fluid Mech. Vol. 298, pp 361-388, 1995.

Rotta, J., 1953, "On the Theory of the Turbulent Boundary Layer", NACA TM No. 1344, 1953.

Seo, J., Castillo, L., Johansson, G., and Hangan, H., 2004, "Reynolds stress in turbulent boundary layers at high Reynolds number", J. Turbul. 5, 015, March 2004.

Spalart, P. R., 1988, "Direct simulation of a turbulent boundary layer up to Reθ = 1410., J. Fluid Mech. Vol. 187, pp 61-98, 1988.

Townsend, A. A. 1976 *The Structure of Turbulent Shear Flow* Cambridge University Press. second edition

Vita

Robert Joe McKee was born in Glendale, California on March 24, 1946, the son of Mildred Ruth McKee and Wayne Clifford McKee. Robert and his wife Catherine have two sons, Dr. David W. McKee and CWO Kevin A. McKee and several grandchildren. After completing his work at John Muir High School, Pasadena, California in 1964, he entered the University of California at Santa Barbara, California where he received his B.S. degree in Mechanical Engineering in 1968. In December 1968 he completed Officer Candidate School and was commissioned as an Ensign in the United States Naval Reserve and reported for active duty at Mare Island Naval Shipyard, Vallejo, California. Robert studied at the Naval Postgraduate School in Monterey, California and received his M.S. in Mechanical Engineering in 1973. Since leaving active duty in the Navy in 1977 Robert has been employed at Southwest Research Institute in San Antonio, Texas actively engaged in research and problem solving for industrial compressors, pumps and piping systems. Robert holds two patents and has nearly a hundred published articles.

Permanent address: 11703 British Arms, San Antonio, TX 78251

This dissertation was typed by the author.